

Modeling of Tensile Properties of Woven Fabrics and Auxetic Braided Structures by
Multi-Scale Finite Element Method

by

Yang Shen

A thesis submitted to the Graduate Faculty of
Auburn University
in partial fulfillment of the
requirements for the Degree of
Master of Science

Auburn, Alabama
December 14, 2013

Keywords: multi-scale mechanical model, finite element method, woven fabric,
helical auxetic yarn, biaxial tubular structure, analysis of mechanical property

Copyright 2013 by Yang Shen

Approved by

Sabit Adanur, Chair, Professor of Polymer and Fiber Engineering
Amnon Meir, Professor of Mathematics and Statistics
Yanzhao Cao, Professor of Mathematics and Statistics
Xinyu Zhang, Associate Professor of Polymer and Fiber Engineering

Abstract

This study is undertaken to build an appropriate mechanical model for the analysis of mechanical properties of forming fabrics by incorporation of multi-scale modeling concept comprising micro-mechanical model, meso-mechanical model and macro-mechanical model. The fabric is analyzed at three different scales: yarn, unit cell and fabric sheet. The micro-mechanical model is to obtain the overall properties of yarn structure. The meso-mechanical model concentrates on the mechanical analysis of the unit cell of the fabric with the periodic boundary conditions by inputting yarns' properties from the micro-mechanical model. The macro-mechanical model is to get the overall properties of desired fabric structure by extracting the results from meso-mechanical model. In the first part, six single-layer woven fabric samples, five two-layer fabric samples are analyzed. In the second part, a tubular braiding fabric structure made of helical auxetic yarns is manufactured and its properties are investigated by a similar multi-scale model. The models for both parts are validated by the comparison of simulation data and experimental data, which had good agreement. Detailed stress-strain field throughout the entire unit cell is determined, which can be further used in the analysis of fatigue and fracture properties.

Acknowledgments

I would like to give my great gratitude to my academic advisor, Dr Sabit Adanur, for his excellent guidance of research as well as courses during my entire academic studies at Auburn. I also would like to thank Dr Ramsis Farag for his help with the test experiments in the lab. My thanks go to Dr. Amnon J. Meir and Dr. Yanzhao Cao from the Department of Mathematics and Statistics for their advice in research.

The financial support from Auburn University Intramural Grants Program is appreciated.

I also would like to appreciate my friends and colleagues at Auburn for their kind help and support at Auburn. Special appreciations go to Song Chen because of his help of finite element method in the research.

Finally, I dedicated this thesis to my loving wife Zi Yan for taking care of me in life and her unconditional love for me.

Table of Contents

| | |
|---|------|
| Abstract | ii |
| Acknowledgments | iii |
| List of Tables | vii |
| List of Figures | viii |
| Chapter 1 Introduction | 1 |
| Chapter 2 Mechanical Model of Fabric Structure | 5 |
| 2.1 Literature Review | 5 |
| 2.1.1 Fibrous Structure and Mechanical Behavior | 5 |
| 2.1.2 Large Deflection and Nonlinearity..... | 6 |
| 2.1.3 Deformation in Textile Structure | 6 |
| 2.1.4 Background..... | 7 |
| 2.1.5 Classification of Mechanical Models of Fibrous Structures | 8 |
| 2.1.6 Analytical Modeling..... | 10 |
| 2.1.6.1 Micro-Mechanical Model by Analytical Method..... | 10 |
| 2.1.6.2 Meso-Mechanical Model by Analytical Method..... | 11 |
| 2.1.6.3 Macro-Mechanical Model by Analytical Method | 14 |
| 2.1.7 Numerical Modeling..... | 15 |
| 2.1.7.1 Micro-Mechanical Model by Numerical Method..... | 15 |

| | |
|--|----|
| 2.1.7.2 Meso-Mechanical Model by Numerical Method | 17 |
| 2.1.7.3 Macro-Mechanical Model by Numerical Method | 19 |
| 2.1.8 Evaluation | 20 |
| 2.2 Experimental | 21 |
| 2.2.1 Material Preparation | 21 |
| 2.2.2 Geometry of Unit Cell | 21 |
| 2.2.3 Measurement of Geometry | 25 |
| 2.2.4 Mechanical Property Tests | 28 |
| 2.2.5 Friction Coefficient Tests | 30 |
| 2.3 Modeling Approach | 33 |
| 2.3.1 Micro-Mechanical Modeling | 33 |
| 2.3.2 Meso-Mechanical Modeling | 36 |
| 2.3.2.1 3D Solid Modeling of Unit Cell Geometry | 37 |
| 2.3.2.2 Material Property Definition | 46 |
| 2.3.2.3 Meshing | 46 |
| 2.3.2.4 Contact Definition | 49 |
| 2.3.2.5 Periodic Boundary Conditions | 51 |
| 2.3.2.6 Derivation of Periodic Boundary Conditions | 52 |
| 2.3.2.7 Implementation of Boundary Conditions | 53 |
| 2.3.3 Macro-Mechanical Modeling | 54 |
| 2.4 Results and Analysis | 55 |
| 2.5 Conclusions | 73 |

Chapter 3 Mechanical Analysis of Auxetic Behavior of a Novel Braiding Tubular Structure

| | |
|--|----|
| by FEM | 74 |
| 3.1 Literature Review | 74 |
| 3.2 Material Preparation | 75 |
| 3.3 Approach..... | 76 |
| 3.4 Analysis of the Properties by FEM..... | 80 |
| 3.4.1 Micro-Mechanical Model..... | 80 |
| 3.4.2 Meso-Mechanical Model..... | 85 |
| 3.5 Results and Discussion | 87 |
| 3.6 Conclusions | 90 |
| References | 91 |

List of Tables

| | |
|--|----|
| Table 1 Geometric properties of six single-layer fabric samples..... | 22 |
| Table 2 Spacing for five two-layer fabric samples | 27 |
| Table 3 Major and minor radius for two-layer fabrics..... | 27 |
| Table 4 Mechanical properties of yarns for single-layer fabrics | 29 |
| Table 5 Mechanical properties of yarns for two-layer fabrics..... | 30 |
| Table 6 Friction coefficients of single-layer fabrics | 32 |
| Table 7 Friction coefficients of two-layer fabrics..... | 32 |
| Table 8 Mesh statistics | 48 |
| Table 9 Mechanical properties of wrap and core yarns as component of the helical auxetic yarn | 74 |
| Table 10 Geometric parameters for the auxetic yarn..... | 78 |
| Table 11 Geometry of the biaxial tubular structure | 79 |

List of Figures

| | |
|--|----|
| Figure 1 Integrated model of micro, meso and macro mechanical model | 9 |
| Figure 2 Geometric model of plain woven fabric by Peirce | 12 |
| Figure 3 3D geometric model of plain woven unit cell by Peirce | 12 |
| Figure 4 3D representation of wove model proposed by Kemp | 12 |
| Figure 5 3D representation of elliptic model proposed by Olofsson | 13 |
| Figure 6 Beam model of filaments for loose structure..... | 16 |
| Figure 7 Beam FE model of 50-filament twisted yarn..... | 16 |
| Figure 8 Solid FE model of unit cell of twill (left) and satin (right) woven structure..... | 17 |
| Figure 9 Cross section of a typical two-layer woven fabric structure with unit cell of 8 columns of weft yarns..... | 22 |
| Figure 10 Geometry of single-layer fabrics in top view (left), right view (middle) and left view (right)..... | 24 |
| Figure 11 Geometry of two-layer fabrics in top view (left), right view (middle) and left view (right) | 25 |
| Figure 12 Peirce’s model of simple woven fabric structure | 25 |
| Figure 13 Illustration for measurement of centerline of warp yarn for two-layer fabric 2 | 26 |
| Figure 14 Universal mechanical testing machine with a camera device..... | 28 |
| Figure 15 Stress strain curves for yarns in six single-layer fabric samples | 29 |
| Figure 16 Schematic of the friction coefficient testing device | 31 |
| Figure 17 Schematic of lenticular cross sections | 41 |
| Figure 18 3D solid model of unit cell of all fabric samples | 46 |

| | |
|--|----|
| Figure 19 Schematic of the meshing of cross section by triangles and rectangles | 47 |
| Figure 20 Coarse mesh of unit cell of single-layer fabric sample 1 | 47 |
| Figure 21 Medium mesh of unit cell of single-layer fabric sample 1 | 48 |
| Figure 22 Fine mesh of unit cell of single-layer fabric sample 1 | 48 |
| Figure 23 A contact pair | 49 |
| Figure 24 Periodicity of boundary of a yarn..... | 51 |
| Figure 25 Displacement constraints on the edge | 53 |
| Figure 26 Periodic boundary conditions on the single-layer fabric sample 5 | 54 |
| Figure 27 The contour of stress distribution throughout the unit cell of single-layer fabric sample 1 in undeformed state (top) and 10% deformed state (bottom) in the warp direction..... | 57 |
| Figure 28 The contour of stress distribution throughout the unit cell of single-layer fabric 2 in undeformed state (top) and 10% deformed state (bottom) in the warp direction | 58 |
| Figure 29 The contour of stress distribution throughout the unit cell of single-layer fabric 3 in undeformed state (top) and 10% deformed state (bottom) in the warp direction | 59 |
| Figure 30 The contour of stress distribution throughout the unit cell of single-layer fabric 4 in undeformed state (top) and 10% deformed state (bottom) in the weft direction..... | 60 |
| Figure 31 The contour of stress distribution throughout the unit cell of single-layer fabric 5 in undeformed state (top) and 10% deformed state (bottom) in the warp direction | 61 |
| Figure 32 The contour of stress distribution throughout the unit cell of single-layer fabric 6 in undeformed state (top) and 10% deformed state (bottom) in the weft direction | 62 |
| Figure 33 The contour of stress distribution throughout the unit cell of two-layer fabric 1 in undeformed state (top) and 10% deformed state (bottom) warp direction..... | 63 |
| Figure 34 The contour of stress distribution throughout the unit cell of two-layer fabric 2 in undeformed state (top) and 10% deformed state (bottom) warp direction..... | 64 |

| | |
|---|----|
| Figure 35 The contour of stress distribution throughout the unit cell of two-layer fabric 3 in undeformed state (top) and 10% deformed state (bottom) warp direction..... | 65 |
| Figure 36 The contour of stress distribution throughout the unit cell of two-layer fabric 4 in undeformed state (top) and 10% deformed state (bottom) warp direction..... | 66 |
| Figure 37 The contour of stress distribution throughout the unit cell of two-layer fabric 5 in undeformed state (top) and 10% deformed state (bottom) warp direction..... | 67 |
| Figure 38 Comparison between experimental data and simulation data of single-layer fabric sample 1 | 68 |
| Figure 39 Comparison between experimental data and simulation data of single-layer fabric sample 2 | 68 |
| Figure 40 Comparison between experimental data and simulation data of single-layer fabric sample 3 | 69 |
| Figure 41 Comparison between experimental data and simulation data of single-layer fabric sample 4 | 69 |
| Figure 42 Comparison between experimental data and simulation data of single-layer fabric sample 5 | 70 |
| Figure 43 Comparison between experimental data and simulation data of single-layer fabric sample 6 | 70 |
| Figure 44 Comparison between experimental data and simulation data of two-layer fabric sample 1 | 71 |
| Figure 45 Comparison between experimental data and simulation data of two-layer fabric sample 2 | 71 |
| Figure 46 Comparison between experimental data and simulation data of two-layer fabric sample 3 | 72 |
| Figure 47 Comparison between experimental data and simulation data of two-layer fabric sample 4 | 72 |
| Figure 48 Comparison between experimental data and simulation data of two-layer fabric sample 5 | 73 |
| Figure 49 Schematic of manufacture of helical auxetic yarn | 76 |
| Figure 50 The cross sectional view of rotating surface..... | 76 |
| Figure 51 The braiding machine used..... | 77 |

| | |
|---|----|
| Figure 52 Geometry of a helical auxetic yarn | 77 |
| Figure 53 Geometrical parameters | 77 |
| Figure 54 Schematic of the biaxial tubular structure | 79 |
| Figure 55 The biaxial tubular structure | 79 |
| Figure 56 3D solid model of the helical auxetic yarn | 81 |
| Figure 57 Application of boundary conditions | 82 |
| Figure 58 The contour of stress distribution before (up) and after (down) deformation | 82 |
| Figure 59 Comparison between simulation data and experimental data for tensile property | 82 |
| Figure 60 Curve fitting with bilinear function..... | 83 |
| Figure 61 Representation of helical auxetic yarn | 84 |
| Figure 62 Poisson's ratio versus longitudinal strain | 85 |
| Figure 63 3D solid model of the unit cell..... | 86 |
| Figure 64 Illustration of tension and shear | 86 |
| Figure 65 Application of boundary conditions | 87 |
| Figure 66 Geometry of the unit cell | 88 |
| Figure 67 The contour of stress distribution before deformation (left) and after deformation (right) | 89 |
| Figure 68 Experimental data and simulation results of each parameter | 89 |

Chapter 1 Introduction

Computer aided designs for conventional engineering materials such as metal and concrete which are widely used in bridges, airplanes and other structures are well established to work out the effects of all the likely forces and aerodynamic properties using computer simulations. In contrast, interlaced fibrous structures and products are still produced largely on the basis of experience, intuition and trial-and-error due to their unique properties of strength, flexibility, inhomogeneous structure and non-linearity. In recent years, the development of new materials and new manufacturing techniques allowed a variety of interlaced fibrous structures to penetrate into high performance areas, from medical to civil engineering, from automotive to military, from space to undersea applications. On the one hand, these ever-expanding new application areas require interlaced structures to be engineered very carefully and precisely since their failure could be devastating. On the other hand, appropriate computer aided design for interlaced fibrous structure and fibrous reinforced composites could maximally utilize overall properties of structures to result in high quality to cost ratio product tailored for very specialized purposes. Such demands considerably stimulate the development of geometric and mechanical modeling of fibrous materials.

Many former researches built analytical models to predict mechanical properties of fibrous materials based on assumptions and simplifications. The main drawbacks of analytical models are that most of them are quite complicated, time consuming and difficult to control the balance between necessary simplifications and accuracy. Application of finite element method emerges with rapid development of computer hardware and CAD programs

and it is gradually accepted as the first priority method to analyze properties of fibrous materials due to its advantages of accuracy, time saving and presentation of detailed stress distribution. After finite element analysis based on numerical method is well established and developed, a multi-level modeling concept by means of finite element method was also proposed and applied into all sorts of traditional materials analysis. Multi-scale concept divides materials into different scale. At each scale, properties data from previous scale is considered as inputs to generate overall properties of a larger unit by finite element method and the latter is then transferred into next scale as inputs to finally get the overall properties of the analyzed object. This concept could be suitably applied for mechanical analysis of interlaced fibrous structure.

The fundamental theory of this multi-level model is that the fabric is considered to be made of many identical repeating units which have exactly the same properties. Each repeating unit comprises continuous and elastic yarns interlaced at a certain structure. The micro scale stage is to calculate the overall properties of each yarn or obtained directly from mechanical tests if the yarn structure is as simple as monofilament.

The overall properties of one single yarn are approached by the homogenization process which connects the micro and meso-modeling. The meso scale stage is to calculate overall properties of repeating unit from yarn properties data of micro-stage. Finally the macro-mechanical modeling stage based on the generation of simplified structure predicts the mechanical performance of extended fabric pieces. The macro-mechanical data are collected from the homogenization process which transfers property of unit cell into property of overall fabric with desired geometry.

The first part of this research is to propose a multi-level model consisting of micro-mechanical model, meso-mechanical model and macro-mechanical model to efficiently and effectively analyze tensile properties of interlaced fibrous structure by finite element method. The multi-level model is constructed in detail so that it could contain most possible aspects from properties of yarn assemble to contact frictional coefficient which could affect the property of final product. Six single-layer woven fabrics and five different two-layer woven fabrics were investigated. Micro-mechanical properties and 3D geometric information both serve as input data for meso-mechanical modeling of repeating unit of each sample. Micro-mechanical properties including modulus, Poisson's ratio and friction coefficient are obtained from test of each yarn. 3D geometric information of one repeating unit containing cross section, spacing and crimp height are directly measured using microscope with CellSens Standard 1.8.1 software (Olympus Corporation). A generative model is used in this research to accurately generate 3D solid geometry of repeating unit of each sample. The meso-mechanical model containing material definition, contact specification and periodic boundary conditions is built in Static Structure module of Ansysworkbench. Finally, homogenization process of stress-strain data obtained from meso-mechanical model extrapolates the macroscopic tensile properties of tested fabrics which are compared with experimental data. Tensile properties of samples in both warp and weft directions were simulated by this model and then compared with experimental data.

The second part of the research introduces a novel auxetic tubular fabric structure by biaxial braiding and its mechanical analysis by FEM.

Considerable research about auxetic materials has been undertaken due to their counter

intuitive mechanical behavior or negative Poisson's ratio. In other words, auxetic materials are expanding in transverse direction while under longitudinal tension. Auxetic materials exhibit various potential applications because the negative Poisson's ratio could improve fundamental mechanical properties such as shear modulus, indentation resistance and toughness. The fundamental mechanism of auxetic behavior ranges from the rotation of the bonds at the molecular level to a honey comb structure at a macroscopic level. Among all auxetic materials, the synthesized auxetics are highly promising because it is possible to carefully tailor mechanical properties and control the structure of synthesized auxetics for specialized applications or purposes. Auxetic fibers also provide a new route to fabricate large textile structures or composites through textile methods such as weaving, knitting and braiding. Under such circumstance, a helical auxetic yarn is proposed by Hook et al. through winding a high modulus yarn helically onto a low modulus yarn [1]. In this research, we use the helical auxetic yarns as basis to fabricate a biaxial tubular structure and study its mechanical properties and variable permeability attributed to helical auxetic yarns.

The whole mechanical model was established on Ansysworkbench 14.0 which is a commercial finite element analysis program. The generative model as the 3D modeling technique was implemented in the modeling module of Ansys.

The literature review gives an introduction of characteristics of mechanical behavior of fabric structures under certain deformations and applications of analytical models and numerical models in mechanical analysis of fabric structures. It is followed by the descriptions of the model. Then results and discussion follow. Finally, conclusions and suggestions are presented.

Chapter 2 Mechanical Model of Fabric Structure

2.1 Literature Review

2.1.1 Fibrous Structure and Mechanical Behavior

Usually, a textile fabric is made of interlaced yarns which consist of elementary units—fibers. Textile structures could be classified according to the manufacturing process such as knitted, woven, braided and non-woven. The major difficulty of computational modeling of textiles is probably the geometrical complexity of the textiles as well as the manufacture pattern. For instance, a plain woven fabric structure could have complicated deformation even under simple loading. A tensile deformation of a spun yarn could result from the combination of bending, tensile, compression and even frictional sliding of the constituent arranged fibers. Furthermore, contact phenomenon such as bonding or frictional contact should also be taken into account as a necessary parameter in the mechanical model. The determination of contact region in the fabric and implementation of contact algorithm undoubtedly increase the complexity of the whole model.

Therefore, many mechanical models or analysis of fabric structures are based on some assumptions and simplifications so that the model is accurate and not costly. For example, the yarn is usually assumed to be an elastic homogeneous material. The elastic property of homogeneous yarn could be either linear or non-linear. A non-linear elastic behavior could come from synergy of mechanical behavior of assemble of micro fibers if the yarn is multifilament. If the yarn is monofilament made of one certain polymer, the yarn would probably exhibit a viscoelastic behavior which is also a non-linear behavior.

As it is mentioned previously, a suitable contact model at where yarns contact with each other must be established in order to effectively analyze mechanics of fabric structure. Actually, the friction effect supports the stability of the whole structure for some certain multifilament fabrics. Frictional contact has great influence on stress and strain distribution in a fabric subjected to deformation because force would be transferred from one yarn to the contacting adjacent yarn.

2.1.2 Large Deflection and Nonlinearity

The complexity of the mechanical behavior of fabric structure could also introduce the large deflection and non-linearity. The relative large deformation is due to the flexibility of yarns and geometries structure of fabric. The yarn is a flexible material which allows large deformation before breakage because of low value of packing factor (the ratio of fibers volume to the total volume of the yarn). The air space left between fibers gives high mobility to fibers resulting high deformability and could be removed by exterior loading. This could also happen in the overall fabric since the fabric structure has air space between yarns [2]. The non-linearity behavior of fabric could be explained by synthesis of straightening of bent yarns and their subsequent elongation [3]. The straightening of yarns usually occurs at the initial stage of loading. Longitudinal elongation of yarns appears with the increase of load. Therefore, the stress-strain curve of a textile structure subjected to tensile deformation is nonlinear.

2.1.3 Deformation in Textile Structure

As discussed in section 2.1.1, even a simple loading condition applied onto a piece of fabric could lead to a complex deformation of straightening, bending, compression and

sliding of yarns in the meso-scale stage and respective deformations of fibers in micro-scale stage.

In addition, huge deformation could occur through fibers in micro-mechanical scale when fabric is subjected to small deformation of macro-mechanical scale. Therefore, a simple deformation behavior happened in macro-mechanical behavior corresponds to a complex deformation in micro-mechanical scale. According to the macro-mechanical scale, deformation can be classified into simple deformations which are tensile, shear, bending and compression of the fabric sheet and complex deformation which is mainly the drape deformation. The drape property is very important characteristic which determines the formability of fabric especially when fabrics are used as reinforcement in composites. This research mainly focuses on the tensile properties of woven fabric structure.

2.1.4 Background

Composite materials exhibit a variety of advantages over conventional materials and have been under rapid development in terms of their design, manufacture and mathematical modeling. Under such circumstances, polymer materials are fabricated to form a tailored structure for a specialized purpose through textile manufacturing methods such as multi-layer weaving, multi-axial braiding and knitting due to their good quality to cost ratio [4]. The prediction of final product properties before the product is actually fabricated is extremely important for design and manufacture process in order to produce high quality to cost ratio product [5-6]. However, mathematical modeling of such fabric reinforced composites or novel fabric structures is complicated due to the complex structure. Fibrous materials present very different properties compared to other engineering materials because of their unique

properties such as strength and flexibility, inhomogeneous structure and visco-elasticity. Besides, the complicated crossover structure in fabric is also difficult to model [7]. The prerequisite of conducting a finite element analysis is to build an accurate geometric model of the object. A generative model which could generate all sorts of 3D fibrous structures has been proposed [8-9].

2.1.5 Classification of Mechanical Models of Fibrous Structures

Analysis of mechanical properties of textile structures has been done during the last decades. Generally speaking, the models can be classified by the scale of the model and the modeling method used. According to the modeling method, the model of textile structure could be divided into analytical model and numerical model. In most cases, the analytical model is to figure out the relationship between the desired properties and parameters as variables. The conceptualization, which is the process from physical reality of textile structure to mathematical model, is of essence. In conceptualization process, some necessary assumptions and simplifications have to be made. The major characteristic of analytical model is the balance between the simplifications introduced and the accuracy of the model. With respect to the numerical model, the first step, conceptualization, is still the same as the analytical model. The entire solution domain could be subdivided into piecewise finite elements and the mathematical model is solved in each finite element. The final solution is approximated by integration of solutions over all finite elements. With rapid development of computer hardware and 3D model programs, now the numerical method is dominating in the field of mechanical modeling of fibrous structures and its reinforced composites. Another classification is based on the scale of the model, namely micro-mechanical model,

meso-mechanical model and macro-mechanical model. The micro-mechanical stage studies the property of yarns by taking into account the orientation, structure and properties of constituent fibers. This stage is actually the process of transferring from properties of constituent fibers to overall property of the yarn assemble. The meso-mechanical model focuses on the study of overall property of fabric unit cell by introduction of geometry of unit cell and considering yarns as homogeneous material. The overall property of homogeneous yarn is calculated from micro-mechanical model. Finally, the macro-mechanical model is to predict complicated deformation of overall fabric such as drape by considering fabric as continuum material [10]. Even though these three model stages were proposed as distinct analysis approaches, there have been efforts for the integration of these three models.

The textile society proposed a modeling hierarchy based on three modeling scales: the micromechanical modeling of yarns, the meso-mechanical modeling of the fabric unit cell and the macro-mechanical modeling of the fabric sheet as shown in Figure 1 [11-12].

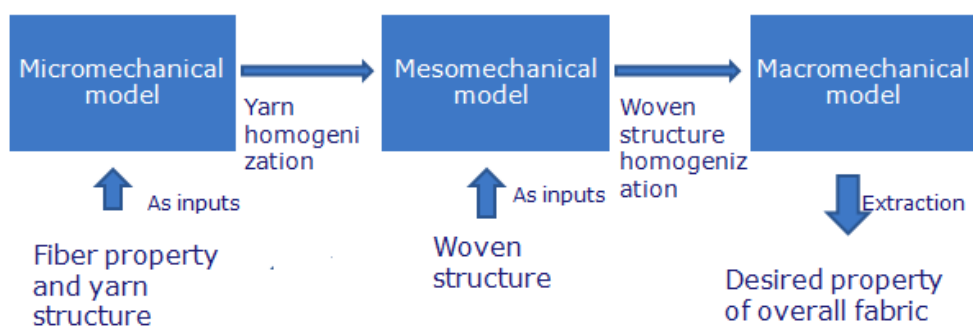


Figure 1 Integrated model of micro, meso and macro mechanical model

According to the integrated textile modeling concept, the only input data over the entire model procedure are the fiber properties, the yarn structure and the fabric structure. In the

first modeling stage, the fiber properties and the yarn structure are introduced as input parameters for the mechanical analysis of the yarn and the calculation of the yarn properties. Then, the yarn properties are transferred to the meso-mechanical stage as inputs. In the meso-mechanical model, the yarn is considered to be homogeneous and the yarns' properties correspond to a homogenization process which connects the first and second model stages. Furthermore, the geometry of fabric unit cell is introduced in this stage to build accurate 3D solid model of the unit cell. The analysis is limited to the fabric unit cell. A second homogenization process is required to connect the second and third stages by calculation of property of unit cell and its attribution in the fabric sheet.

Finally, the macro-mechanical modeling stage based on the assumption of continuum materials predicts the mechanical performance of extended fabric pieces in complex deformations. Each individual modeling procedure presents significant obstacles [12].

2.1.6 Analytical Modeling

The first mechanical analysis of fabric structure was probably proposed by Peirce [13]. Most of the analytical models are based on the elastica theory and energy minimization.

2.1.6.1 Micro-Mechanical Model by Analytical Method

Some research concentrates on the study of multifilament twisted yarn in terms of micro-mechanical model. The objective of such research is to investigate the response of twisted yarn subjected to certain deformations. In most cases, yarn is considered to be homogeneous continuum of constant cross section and density along the length. And all fibers are assumed to have identical properties and perfectly elastic. Stress-strain curve of fibers, twist density and the initial specific volume are taken into account as input parameters.

The cylindrical- helix model by Hearle et al and the conical-helix model by Onder and Başer were established from the point of view of arrangement of fibers and geometry of fibers' assemble [14-15]. Detailed descriptions of mechanical behavior of yarns were studied. Tension, bending and torsion behavior of yarns were approached by means of force, stress-analysis and energy methods [16-20]. Komori employed a statistical approach by introduction of large quantity of data to analyze mechanical properties of yarn assemble [21]. The major challenge of multifilament yarn model is the balance between physical reality and idealistic condition of yarn assemble.

2.1.6.2 Meso-Mechanical Model by Analytical Method

The first attempt of analytical modeling of fabric unit cell is to predict the uniaxial or biaxial deformation of plain woven structure. Peirce proposed three principal fundamental assumptions of geometrical model of plain woven fabric [13]. The flexible thread is assumed to be infinitely flexible, incompressible and inextensible with circular cross-sections as shown in Figure 2 and Figure 3 [13] [22]. This model has one main drawback which is the assumption of circular cross section shape because in most cases cross section shape is not perfectly circular due to exterior forces in manufacture processes. Thus, later, the Peirce's geometry model was improved by changing the cross sectional shape for a better representation of interlaced structure. The racetrack and elliptical cross sectional shapes were employed into Peirce's model as shown in Figure 4 and Figure 5 [23-24].

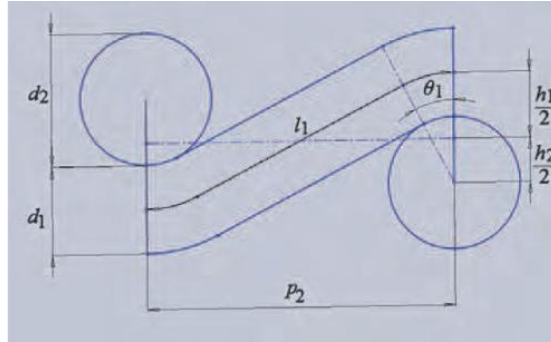


Figure 2 Geometric model of plain woven fabric by Peirce [13]

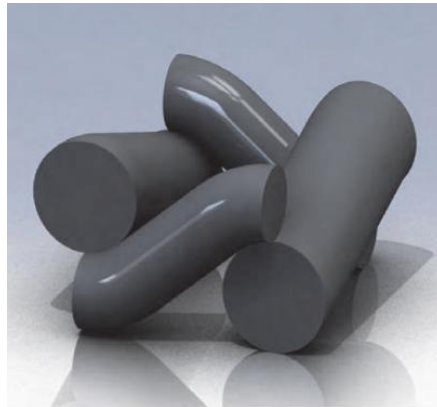


Figure 3 3D geometric model of plain woven unit cell by Peirce [13]

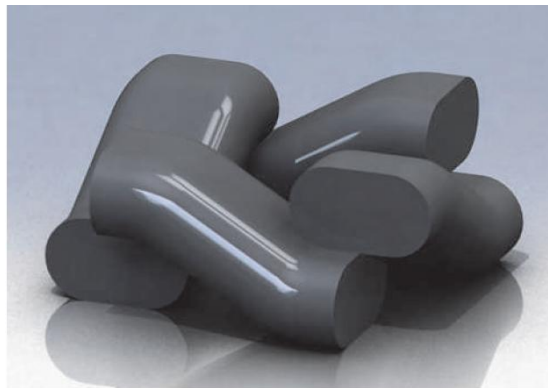


Figure 4 3D representation of woven model proposed by Kemp [23]

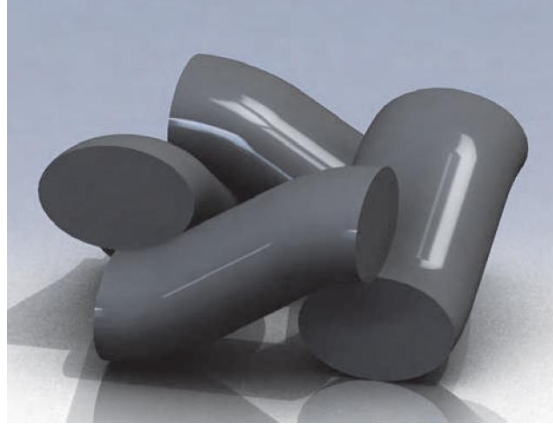


Figure 5 3D representation of elliptic model proposed by Olofsson [24]

In Peirce's model, the theory of elastica was proposed to treat the yarns as elastic slender rods. The shape of the yarn axis can be determined by the energy minimization of elastic slender while subjected to transverse forces. In short, the Peirce's model and its corresponding models were all developed according to the equilibrium, energy or elastica method for the mechanical analysis.

Another flexible thread model including the consideration of crimp and yarn extension was proposed by Freeston et al. [25]. This flexible thread model was based on the assumption of homogeneous, linear elasticity as well as linear work-hardening. Olofsson improved the Peirce's model by changing the yarn cross section shape into a function of the forces acting on them [24]. Mathematical equations were derived in terms of equilibrium conditions, stress-strain relationship of tension and compression and energy in bending. Grosberg and Kedia employed an energy method on the analysis of initial load extension modulus of completely relaxed woven fabric with the assumptions of inextensible and incompressible yarn [26]. Dastoor et al also proposed a similar elastica method taking into account linear extensibility of the yarns by regarding the yarns as homogeneous, weightless slender rods, frictionless material [27]. In this analytical approach, a computational algorithm was

implemented for the solution of the equilibrium equations. Another analysis of the large deformation of partially and completely set plain woven fabrics was performed by Huang [28-29]. Both effects of extension and bending of yarns were considered based on the elastic model. His model introduces the bilinear moment –curvature relation to explain the sliding of the fibers within the yarn, increasing the reliability of the study. The ‘sawtooth’ geometrical model which contains the force equilibrium and the displacement of the warp and weft yarns in thickness direction at contact points of crossing threads was proposed to elaborate finite deformation and biaxial deformation theory [30]. Dolatabadi and Kovař suggested an alternative geometrical model of woven fabric considering the yarn’s packing density as well as general fabric data as parameters [31-32].

2.1.6.3 Macro-Mechanical Model by Analytical Method

An improvement of elastic theory based on the concept of planar and spatial elastica was developed to study complex deformation of fibers and fiber assembly by Konopasek [33-34]. This model includes considerations of nonlinear behavior of material, friction elasticity, elastic-plasticity and visco-elasticity.

To be more specific, the planar elastica theory was proposed to study the large deflections of yarn in a plane and the bending behavior of fabric sheet. The spatial elastic was proposed to analyze fiber buckling and crimp. Computational tools were utilized in order to solve the nonlinear differential equations. Lloyd et al. published an alternative method to the theoretical mechanics of static drape of fabrics by solving the differential geometry of surfaces [35]. In addition, they developed a convenient implementation of the theoretical mechanics of fabrics since the fabric was considered as 2D continuum represented by a

surface with very small thickness embedded in the 3D Euclidean space. The dynamic deformation of fabrics was studied by means of differential geometry of surfaces [36]. A model was established to generate the surfaces made of a series of twisted curves. The relationship between the curvature of surface and the mechanical properties of material was investigated by checking differential geometry parameters. The concept of homotopy was applied in the mathematical model of deformation of the surface from the initial state to the final state.

2.1.7 Numerical Modeling

The expansion of powerful commercial software codes considerably stimulates the application of numerical method into research of textile structures. Two dominant methods in mechanical modeling of textile structure and its respective reinforced composite are Finite Element Method (FEM) and Boundary Element Method (BEM) [37-38]. 2D and 3D representations for the plain woven fabric structure were the first attempts to build mechanical model by numerical method. Keefe et al. proposed a 3D geometrical model with various compactions and angles based on the geometry of woven fabric [39]. Later, these models were validated for numerical methods [40-41]. The application of numerical methods such as FEM and BEM guides the direction of the approaches for textile micro and meso-mechanical models in the future.

2.1.7.1 Micro-Mechanical Model by Numerical Method

Munro et al [42] suggested a new approach using FEM to analyze the properties of aligned fiber assembly. The element used in the model is a cuboid cell with 8 nodes and each node contains 6 degrees of freedom. The model could correlate the energy contributions to

element stiffness with various user defined properties in which nonlinear behavior is successfully applied. The yarn models were discretized by dividing them into layers which was again split into finite element ranging from 1 to 22. The fibers were initially arranged to form the idealized helical-yarn geometry. The result from this model fit well with the expectation. The necking phenomenon of the yarn assemblies appeared under tension and elements of the model were opened significantly under axial compression.

The fast development of CAD tools makes the construction of 3D solid models of even complex textile structure possible. An FEM modeling of yarn of the loose condition and dense condition supported by the assumption of helicoidal filaments with a constant helix radius are given in Figures 6 and 7 [43].



Figure 6 Beam model of filaments for loose structure [43]



Figure 7 Beam FE model of 50-filament twisted yarn [43]

2.1.7.2 Meso-Mechanical Model by Numerical Method

Parametric solid modeling software programs have been developed to generate 3D solid model of complex woven structures with weave pattern, yarn size or spacing as parameters. In the unit cell, the yarn is still assumed to be homogeneous material in order to reduce the cost and time consumption during calculation [44]. The meso-mechanical model was greatly improved by various types of finite elements and implementation of material property pool which includes linear, nonlinear, elastic, plastic, viscoelastic, isotropic, orthotropic, anisotropic options etc. In addition, contact algorithms and large strain effects were also taken into account in the mechanical model of unit cell since they have great influence on the final result. Durville [45] proposed a 3D beam model to simulate mechanical behavior of woven fabrics in fibers scale. Tarfaoui and Akesbi [46] presented a more complicated structure of twill woven fabric whose unit cell comprises of three warp and three weft yarns. B-spline function was used in order to generate more precise 3D solid model of yarn in FEM [47]. Vassiliadis et al built a 3D model of complex interlaced woven fabric for the mechanical properties analysis as shown in Figure 8 [48].



Figure 8 Solid FE model of unit cell of twill (left) and satin (right) woven structure [48]

Fibrous structure reinforced composites have been widely used in fields of automotive, marine and aerospace industry due to their high ratio of stiffness and strength to weight and multiple functions. Zhang and Harding used strain energy method of FEM to predict the elastic properties of plain woven composite structures [49]. The drawback of this approach pointed out by the authors was that the two undulations in one direction were not realistic for woven fabric. Naik improved this approach by considering the strand cross section geometry, possible gap between two adjacent yarns and the two direction undulation [50]. Whitcomb studied the effect of quadrature order, mesh density and material degradation on the predicted failure from in-plane loading [51]. The 3D solid model of composite is made of the volumes of woven unit cell and the volumes of matrix. The volume of matrix could be obtained by subtracting the volumes of fabric unit cell from the overall volume of composite unit cell. Some approaches were undertaken to investigate the homogenized elastic properties of fabric composites using the unit cell of composite structure. Circular, elliptic, compressed hexagonal and lenticular cross section shapes were assumed for the 3D construction of tows. The material properties of tows in the composite were defined as transverse isotropic and the matrix as isotropic. An approach proposed by Ng et al. [52] predicted the inplane elastic properties of a single layer 2/2 twill woven fabric composite. The mechanical model was programmed by the ANSYS Parametric Design Language (APDL). The 8-node solid elements with 3 degrees of freedom per node were used in the model. The whole model contains approximately 52000 finite elements and 12000 nodes. The contact areas were generated by subtracting the volume of fabric unit cell from the overall volume of composite unit cell and were then defined to be a shared entity for both the yarn and the matrix volumes.

Choi and Tamma [53] successfully predicted the in-plane elastic properties of a composite structure reinforced with plain woven fabric. The predicted elastic properties were then used for the damage analysis of laminated composite structures. The superposition principle was used for the prediction of homogenized properties of woven fabric reinforced composites. The overall model contains 520 wedge elements for the yarns and 256 brick elements for the matrix. In-plane tensile and shear deformation was obtained with a gradually incrementing load. A novel research in terms of generalized description of the internal structure of textile reinforcement was conducted by Leuven. Lomov et al. proposed a model for the internal geometry of 2D and 3D woven structure based on the minimization of total energy throughout unit cell and yarn mechanical properties. And this method could be extended to all sorts of fibrous structures such as woven, braided, knitted structures [54-56]. They also established a three-level hierarchy: the micro-, meso- and macro-level. The micro-level deals with the arrangement of fibers in the representative volume of yarn. The meso-level defines the internal structure of the reinforcement and direction and volume fraction within the yarn. Finally, the macro-level prescribes the 3D geometry of composite unit cell and distribution of the reinforcement properties.

2.1.7.3 Macro-Mechanical Model by Numerical Method

Macro-mechanical modeling of fabric or cloth mainly concentrates on the prediction of drape behavior and the virtual representation. According to the purpose and application of fabric, different techniques have been developed in the last decades. Numerical model such as the particle-model, the deformable node-bar model and the FEM were proposed for the purpose of better understanding of fabric behavior under deformation. Most

macro-mechanical models by numerical method mainly focus on drape properties of fabric, whereas meso-mechanical models with appropriate boundary condition are accurate enough to solve simple macro-deformation of tension, compression and shearing. Since this research only concentrates on the prediction of tensile property of fabric structure, there is no further introduction of macro-mechanical model of drape properties of fabric.

2.1.8 Evaluation

The review of literature of analytical models for the mechanical analysis of woven fabrics indicates that a globally accepted analytical model in terms of accuracy still remains as a goal. Even though there are so many different analytical models, most of which are based on totally distinct theories or principles, all of them were established on simplifications and assumptions in order to decrease the complexity of the model. The major drawback in analytical models is the balance between simplifications and the accuracy of the results. The two-dimensional approach and the attribution of linear isotropic properties defined for materials would result in inaccuracy. In addition, the analytical models have the difficulty of integrating of micro-, meso- and macro-level models. Analytical models have been replaced by or incorporated into the numerical models. The numerical methods have unique advantages to overcome obstacles such as geometrical representation, complex deformations, particular material properties, contact phenomena and large deflection effects. Moreover, numerical approach tools are able to generate good virtual representation of fabric under deformation. Most numerical methods are based on the Finite Element Method which could simplify the mechanical analysis by avoiding calculation of the bending rigidity of the yarn and its attribution at the modeled yarn. The homogenization process could be achieved

between each model level by application of boundary conditions so that the micro-, meso- and macro-level models are well connected. However, homogenization process may become problematic if the interpretation of data from previous stage is difficult for the next stage. There is still much work to collaborate each stage in order to generate realistic model and equivalent properties.

2.2 Experimental

2.2.1 Material Preparation

Six single-layer woven fabrics and five two-layer woven fabrics were used for this research. Each yarn in the fabric is polyester monofilament with different diameter and mechanical properties. The detailed information of unit cell of each woven fabric was examined by observation under microscope.

2.2.2 Geometry of Unit Cell

The geometry of unit cell of each fabric samples was examined using computer software associated with a microscope (cellSens Standard 1.8.1 by Olympus Corporation). The CellSens Standard program is capable to measure the length and angle up to magnitude of micrometer. The yarns in the fabric structure are classified into warp yarn and weft yarn. The warp yarn is along the machine direction, while weft yarn is perpendicular to the warp yarn. For the two-layer woven fabrics, the top layer and bottom layer are made of weft yarns, while a warp yarn crosses over each weft yarn as shown in Figure 9.

The unit cells geometry of each fabric sample are presented in Figures 10 and 11. The top view, right view (weft yarn direction) and left view (machine direction) of single-layer woven fabrics and two-layer fabrics are shown in the figures. The properties of single-layer

woven fabrics are given in Table 1. The patterns for two-layer fabrics are little bit complicated. The two-layer fabric samples 1, 4 and 5 have extra yarns in the top weft layer.

Table 1 Geometric properties of six single-layer fabric samples (w: warp, f: filling)

| Fabric | 1w | 1f | 2w | 2f | 3w | 3 f | 4w | 4f | 5w | 5f | 6 w | 6 f |
|-------------------|-------|-------|-------|-------|-------|-------|-------|-------|-------|-------|-------|-------|
| Major radius (mm) | 0.575 | 0.525 | 0.555 | 0.555 | 0.445 | 0.355 | 0.435 | 0.255 | 0.25 | 0.21 | 0.22 | 0.175 |
| Minor radius (mm) | 0.51 | 0.485 | 0.45 | 0.45 | 0.415 | 0.305 | 0.405 | 0.195 | 0.195 | 0.195 | 0.195 | 0.15 |
| Spacing (mm) | 3.57 | 3.57 | 1.89 | 1.89 | 1.29 | 1.06 | 1.13 | 1.09 | 1.28 | 1.58 | 0.90 | 0.50 |
| Crimp height (mm) | 1.65 | | 1.94 | | 0.9 | | 1 | | 0.9 | | 0.65 | |
| Structure | 1/1 | | 2/1 | | 4/1 | | 3/1 | | 3/1 | | 3/1 | |

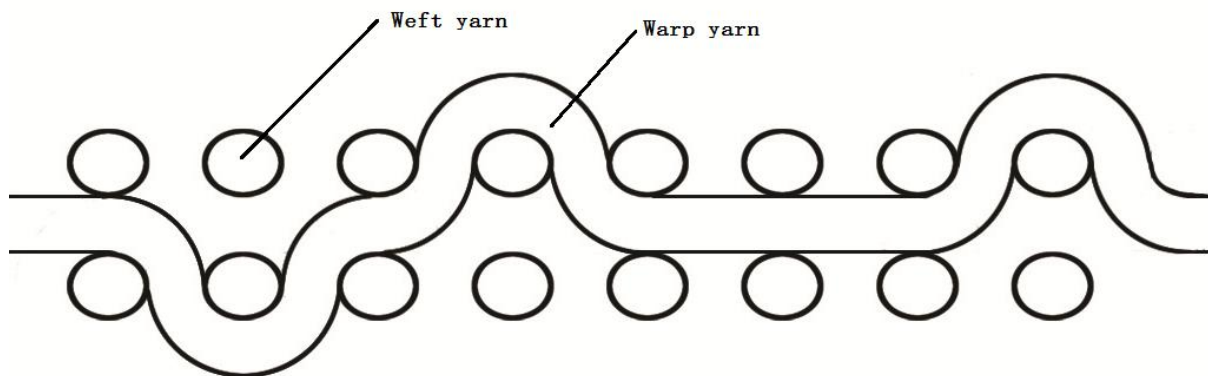
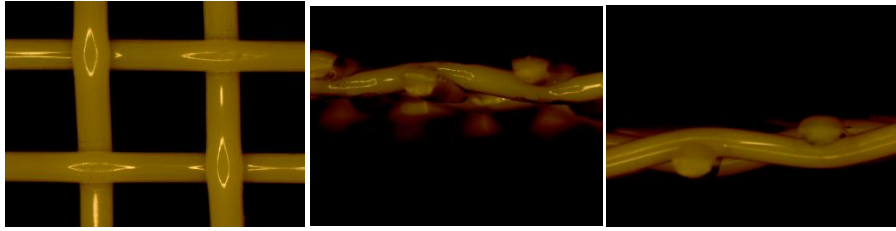
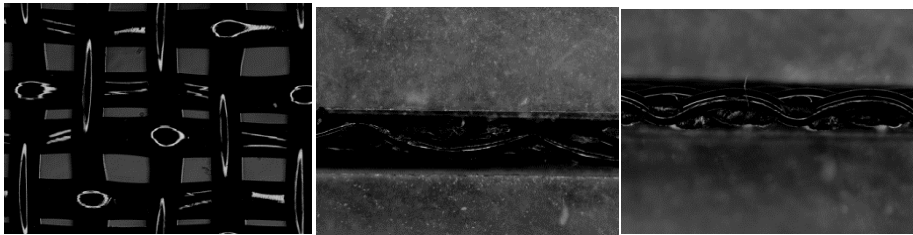


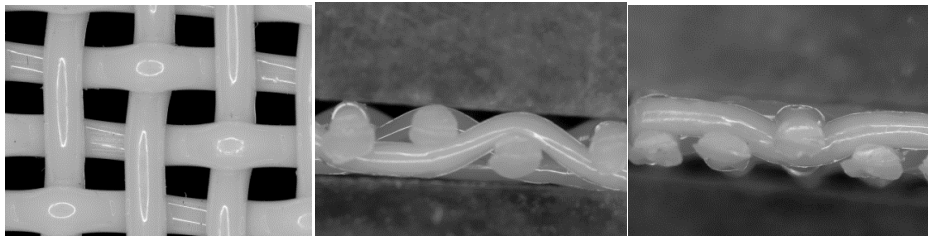
Figure 9 Cross section of a typical two-layer woven fabric structure with unit cell of 8 columns of weft yarns



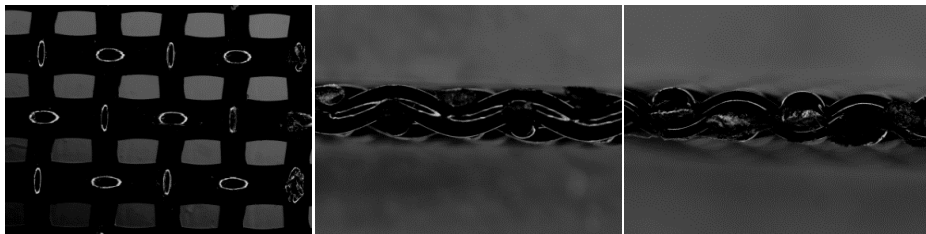
Single-layer fabric sample 1



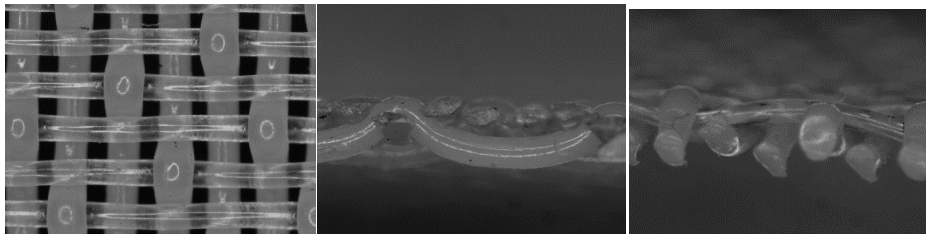
Single-layer fabric sample 2



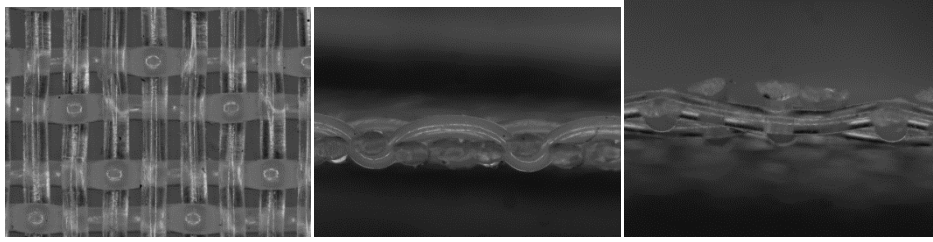
Single-layer fabric sample 3



Single-layer fabric sample 4

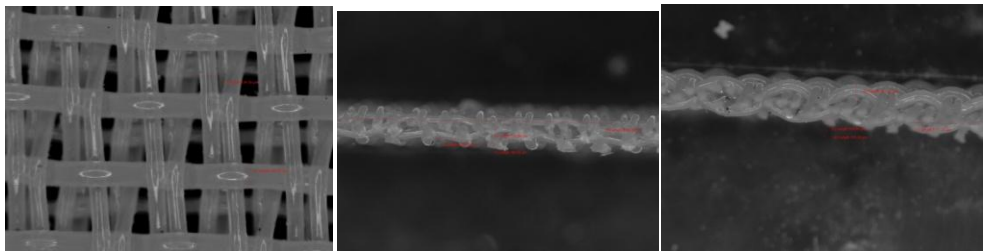


Single-layer fabric sample 5

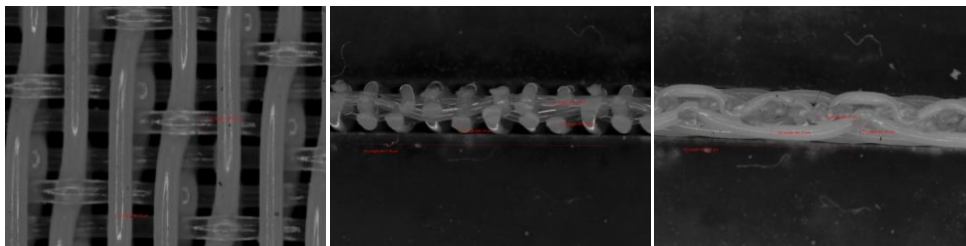


Single-layer fabric sample 6

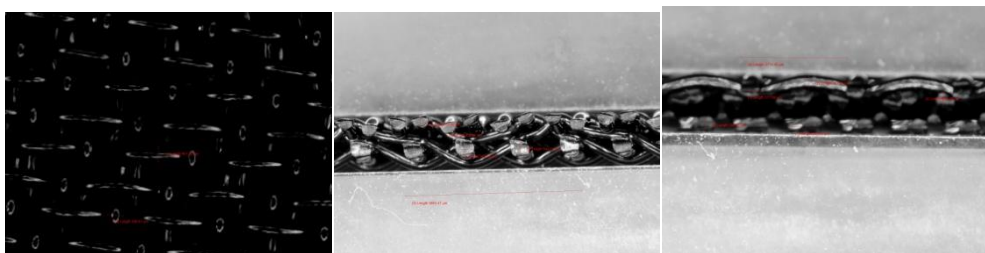
Figure 10 Geometry of single-layer fabrics in top view (left), right view (middle) and left view (right)



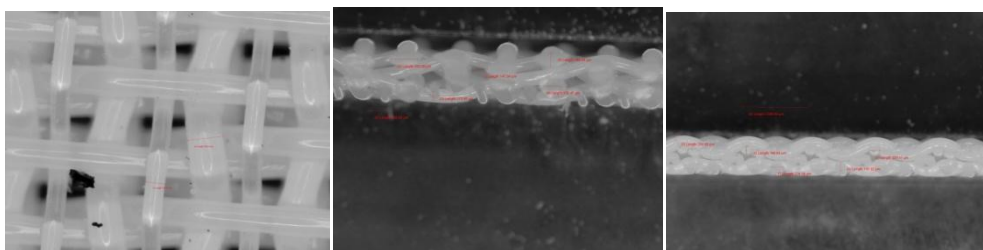
Two-layer fabric sample 1



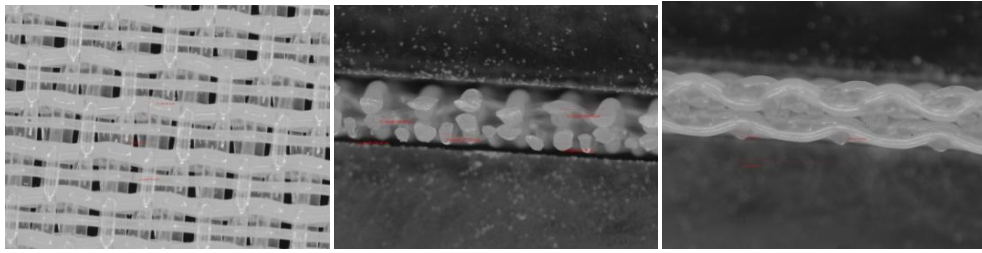
Two-layer fabric sample 2



Two-layer fabric sample 3



Two-layer fabric sample 4



Two-layer fabric sample 5

Figure 11 Geometry of two-layer fabrics in top view (left), right view (middle) and left (right) view

2.2.3 Measurement of Geometry

The 3D model construction depends on the measurement of geometry of each unit cell. What geometrical parameters need to be measured matters. According to the Peirce's model, the intact geometry of the unit cell of fabric can be determined as long as the spacing between yarns (p in Figure 12), diameter and crimp height (h in Figure 12) are given. Then, the crimp angle, θ in Figure 12, can be calculated so that the contact area at cross over point is determined.

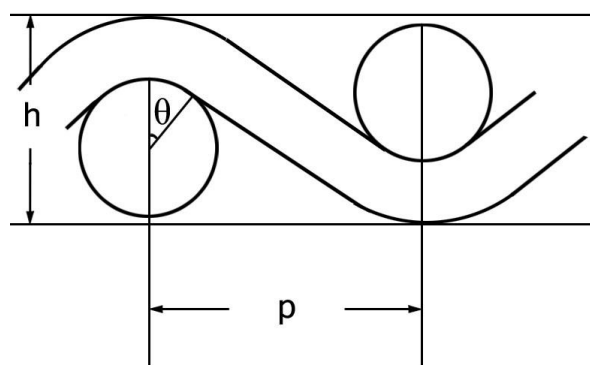


Figure 12 Peirce's model of simple woven fabric structure

CellSens Standard 1.8.1 can measure fine distances between two points. The spacing is measured through the distance between centroids of two adjacent yarns. It was found that the

cross sectional shape of yarns is not perfectly circular. To build a more accurate model, elliptic shape is used to describe cross section of each yarn. The major radius and minor radius of each yarn are measured. Finally, the crimp is measured through the distance between the highest point and lowest point over an undulated yarn. Table 1 summarizes the geometrical information of 6 samples of single-layer fabrics

However, this principle is only suitable for simple woven structures which, in this case, are single-layer fabrics. It does not work for the more complicated woven structures such as 2 layer fabrics. A generative model which contains an interpolated spline function and elliptical surface is applied into generation of 3D solid geometry of unit cell for 2 layer fabrics. This technique will be explained later in the modeling section. An undulated yarn could be described by the path of the centerline of its cross section. Besides major and minor radius and spacing, the coordinates of the nodes along the centerline are also measured. In order to draw an intact curve for the centerline of the warp yarn for a two-layer structure as shown in Figure 9, at least 8 nodes which are exactly above the centroids of bottom weft yarns have to be determined. Figure 13 shows the 8 centerline nodes (black dots) for the unit cell of two-layer fabric 2. This method for generating 3D solid model of fabrics could be extended to all sorts of fabric structures

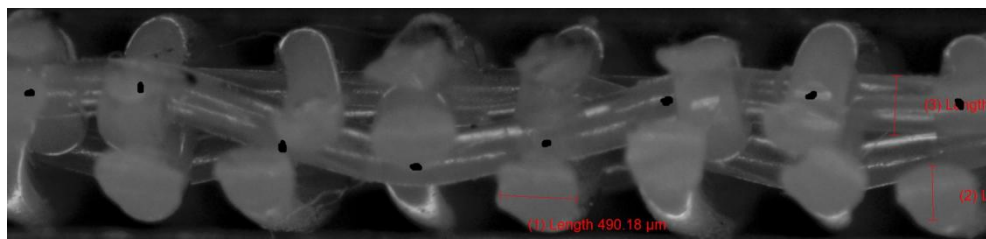


Figure 13 Illustration for measurement of centerline of warp yarn for two-layer fabric 2

Table 2 presents the spacing information for five two-layer fabric samples. Since spacing between top weft, bottom weft and warps could be different, each of them has to be measured separately. Table 3 shows the major and minor radius for two-layer fabrics.

Table 2 Spacing for five two-layer fabric samples

| | spacing between top and bottom layer (mm) | spacing between warp yarns (mm) | spacing between top weft yarns (mm) | spacing between bottom weft yarns (mm) |
|----------|---|---------------------------------|-------------------------------------|--|
| Sample 1 | 0.234 | 0.187 | 0.280 | 0.560 |
| Sample 2 | 0.786 | 0.475 | 0.930 | 0.930 |
| Sample 3 | 0.881 | 0.384 | 0.877 | 1.755 |
| Sample 4 | 0.390 | 0.241 | 0.434 | 0.868 |
| Sample 5 | 0.303 | 0.222 | 0.377 | 0.755 |

Table 3 Major and minor radius for two-layer fabrics

| | | Major radius(mm) | Minor radius(mm) |
|----------|-------------|------------------|------------------|
| Sample 1 | Warp yarn | 0.072 | 0.058 |
| | Weft bottom | 0.091 | 0.080 |
| | Weft top | 0.066 | 0.053 |
| Sample 2 | Warp yarn | 0.208 | 0.175 |
| | Weft bottom | 0.221 | 0.173 |
| | Weft top | 0.221 | 0.173 |
| Sample 3 | Warp yarn | 0.258 | 0.202 |
| | Weft bottom | 0.284 | 0.272 |
| | Weft top | 0.227 | 0.165 |
| Sample 4 | Warp yarn | 0.115 | 0.090 |
| | Weft bottom | 0.175 | 0.091 |
| | Weft top | 0.175 | 0.091 |
| | Top extra | 0.056 | 0.044 |
| Sample 5 | Warp yarn | 0.098 | 0.069 |
| | Weft bottom | 0.120 | 0.095 |
| | Weft top | 0.120 | 0.095 |
| | Weft extra | 0.078 | 0.063 |

2.2.4 Mechanical Property Tests

Since this model assumes that the yarn is homogeneous and isotropic, the linear isotropic material model is used to define elastic properties of yarns. A linear relationship is applied to fit the stress-strain curve of each yarn to describe mechanical properties. Thus, both stress-strain curve and Poisson's ratio are measured by universal mechanical testing machine (INSTRON) according to the ASTM D3822 – 07. A camera device associated with the mechanical test machine can capture the image of yarns under tension test (Figure 14). The width of each yarn can be measured under different tensile deformation from which the Poisson's ratio can be calculated.

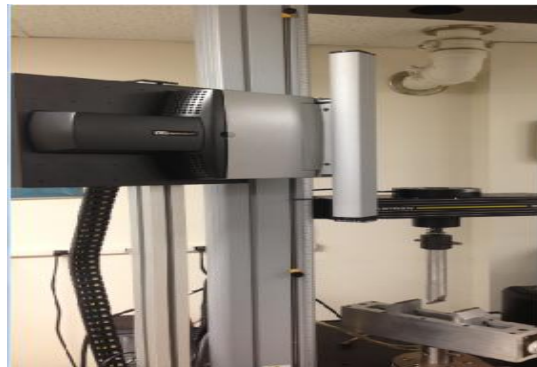


Figure 14 Universal mechanical testing machine with a camera device (INSTRON Technology)

The stress-strain curves of yarns in 6 single-layer fabric samples are given in Figure 15, which shows that some of them exhibit non-linear behavior. In an ideal realization of the model, the non-linear behavior should be taken into account. However, in this research, a simplified linear model is used.

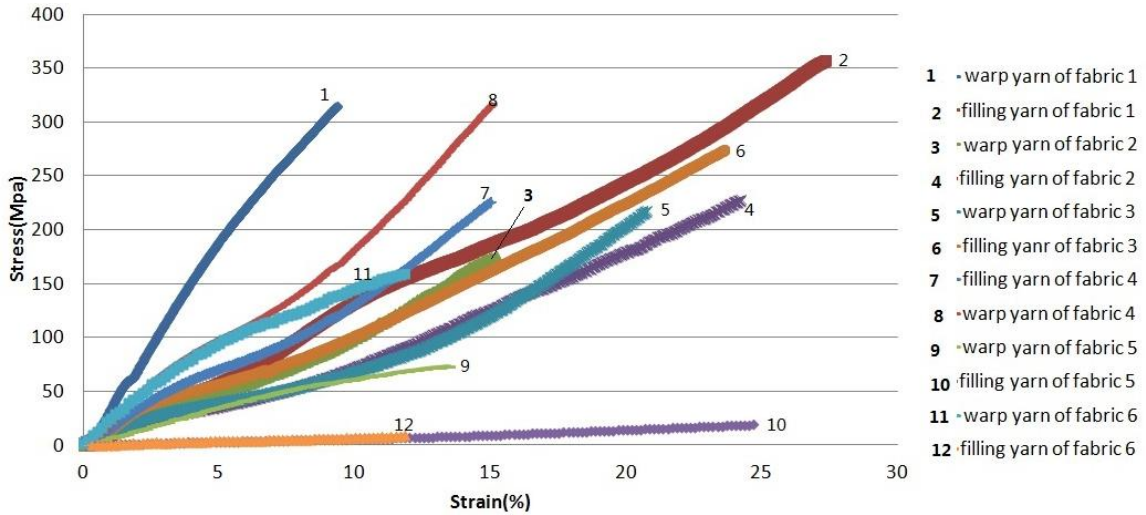


Figure 15 Stress strain curves for yarns in six single-layer fabric samples

The mechanical properties of each yarn are summarized in Tables 4 and 5. For single-layer fabric structure, both warp yarn and weft yarn have different modulus and Poisson's ratio. Usually, the modulus of warp yarn is higher than that of weft yarn. With respect to two-layer fabric structure, the unit cell of two-layer structure contains top weft, bottom weft, warp yarn and even extra yarn. Each of them may have different mechanical properties.

Table 4 Mechanical properties of yarns for single-layer fabrics

| Samples | Direction | Modulus (MPa) | Poisson's ratio |
|-----------------------|-----------|---------------|-----------------|
| single-layer sample 1 | Warp yarn | 3990 | 0.39 |
| | Weft yarn | 1260 | 0.32 |
| single-layer sample 2 | Warp yarn | 1080 | 0.35 |
| | Weft yarn | 870 | 0.36 |
| single-layer sample 3 | Warp yarn | 1110 | 0.42 |
| | Weft yarn | 870 | 0.35 |
| single-layer sample 4 | Warp yarn | 1440 | 0.4 |
| | Weft yarn | 890 | 0.37 |
| single-layer sample 5 | Warp yarn | 610 | 0.41 |
| | Weft yarn | 74.1 | 0.34 |
| single-layer sample 6 | Warp yarn | 1541 | 0.39 |
| | Weft yarn | 88.4 | 0.44 |

Table 5 Mechanical properties of yarns for two-layer fabrics

| | | Modulus(MPa) | Poisson's ratio |
|----------|-------------|--------------|-----------------|
| Sample 1 | Warp yarn | 3320 | 0.34 |
| | Weft bottom | 788 | 0.32 |
| | Weft top | 1240 | 0.34 |
| Sample 2 | Warp yarn | 3510 | 0.33 |
| | Weft bottom | 931 | 0.33 |
| | Weft top | 382 | 0.35 |
| Sample 3 | Warp yarn | 2080 | 0.37 |
| | Weft bottom | 3452 | 0.36 |
| | Weft top | 2219 | 0.37 |
| Sample 4 | Warp yarn | 2637 | 0.43 |
| | Weft bottom | 453 | 0.41 |
| | Weft top | 194.6 | 0.43 |
| | Top extra | 1699 | 0.41 |
| Sample 5 | Warp yarn | 3599 | 0.39 |
| | Weft bottom | 703.2 | 0.39 |
| | Weft top | 333.5 | 0.38 |
| | Weft extra | 2469 | 0.40 |

2.2.5 Friction Coefficient Tests

Previous research indicated that friction coefficient between fibers does not have much effect on mechanical properties while fabric is under axial or biaxial loading because relative sliding can be neglected when fabric is subjected to axial or biaxial loading. However, the friction coefficient turns out to be a very important aspect in terms of manufacturing process and behavior under shear loading or cyclic loading [56]. In addition, friction between yarns at crossover points directly supports the geometric integrity. For the completeness of the mechanical model, the friction coefficient has been taken into account in the FEA by

incorporating a friction model at the contact zone. The friction coefficient was experimentally obtained using a device whose schematic is shown in Figure 16. Five samples were tested for each pair of yarns contacting to each other and the final value of friction coefficient was obtained by taking the average. The friction coefficient is calculated using:

$$\mu = \left(\frac{1}{\pi\tau\beta} \right) * \ln T_1/T_0 \quad (1)$$

where τ is the number of turns per unit length, T_0 is the initial tension on the lower free ends, T_1 is the measured friction force, and β is the twist angle which can be calculated from the following equation:

$$\beta = 2 * \tan \frac{L_2}{(L_1-L)} \quad (2)$$

where L , L_1 and L_2 are distances indicated in Figure 16. Friction coefficients of each fabric measured from experiments are shown in Tables 6 and 7. The single-layer fabrics only have one type of contacting condition which is the contact between the warp and weft yarn at crossover point, whereas the two-layer fabrics have more than one contacting condition since there are two or three different types of weft yarns including the extra yarn in the two-layer structure.

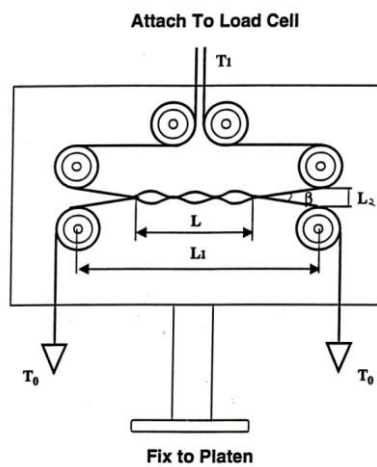


Figure 16 Schematic of the friction coefficient testing device

Table 6 Friction coefficients of single-layer fabrics

| Fabric | 1 | 2 | 3 | 4 | 5 | 6 |
|---|-------|-------|-------|-------|-------|-------|
| Yarn to yarn average dynamic friction coefficient | 0.102 | 0.112 | 0.104 | 0.109 | 0.112 | 0.109 |
| Coefficient of variation | 2.2% | 3.2% | 2.9% | 2.5% | 2.4% | 2.4% |

Table 7 Friction coefficients of two-layer fabrics

| Sample | | Yarn to yarn average dynamic friction coefficient | Coefficient of variation |
|----------|--------------------------|---|--------------------------|
| Sample 1 | Warp yarn to top weft | 0.117 | 3.0% |
| | Warp yarn to bottom weft | 0.116 | 2.9% |
| Sample 2 | Warp yarn to top weft | 0.103 | 2.1% |
| | Warp yarn to bottom weft | 0.103 | 2.2% |
| Sample 3 | Warp yarn to top weft | 0.114 | 1.9% |
| | Warp yarn to bottom weft | 0.116 | 1.7% |
| Sample 4 | Warp yarn to top weft | 0.115 | 1.9% |
| | Warp yarn to bottom weft | 0.114 | 2.0% |
| | Warp yarn to extra weft | 0.111 | 2.1% |
| Sample 5 | Warp yarn to top weft | 0.112 | 2.3% |
| | Warp yarn to bottom weft | 0.112 | 2.9% |
| | Warp yarn to extra weft | 0.109 | 2.9% |

2.3 Modeling Approach

2.3.1 Micro-Mechanical Modeling

The objective of micro-mechanical model is to describe the stress-strain relationship of the yarn and to ultimately obtain what displacements would result from given forces in different directions. The properties of yarn calculated from this stage will be further used in the meso-mechanical modeling.

To begin with, the strain represents the deformation of a body in a certain direction.

Engineering strain, is defined by the following equation.

$$\varepsilon = \frac{L_1 - L_0}{L_0} \quad (3)$$

where L_0 is the body length before deformation, L_1 is the body length after deformation in the same direction. This is the simple definition of engineering strain in the uniform deformation scenario. If the deformation of the body is no longer uniform, the engineering strain can be defined by a more generic form:

$$\varepsilon = \frac{du}{dx} \quad (4)$$

where u is the displacement vector. So this expression can be extended to three orthogonal directions:

$$\begin{aligned} \varepsilon_x &= \frac{\partial u_x}{\partial x} \\ \varepsilon_y &= \frac{\partial u_y}{\partial y} \\ \varepsilon_z &= \frac{\partial u_z}{\partial z} \end{aligned} \quad (5)$$

According to the mechanics of materials, the shear strains are defined in the following equations.

$$\begin{aligned}
\varepsilon_{xy} &= \varepsilon_{yx} = \frac{1}{2} \left(\frac{\partial u_x}{\partial y} + \frac{\partial u_y}{\partial x} \right) \\
\varepsilon_{xz} &= \varepsilon_{zx} = \frac{1}{2} \left(\frac{\partial u_x}{\partial z} + \frac{\partial u_z}{\partial x} \right) \\
\varepsilon_{yz} &= \varepsilon_{zy} = \frac{1}{2} \left(\frac{\partial u_z}{\partial y} + \frac{\partial u_y}{\partial z} \right)
\end{aligned} \tag{6}$$

The deformation at any point in a body can be defined by tensile and shear strain $\varepsilon_x, \varepsilon_y, \varepsilon_z, \varepsilon_{xy}, \varepsilon_{xz}, \varepsilon_{yz}$. The strain occurred in the body would cause the internal force within the body to resist the deformation. This internal force can be expressed by stress. The stress is the internal distribution of force per unit area. The stress is usually calculated as the function of the strain.

$$\sigma = E\varepsilon \tag{7}$$

This function describing the relationship between stress and strain is usually called the material model or constitutive equation, which is what the micro-mechanical model seeks for. If the stress-strain relationship of the material is the same regardless of directions, then it is called isotropic material. The stress-strain relationships in different directions might not be identical for the same body. If so, the material is then named anisotropic material. Typically, the yarn material is an anisotropic material; however, it is not completely anisotropic. The stress response in the cross section plane is isotropic. So the yarn material is considered to be transverse isotropic material. If the material is assumed to be linear elastic, the stress can be defined as a function of strain with 5 constants. The constants are longitudinal modulus E_L , transverse modulus E_T , transverse Poisson's ratio ν_{TT} , transverse-longitudinal Poisson's ratio ν_{TL} and transverse-longitudinal shear modulus G_{TL} . From these 5 constants, the longitudinal-transverse Poisson's ratio ν_{LT} and transverse shear modulus G_{TT} can be calculated by the following equations:

$$V_{LT} = \frac{v_{TL}E_L}{E_T} \quad (8)$$

$$G_{TT} = \frac{E_T}{2(1+v_{TT})} \quad (9)$$

In this case, the stiffness matrix equation of transverse isotropic property can be established assuming that z axis is the yarn path direction and x and y axes are two orthogonal directions perpendicular to the z axis. The overall stiffness matrix can be expressed by the following equation:

$$\begin{bmatrix} \sigma_x \\ \sigma_y \\ \sigma_z \\ \sigma_{xy} \\ \sigma_{yz} \\ \sigma_{zx} \end{bmatrix} = \begin{bmatrix} \frac{E_T(1-v_{TL}v_{LT})}{\Delta} & \frac{E_T(v_{TT}+v_{TL}v_{LT})}{\Delta} & \frac{E_L(v_{TL}+v_{TT}v_{TL})}{\Delta} & 0 & 0 & 0 \\ \frac{E_T(v_{TT}+v_{TL}v_{LT})}{\Delta} & \frac{E_T(1-v_{TL}v_{LT})}{\Delta} & \frac{E_L(v_{TL}+v_{TT}v_{TL})}{\Delta} & 0 & 0 & 0 \\ \frac{E_T(v_{TL}+v_{TT}v_{LT})}{\Delta} & \frac{E_T(v_{TL}+v_{TT}v_{LT})}{\Delta} & \frac{E_L(1-v_{TT}^2)}{\Delta} & 0 & 0 & 0 \\ 0 & 0 & 0 & G_{TT} & 0 & 0 \\ 0 & 0 & 0 & 0 & G_{TL} & 0 \\ 0 & 0 & 0 & 0 & 0 & G_{TL} \end{bmatrix} \begin{bmatrix} \varepsilon_x \\ \varepsilon_y \\ \varepsilon_z \\ \gamma_{xy} \\ \gamma_{yz} \\ \gamma_{zx} \end{bmatrix} \quad (10)$$

$$\Delta = (1 + v_{TT})(1 - v_{TT} - 2v_{TL}v_{LT})$$

However, all the yarns in this research are monofilaments which mean that each yarn is formed evenly by extruding and polyester is uniformly distributed throughout the entire yarn. Therefore it is quite reasonable to assume that the yarn is an isotropic homogeneous material. In order to have a simplified model for the description of mechanical properties of yarn, the isotropic model is defined for the homogeneous yarn. The isotropic mechanical property has only two independent variables (E for modulus and v for Poisson's ratio). The expression of relationship between the stress and strain is simplified from equation (10) to equation (11). The modulus and Poisson's ratio are experimentally measured using universal mechanical testing with a camera device. The data of modulus and Poisson's ratio of each yarn are given in Section 3 experimental part.

$$\begin{bmatrix} \sigma_{xx} \\ \sigma_{yy} \\ \sigma_{zz} \\ \sigma_{yz} \\ \sigma_{zx} \\ \sigma_{xy} \end{bmatrix} = \frac{E}{(1+\nu)(1-2\nu)} \begin{bmatrix} 1-\nu & \nu & \nu & 0 & 0 & 0 \\ \nu & 1-\nu & \nu & 0 & 0 & 0 \\ \nu & \nu & 1-\nu & 0 & 0 & 0 \\ 0 & 0 & 0 & 1-2\nu & 0 & 0 \\ 0 & 0 & 0 & 0 & 1-2\nu & 0 \\ 0 & 0 & 0 & 0 & 0 & 1-2\nu \end{bmatrix} \begin{bmatrix} \varepsilon_{xx} \\ \varepsilon_{yy} \\ \varepsilon_{zz} \\ \varepsilon_{yz} \\ \varepsilon_{zx} \\ \varepsilon_{xy} \end{bmatrix} \quad (11)$$

Usually, a homogenization process is required as the last step in this stage to obtain the overall property of a yarn if the yarn is multifilament assembled by many fibers. However, the overall property of yarn is self-explained by the modulus and Poisson's ratio because the yarn is homogeneous monofilament with isotropic properties.

2.3.2 Meso-Mechanical Modeling

The meso-mechanical modeling stage is to analyze mechanical properties of the unit cell. According to the multi-scale model concept, the behavior of a micro heterogeneous medium can be described by that of an equivalent homogeneous medium with appropriate boundary conditions according to the macroscopic geometry and boundary. In particular, the fabric is a heterogeneous material. However, one can consider fabric structure to be homogeneous material made of identical repeating unit cells which have exactly same properties. In this case, the behavior of fabric structure can be described by repeating unit cell structure with appropriate boundary conditions. The overall fabric's simple deformation behavior such as unidirectional tension and shearing can be retrieved as long as the corresponding mechanical properties of unit cell are calculated. In this research, the tensile properties in longitudinal and transverse direction of unit cells are obtained through FEM in which the geometry of unit cell, modulus and Poisson's ratio are introduced as input data. An appropriate boundary condition is applied onto the unit cell to simulate the real physical conditions over the unit cell and

more importantly to homogenize the mechanical properties throughout the unit cell.

2.3.2.1 3D Solid Modeling of Unit Cell Geometry

3D solid model of a single yarn can be described by its 2D shape of cross section and yarn path, which is similarly defined by an array of nodes of centroids. This kind of modeling is called generative model, which is formed by transformation of a lower dimensional shape to a higher dimensional shape [57].

Consider a cross sectiona shape:

$$z=f_1(x, y), x \in R_1, y \in R_2 \quad (12)$$

And a curve in 3D space:

$$z=f_2(v), v \in R_3 \quad (13)$$

Now the cross sectional shape (12) is translated along the tangent direction of the 3D curve (13) so that the new coordinate z is expressed as function of v for every point $(x, y) \in [R_1, R_2]$ given a v . Then, a 3D solid structure $V(x, y, v)$ may be generated. In particular, the cross sectional shape of a yarn is the generator. This generator can be translated along the centerline curve of the yarn path in order to generate a 3D solid model.

- **Yarn Path Representation**

Adanur and Liao proposed a geometric modeling technique by generative model which can actually generate all sorts of fabric structures such as woven, knitted and braided [8]. However, the yarn path function they used for the description of undulation of yarn is limited to cosine and sine. Cosine and sine functions are probably appropriate to describe undulation of the yarn in simple woven fabric; however, they are no longer precise for the undulation of

warp yarn in the two-layer woven fabric. Therefore, a more accurate yarn path function has to be used to represent the centerline path of the yarn.

The path of a yarn can be considered as one dimensional line representing the yarn's centerline in three dimensional space. Thus, the yarn path can be defined in 3D space as a function of distance along the yarn. The most generic and accurate way to describe such a yarn path is to specify a number of discrete positions along the yarn length, known as master nodes, and have the rest part interpolated [57] between these points rather than to define a certain cosine or sine function which is not precise enough to represent yarn path in this case. Generally speaking, the more master nodes are defined, the more accurate model of the yarn path. In order to get an accurate yarn path model, it is sufficient to specify one or two master nodes per crossover as long as the interpolation function is suitable. The continuity C must be required in the interpolation function so that there is no gap in the yarn path and the tangent of yarn path varies smoothly. A common solution to make sure the continuity and smoothness of the yarn path is to use spline functions. A spline is a function defined piecewise by polynomials. In its most general form a polynomial spline $S : [a, b]$ consists of polynomial pieces $S_i : [t_i, t_{i+1}]$, where

$$a = t_0 < t_1 < \dots < t_{k-2} < t_{k-1} = b \quad (14)$$

That is:

$$S_t = \begin{cases} S_0(t) & t_0 \leq t < t_1 \\ S_1(t) & t_1 \leq t < t_2 \\ & \vdots \\ S_{k-2}(t) & t_{k-1} \leq t < t_{k-2} \end{cases} \quad (15)$$

Since it is impractical to measure so many master nodes along the yarn path, another requirement of this interpolation function is that it can generate the curve of yarn path with the master nodes as little as possible. In this case no extra points need to be defined in order to specify the yarn path. A natural cubic spline function is used for the model of yarn path [57]. A detailed definition of natural cubic spline function is introduced below:

The continuity conditions C^0 , C^1 and C^2 are applied by the equation:

$$S_i(t_i + 1) = S_{i+1}(t_i + 1), \quad 0 \leq i \leq k - 3 \quad (16)$$

$$S_i'(t_i + 1) = S_{i+1}'(t_i + 1), \quad 0 \leq i \leq k - 3 \quad (17)$$

$$S_i''(t_i + 1) = S_{i+1}''(t_i + 1), \quad 0 \leq i \leq k - 3 \quad (18)$$

The boundary conditions at $t = a$ and $t = b$ are given in equation:

$$S'(a) = S'(b) = 0 \quad (19)$$

The derivatives of the spline at the knots can be calculated by solving the matrix equations:

$$\begin{bmatrix} 2 & 1 & 0 & 0 & 0 & 0 \\ 1 & 4 & 1 & 0 & 0 & 0 \\ 0 & 1 & 4 & 1 & 0 & 0 \\ 0 & 0 & \ddots & \ddots & \ddots & 0 \\ & 0 & & 1 & 4 & 1 \\ & & 0 & 0 & 1 & 4 \\ & & & 0 & 0 & 1 \end{bmatrix} \begin{bmatrix} S'(t_0) \\ S'(t_1) \\ S'(t_2) \\ \vdots \\ S'(t_{k-3}) \\ S'(t_{k-2}) \\ S'(t_{k-1}) \end{bmatrix} = \begin{bmatrix} 3(S(t_1) - S(t_0)) \\ 3(S(t_2) - S(t_0)) \\ 3(S(t_3) - S(t_1)) \\ \vdots \\ 3(S(t_{k-2}) - S(t_{k-4})) \\ 3(S(t_{k-1}) - S(t_{k-3})) \\ 3(S(t_{k-1}) - S(t_{k-2})) \end{bmatrix} \quad (20)$$

Once the derivatives are known, the coefficients of the spline pieces can easily be determined.

For each cubic spline piece, there are 4 equations with 4 unknown coefficients a_i , b_i , c_i and d_i :

$$S_i(t_i) = a_i + b_i t_i + c_i t_i^2 + d_i t_i^3 \quad (21)$$

$$S_i(t_i + 1) = a_i + b_i t_{i+1} + c_i t_{i+1}^2 + d_i t_{i+1}^3 \quad (22)$$

$$S_i'(t_i) = b_i + 2c_i t_i + 3d_i t_i^2 \quad (23)$$

$$S_i'(t_i + 1) = b_i + 2c_i t_{i+1} + 3d_i t_{i+1}^2 \quad (24)$$

The natural spline interpolation function also has a very important characteristic of

minimization of the total curvature. Equation 25 is the expression for approximation of the total curvature through the entire domain. The natural spline interpolation method can minimize the value of the total curvature. Since the total energy of elastic strip is proportional to the curvature, it turns out that the natural spline interpolation is actually the approximation of geometry of elastic strip with minimal energy constraint in k knots [57].

$$J(s) = \int_a^b \|S''(t)\|^2 dt \quad (25)$$

- **Yarn Cross Section**

As discussed previously, the 3D solid model of a yarn is generated through the translation of cross section of yarn along its centerline yarn path. Thus, the shape of cross section is critical to determine the 3D solid model of a yarn. The cross section of yarn is defined as the 2D surface cut by plane perpendicular to the yarn path tangent. When it comes to multifilament which is assembled by fibers, the cross section shape would no longer be constant shape and rather difficult to determine. Therefore, the cross section of the multifilament yarn can be assumed to be the smallest region which encompasses all of the fibers within the yarn. The outline of cross sections can be defined using parametric equations in 2 dimensions. Various shapes have been explored including the ellipse proposed by Peirce [13], power ellipse [58] and a modified lenticular shape [59]. All of these cross sections are summarized as follows.

- Ellipse

The elliptical cross-section is one of the simplest approximations. With given width A and height B the equation is defined as follows:

$$\frac{4x^2}{A^2} + \frac{4y^2}{B^2} = 1 \quad (26)$$

$$x(t) = \frac{A}{2} \cos(2\pi t), 0 \leq t \leq 1 \quad (27)$$

$$y(t) = \frac{B}{2} \sin(2\pi t), 0 \leq t \leq 1 \quad (28)$$

- Lenticular

The lenticular cross-section is defined by the intersection part of two circles of radius r_1 and r_2 each of which offsets vertically by distances o_1 and o_2 respectively. The parameters r_1 , r_2 , o_1 and o_2 can be calculated from w , h and distortion d in the following equations (Figure 17):

$$r_1 = \frac{w^2 + (h-2d)^2}{4(h-2d)} \quad (29)$$

$$r_2 = \frac{w^2 + (h+2d)^2}{4(h+2d)} \quad (30)$$

$$o_1 = -r_1 + \frac{h}{2} \quad (31)$$

$$o_2 = r_2 - \frac{h}{2} \quad (32)$$

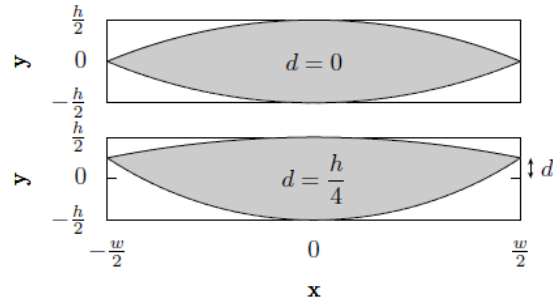


Figure 17 Schematic of lenticular cross sections

The outline of cross-section can be defined as:

$$x(t) = \begin{cases} r_1 \sin(\theta), & 0 \leq t \leq 0.5 \\ r_2 \sin(\theta), & 0.5 \leq t \leq 1 \end{cases} \quad (33)$$

$$y(t) = \begin{cases} r_2 \cos(\theta) + o_1, & 0 \leq t \leq 0.5 \\ -r_2 \cos(\theta) + o_2, & 0.5 \leq t \leq 1 \end{cases} \quad (34)$$

where:

$$\theta = \begin{cases} (1 - 4t)\sin^{-1}\left(\frac{w}{2r_1}\right), & 0 \leq t \leq 0.5 \\ (-3 + 4t)\sin^{-1}\left(\frac{w}{2r_2}\right), & 0.5 \leq t \leq 1 \end{cases} \quad (35)$$

- Power ellipse

The power ellipse is a cross-sectional shape between ellipse and lenticular. The power ellipse is a slight modification to the elliptical cross-section where the y coordinate is assigned a power n to make the section resemble a rectangle with rounded edges when $n < 1$ or a shape similar to a lenticular cross-section when $n > 1$ [57]. It is defined as follows:

$$x(t) = \frac{A}{2} \cos(2\pi t), 0 \leq t \leq 1 \quad (36)$$

$$y(t) = \begin{cases} \frac{B}{2} \sin(2\pi t)^n, & 0 \leq t \leq 0.5 \\ -\frac{B}{2} (-\sin(2\pi t))^n, & 0.5 \leq t \leq 1 \end{cases} \quad (37)$$

- **Specification of Centroids.**

The computer software associated with the microscope device (CellSells Standard 1.8.1 Olympus Corporation) is used in this research to measure the geometry including major and minor radius of each yarn, spacing between top and bottom layer, spacing between warp yarns and spacing between weft yarns as well as configuration. In this case, the spacing is defined as the distance between centroids of cross-sections. Another critical factor for accuracy of 3D solid model is the crimp height at crossover points. Theoretical speaking, crimp of weft yarns for two-layer fabric structure is not developed until heat-setting procedure. Therefore, 3D model is of little practical value without taking into account the crimp of weft yarns. This is another reason to use the generative modeling technique and interpolation method. Two assumptions are made in order to simplify the model without losing much accuracy. First, the cross-section of each yarn is elliptical. Second, there is no

penetration at contact region and yarns contact perfectly at tangent plane to the line crossing two centroids at crossover point.

The number of centerline nodes is determined from the number of weft yarns and warp yarns in one repeating unit. For instance, Figure 9 exhibits the configuration of two-layer fabric sample 2. This two-layer fabric structure has 16 weft yarns in one unit cell. Horizontal number from 1~8 indicates the horizontal position of each weft yarn and vertical number 1, 2 represent for vertical position of each weft yarn. There are at least 10 nodes to be defined for warp yarn in order to smoothly draw the curve of centerline of warp yarn. Likewise, minimum 10 nodes need to be defined along the weft yarn to smoothly draw the weft yarn.

The related variables are defined as follows:

The number of columns of weft yarn in one repeating unit: M

The number of warp yarns in one repeating unit: N

One single warp yarn could be described by a vector:

$$a_i = (a_{i1}, a_{i2}, \dots, a_{i(M+2)}), \quad i \in [1, N] \quad (38)$$

where $a_{ij} = (x_{ij}, y_{ij}, z_{ij})$, $j \in [1, M + 2]$ represents the coordinate of centerline node. Due to the periodic relationship between adjacent warp yarns, the relationship between adjacent warp yarns could be described by the following equation:

$$a_{i+1} = a_i + \vec{p} \quad (39)$$

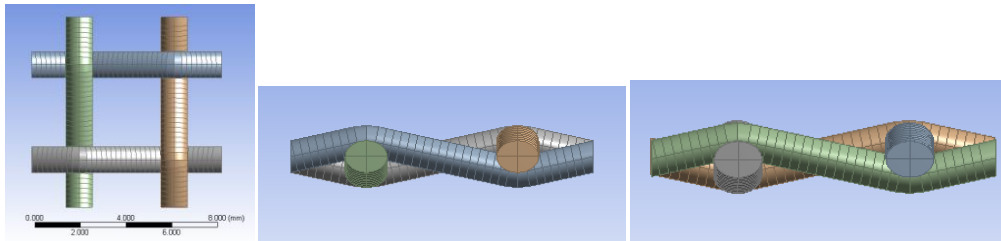
where \vec{p} stands for the periodic vector.

This could be applied to weft yarns:

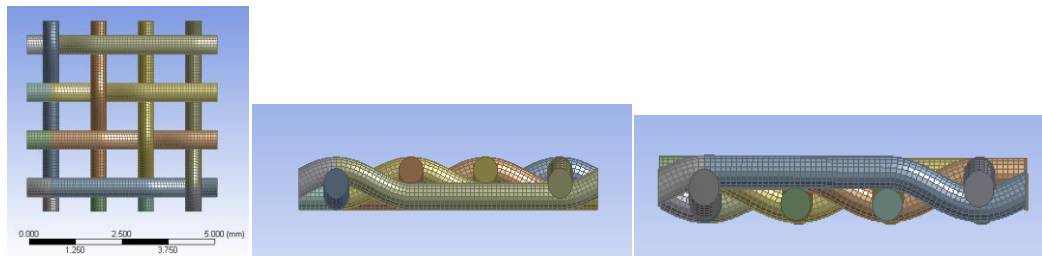
$$b_i = (a_{i1}, a_{i2}, \dots, a_{i(N+2)}), \quad i \in [1, 2M] \quad (2M \text{ means } 2 \text{ weft layers})$$

$$b_{ij} = (x_{ij}, y_{ij}, z_{ij}) \quad j \in [1, N + 2] \quad (40)$$

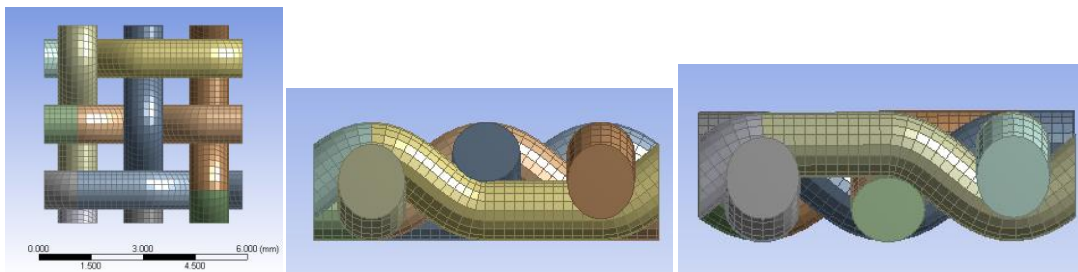
This method could be applied to 3D modeling software such as Solidworks. All configurations of single-layer woven fabrics and two-layer woven fabrics are given in Figure 18.



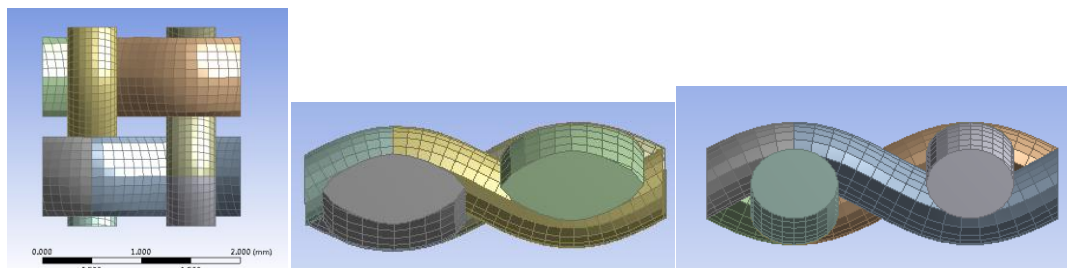
Single-layer fabric sample 1



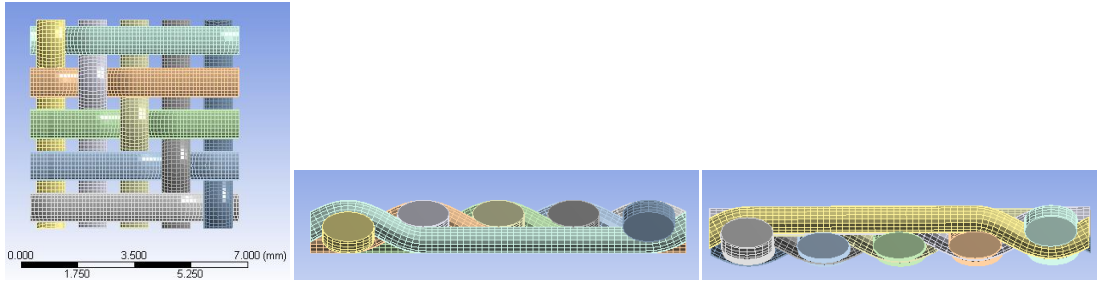
Single-layer fabric sample 2



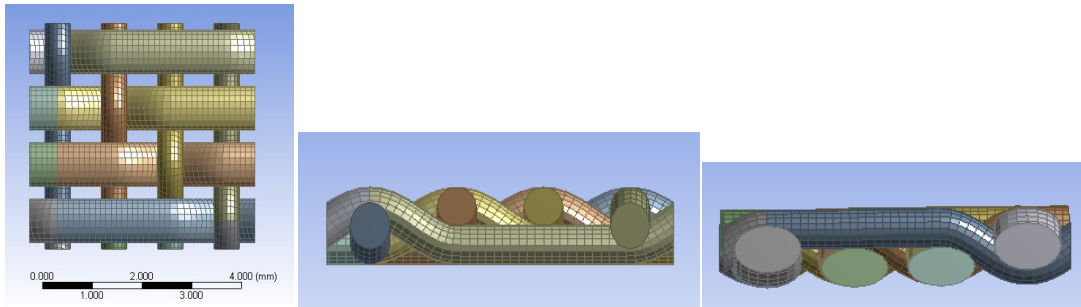
Single-layer fabric sample 3



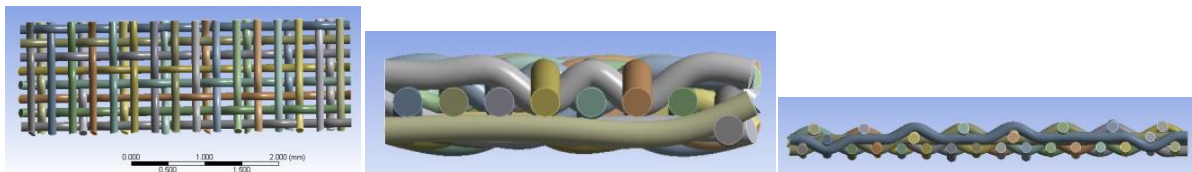
Single-layer fabric sample 4



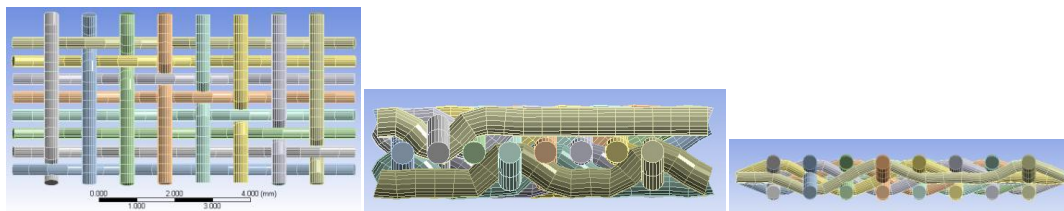
Single-layer fabric sample 5



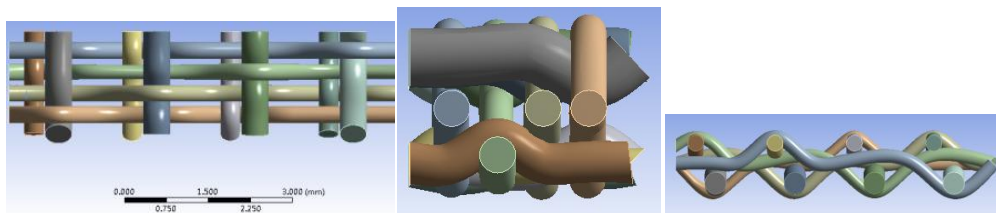
Single-layer fabric sample 6



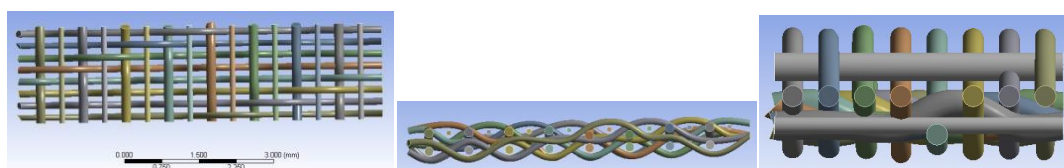
Two-layer fabric sample 1



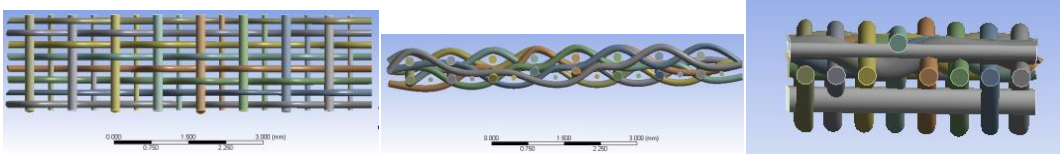
Two-layer fabric sample 2



Two-layer fabric sample 3



Two-layer fabric sample 4



Two-layer fabric sample 5

Figure 18 3D solid model of unit cell of all fabric samples

2.3.2.2 Material Property Definition

The data of modulus and Poisson's ratio are used as inputs retrieved from the micro-mechanical model.

2.3.2.3 Meshing

In order to perform the finite element analyses, the geometry of the fabric must be meshed. The only specific requirement about the mesh is that the cross section mesh at one end must be identical to that at the other end in a unit cell. This is due to the periodicity of the unit cell. The overall fabric is periodically made of repeating units. Hence, the nodes at both cross-sections at the end must be periodically related. The meshes at both cross-section ends have to be identical to ensure that the elements generated from meshing are the same. Figure 19 shows a typical mesh of cross-sections at both ends. This requirement can be achieved by the mapped face mesh with triangle and rectangle elements in Ansysworkbench. The rest of the meshing steps could follow the standard procedure of meshing in Ansysworkbench. Figures 20, 21 and 22 present the coarse, medium and fine mesh of single-layer fabric sample 1 respectively. Table 8 presents the mesh data of coarse, medium and fine mesh.

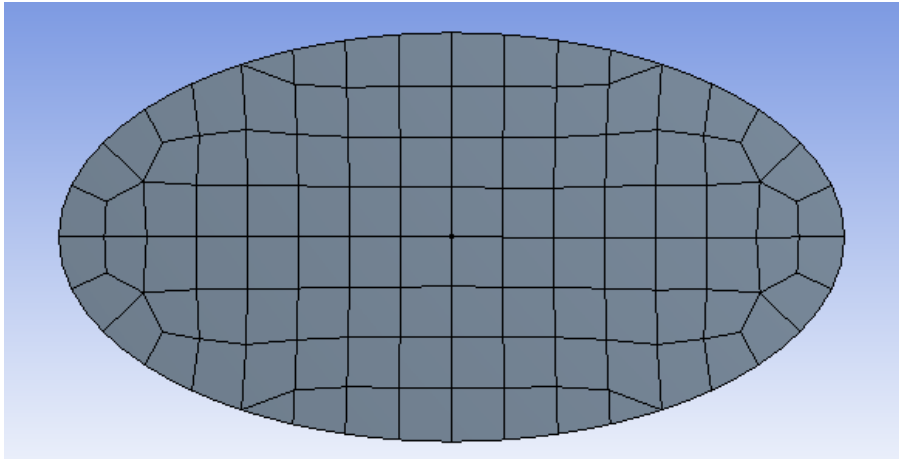


Figure 19 Schematic of the meshing of cross section by triangles and rectangles

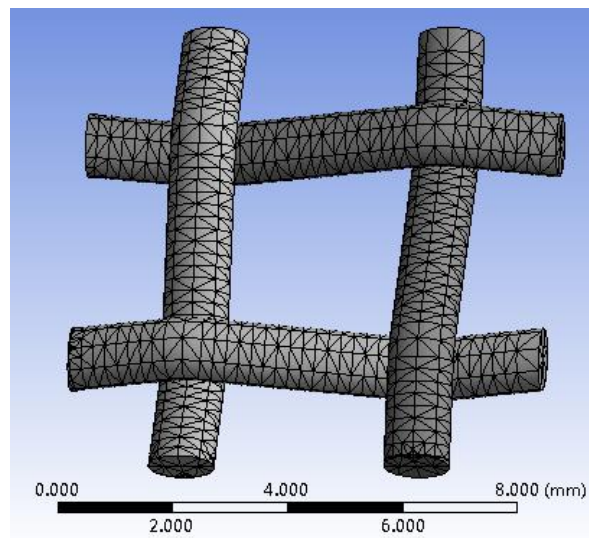


Figure 20 Coarse mesh of unit cell of single-layer fabric sample 1

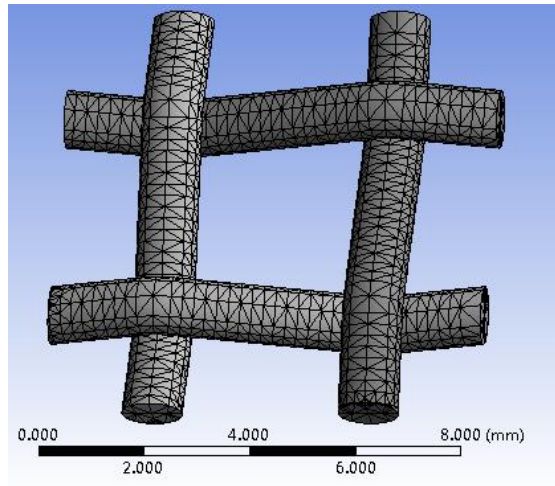


Figure 21 Medium mesh of unit cell of single-layer fabric sample 1

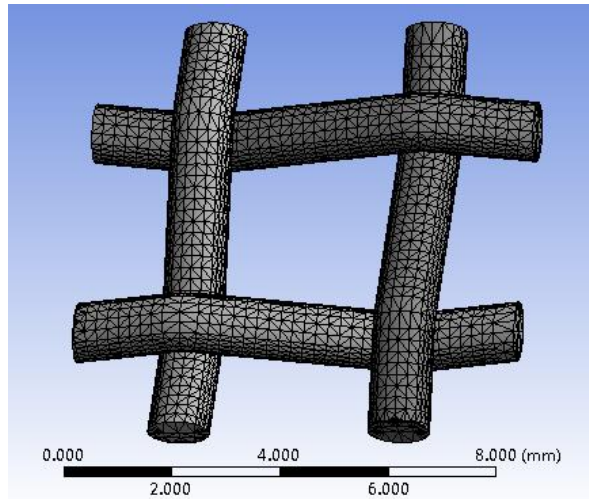


Figure 22 Fine mesh of unit cell of single-layer fabric sample 1

Table 8 Mesh statistics

| | Number of Nodes | Number of elements |
|-------------|-----------------|--------------------|
| Coarse mesh | 8576 | 4152 |
| Medium mesh | 13476 | 6876 |
| Fine mesh | 29943 | 16175 |

2.3.2.4 Contact Definition

- **Contact Pair**

In this case, a surface to surface contact model is used for contact behavior at crossover points. The contact pairs are defined according to the contact algorithm in ANSYS to handle the interpenetration. 3D eight-node surface-to-surface contact elements CONTA174/TARGE170 are used. CONTA174 is an 8-node element that is intended for general rigid-flexible and flexible-flexible contact analysis [60].

In studying the contact between two bodies, the surface of one body is conventionally taken as a contact surface and the surface of the other body as a target surface. For rigid-flexible contact, the contact surface is associated with the deformable body; and the target surface must be the rigid surface. For flexible-flexible contact, both contact and target surfaces are associated with deformable bodies. The contact and target surfaces constitute a "Contact Pair" (Figure 23). The yarn is considered to be flexible body, so flexible-flexible contact is applied.

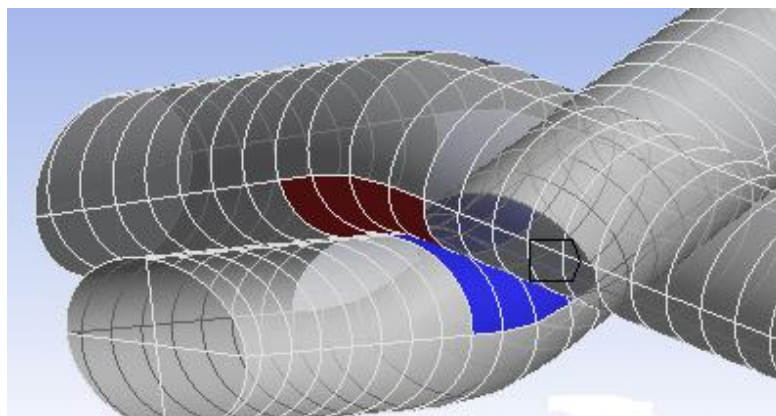


Figure 23 A contact pair

● Frictional Model

In this research, the yarn is considered to be contacted with another yarn at the crossover point and the friction effect between them sustains the stability of interlaced structure. Therefore, a Coulomb friction model is used according to Ansys contact options [60]. In the basic Coulomb friction model, two contacting surfaces can carry shear stresses. When the equivalent shear stress is less than a limit frictional stress (τ_{lim}), no motion occurs between the two surfaces. This state is known as sticking. The Coulomb friction model is defined as:

$$\tau_{lim} = \mu P + b \quad (41)$$

$$\tau \leq \tau_{lim} \quad (42)$$

where:

τ_{lim} = limit frictional stress

τ = equivalent stress for 3D contact

μ = coefficient of friction for isotropic material

P = contact normal pressure

b = contact cohesion

Once the equivalent frictional stress exceeds τ_{lim} , the contact and target surfaces will slide relative to each other. This state is known as sliding. The sticking/sliding calculations determine when a point transitions from sticking to sliding or vice versa. The contact cohesion provides sliding resistance even with zero normal pressure. The contact cohesion is assumed to be zero for the yarn to yarn contact. The friction coefficients in each fabric samples are experimentally measured.

2.3.2.5 Periodic Boundary Conditions

Because the overall fabric is considered to be made of repeatable repeating units or representative volumes, a periodic boundary condition is imposed on the model to ensure symmetry and repeatability of the repeating unit. By applying such boundary conditions, the model is equivalent to an infinitely large fabric undergoing uniform deformation. If a large fabric needs to be modelled with non-uniform deformation as is usually the case, the unit cell model is still useful. A macroscopic model is required which takes effective properties from the unit cell model in a multi-scale modelling approach. Since this research only concentrates on the unidirectional tensile behaviour of fabrics, there is no need to use a well established macroscopic model to calculate the macroscopic behaviour. That is to say, in this particular case, periodic boundary condition serves as the equivalent function of homogenization which calculates the macroscopic response of fabrics.

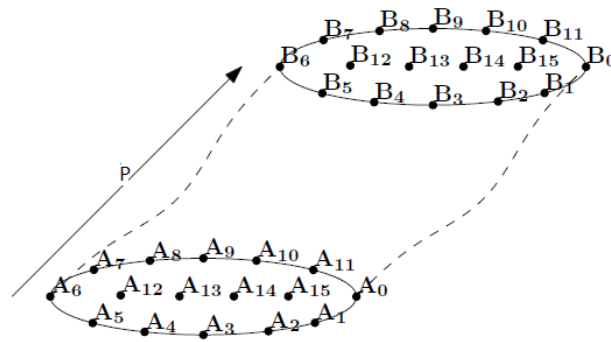


Figure 24 Periodicity of boundary of a yarn [57]

Figure 24 illustrates a section of a periodic yarn, where the yarn is repeatable along the repeat vector P . Nodes A_i and B_i lie on opposite sides of the yarn section. Their positions are initially related by the following equation:

$$B_i = A_i + \vec{P} \quad (43)$$

Where B_i is the coordinates of points on one surface, A_i is the coordinates of points on another surface and \vec{P} is the periodicity vector.

This is a requirement for applying periodic boundary conditions and it is a consideration to be taken into account when the mesh is generated for the yarn.

2.3.2.6 Derivation of Periodic Boundary Conditions

The global constitutive law describes the relation between macroscopic stresses ($\underline{\underline{\delta}}$) and strains ($\underline{\underline{E}}$) which are defined as volumetric averages of the relevant microscopic stresses ($\underline{\underline{\sigma}}$) and strains ($\underline{\underline{\varepsilon}}$) respectively:

$$\underline{\underline{E}} = \frac{1}{V} \int \underline{\underline{\varepsilon}} dV \quad (44)$$

$$\underline{\underline{\delta}} = \frac{1}{V} \int \underline{\underline{\sigma}} dV \quad (45)$$

The microscopic stress and strain fields must fulfill the periodicity of the heterogeneous material [61-62]. This principle can be expressed by the following equation:

$$\underline{\underline{u}}(\underline{\underline{x}}) = \underline{\underline{u}}^0 + \underline{\underline{\Omega}} * \underline{\underline{x}} + \underline{\underline{E}} * \underline{\underline{x}} + \underline{\underline{u}}(\underline{\underline{x}}) \quad (46)$$

where:

$\underline{\underline{u}}^0$ = a rigid displacement of the unit cell

$\underline{\underline{\Omega}}$ = anti-symmetric tensor related to the small rigid rotation of the unit cell

$\underline{\underline{x}}$ = position vector in the RV

$\underline{\underline{u}}$ = periodic part of microscopic displacement field

For the problem of elastic behavior of unit cell, Equation 46 could be further simplified to:

$$\underline{\underline{\Omega}} = 0 \quad (47)$$

$$\underline{\underline{u}}^0 = 0 \quad (48)$$

Then we get:

$$\underline{\underline{E}} * \underline{\underline{x}} = \underline{\underline{u}}(\underline{\underline{x}}) \quad (49)$$

The equation could be further rearranged into [62]:

$$\vec{U}(A + \vec{b}) - \vec{U}(A) = \langle \epsilon \rangle * \vec{b} \quad (50)$$

$$\langle \epsilon \rangle = \begin{bmatrix} \epsilon_x & 0 & 0 \\ 0 & \epsilon_y & 0 \\ 0 & 0 & 0 \end{bmatrix} \quad (51)$$

where $\vec{U}(A + \vec{b})$ and $\vec{U}(A)$ are displacement vector of corresponding nodes on the surfaces of one side and the other, respectively. $\langle \epsilon \rangle$ is average strain tensor applied on the repeating unit, \vec{b} is the periodicity vector. The periodic boundary conditions can be set up by constraint equations in Ansys [60]. Detailed information is given in the following. Equation (50) is a more general form of Equation (49) in mechanical model.

2.3.2.7 Implementation of Boundary Conditions

There two types of boundary conditions defined for the unit cell. The first one is actually the displacement constraints on the edge in order to make the convergence of solution easier. In particular, nodes on the edge have no displacement along the y axis while fabric is subjected to tension along the x axis. This can be achieved by specifying the displacements along the y axis to be zero (Figure 25).

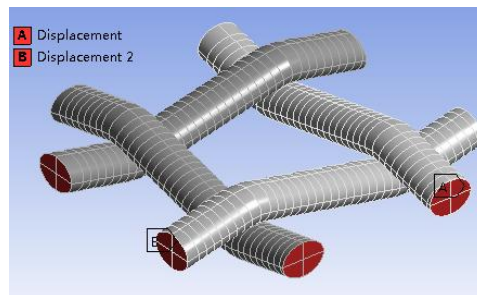


Figure 25 Displacement constraints on the edge

The second one is periodic boundary condition which could be implemented as follows:

$$U_1 - U_2 = \underline{\underline{E}}(X_1 - X_2) \quad (52)$$

$$U_3 - U_4 = \underline{\underline{E}}(X_3 - X_4) \quad (53)$$

where U_1 , U_2 , U_3 , and U_4 are displacement vectors of points on the edges of 1, 2, 3, and 4 respectively (Figure 26). $\underline{\underline{E}}$ stands for macroscopic strain tensor of the fabric

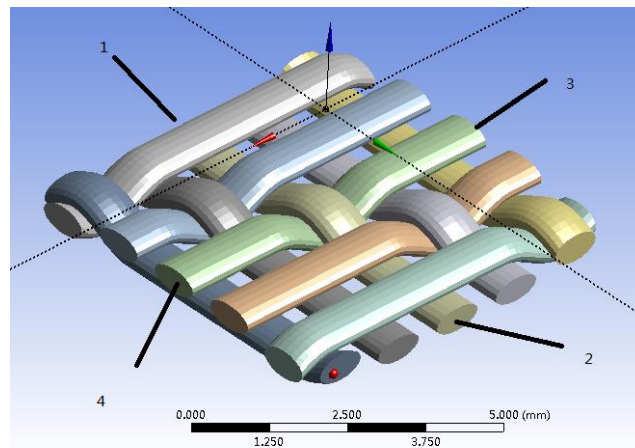


Figure 26 Periodic boundary conditions on the single-layer fabric sample 5

2.3.3 Macro-Mechanical Modeling

As discussed previously, there is no need to apply a specific macro-mechanical model for the calculation of macro-mechanical behavior. The macro-mechanical behavior can be obtained from the meso-mechanical model as long as the boundary conditions are appropriately established. On the macro-scale level, the fabric is considered as homogeneous material which can be described by the constitutive equation between macro strains E and macro-stresses δ :

$$\delta = C * E \quad (54)$$

The aim of macro-mechanical model is to find macro-stiffness matrix C . The solution to this question is actually the homogenization process. The homogenization process is

approached by considering the unit cell of a textile as a repetitive part of an infinite array of identical cells [1, 35, 38 124]. Then the meso-mechanical modeling of unit cell can calculate the stiffness matrix C_c of infinite array of identical cells through the appropriate periodic boundary conditions with given macro strain E . The macro stress can be calculated by volumetric average of microscopic stresses throughout the unit cell.

2.4 Results and Analysis

Figures 27-37 exhibit the contour of stress distribution throughout the unit cell under undeformed state and 10% deformed state in unidirectional tension for single-layer and two-layer fabrics. It is clearly indicated that stress concentration occurred at crossover points. The middle part between the edge and crossover point has less stress concentration than the crossover point. The positions at the crossover points in the fabric structure have the highest possibility to break or deform. Moreover, the translation of stress from weft yarns to warp yarns of single-layer fabrics and warp yarns to weft yarns of two-layer fabrics at the contact region can be observed. The detailed stress distribution indicates that stress from tensile force is translated to the yarns in perpendicular direction through the crossover points. This information could be further used for fracture analysis and ballistic resistance.

Figure 38-48 show the comparison between simulation data and experimental data. Generally speaking, the simulation data agreed well with the experimental data at initial stage, i.e. below 40%~50% of total deformation. However, the variation between simulation and experimental data is continuously increasing with growing deformation. This is probably due to the fact that the solid yarn is going to have plastic deformation at certain point which no longer indicates linear tensile behavior. Another reason is probably the simplification by

using isotropic properties instead of anisotropic properties. However, since this work mainly focuses on the mechanical properties under unidirectional tensile tests, the assumption of isotropic properties does not affect the simulation results much. Isotropic property assumption is a reasonable choice to simplify the model without losing the accuracy in the simulation. There are variations between contact simulations and actual contact conditions, which could also result in the inaccuracy of the model.

The warp direction usually has higher force to extension ratio because the warp yarn has higher modulus than filling yarn. Even though the number of weft yarns is more than the number of warp yarns, the slope of force to extension in warp direction is still higher than the slope in weft direction. The initial modulus dominates unidirectional tensile property.

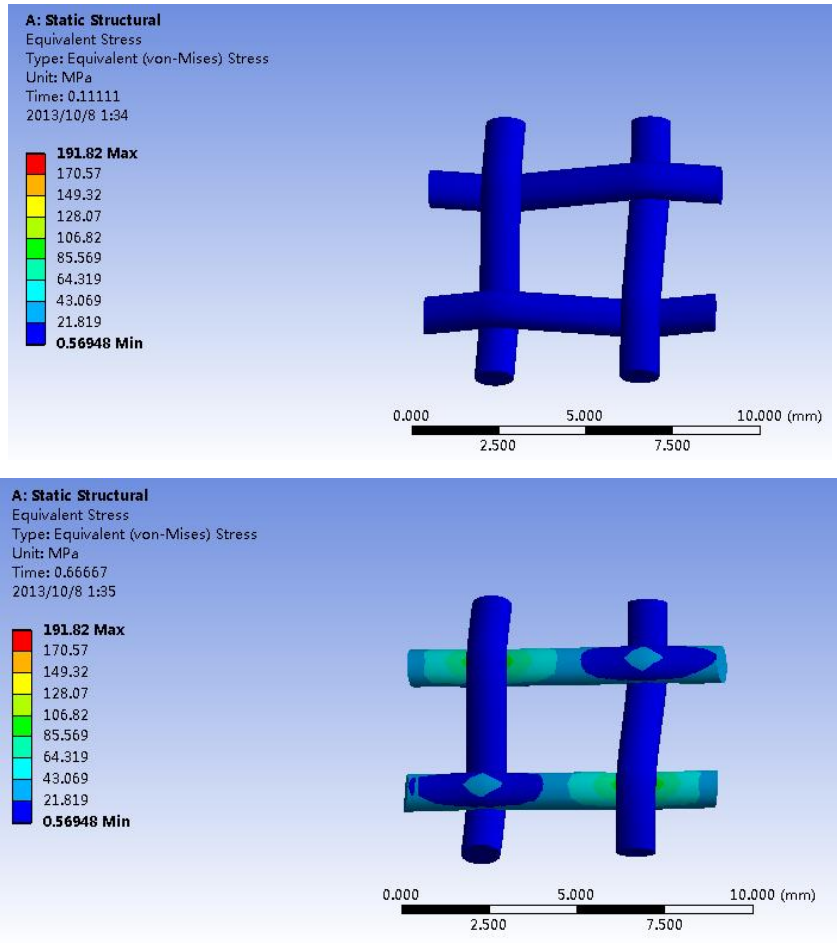


Figure 27 The contour of stress distribution throughout the unit cell of single-layer fabric sample 1 in undeformed state (top) and 10% deformed state (bottom) in the warp direction

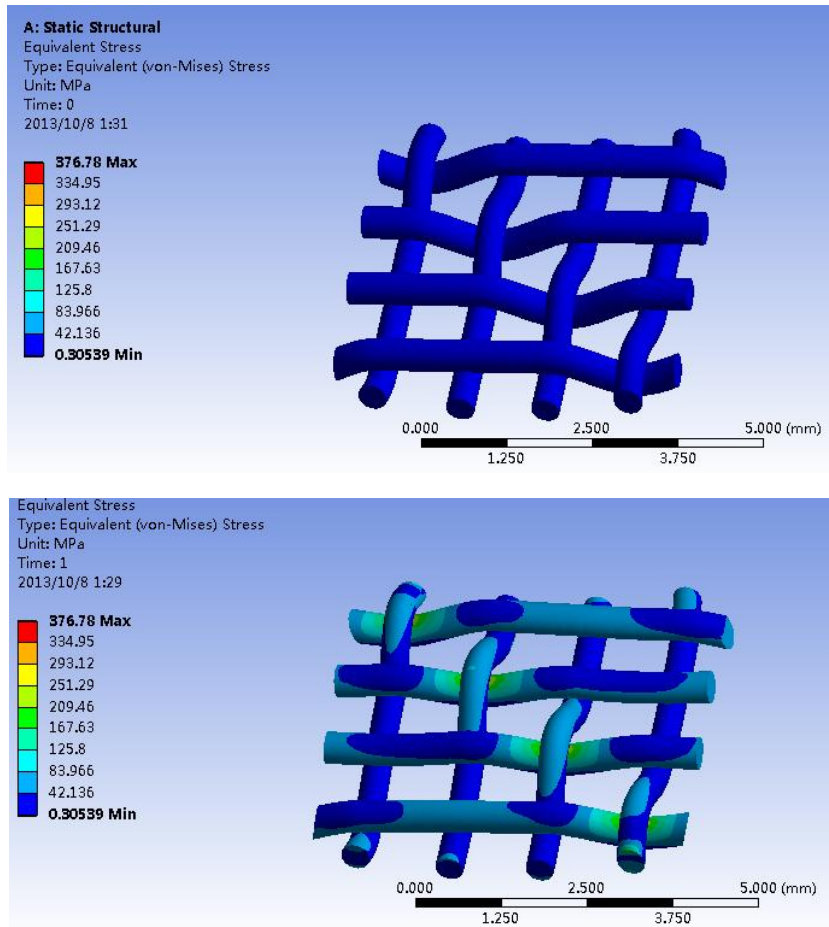


Figure 28 The contour of stress distribution throughout the unit cell of single-layer fabric 2 in undeformed state (top) and 10% deformed state (bottom) in the warp direction

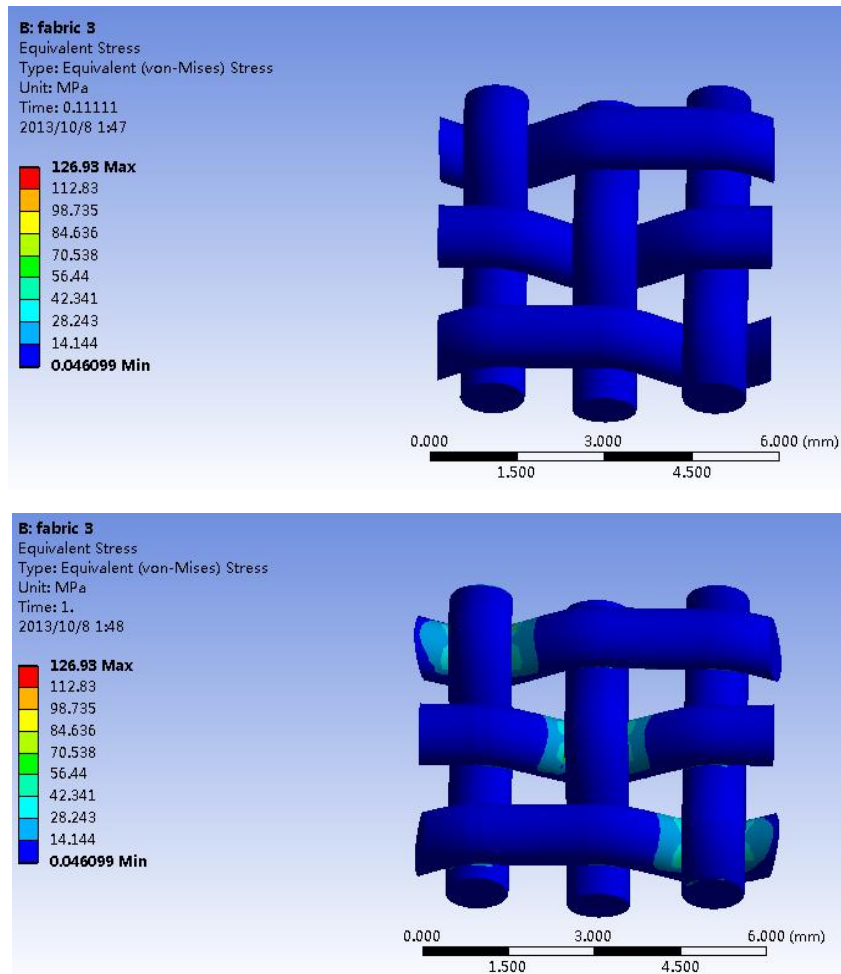


Figure 29 The contour of stress distribution throughout the unit cell of single-layer fabric 3 in undeformed state (top) and 10% deformed state (bottom) in the warp direction

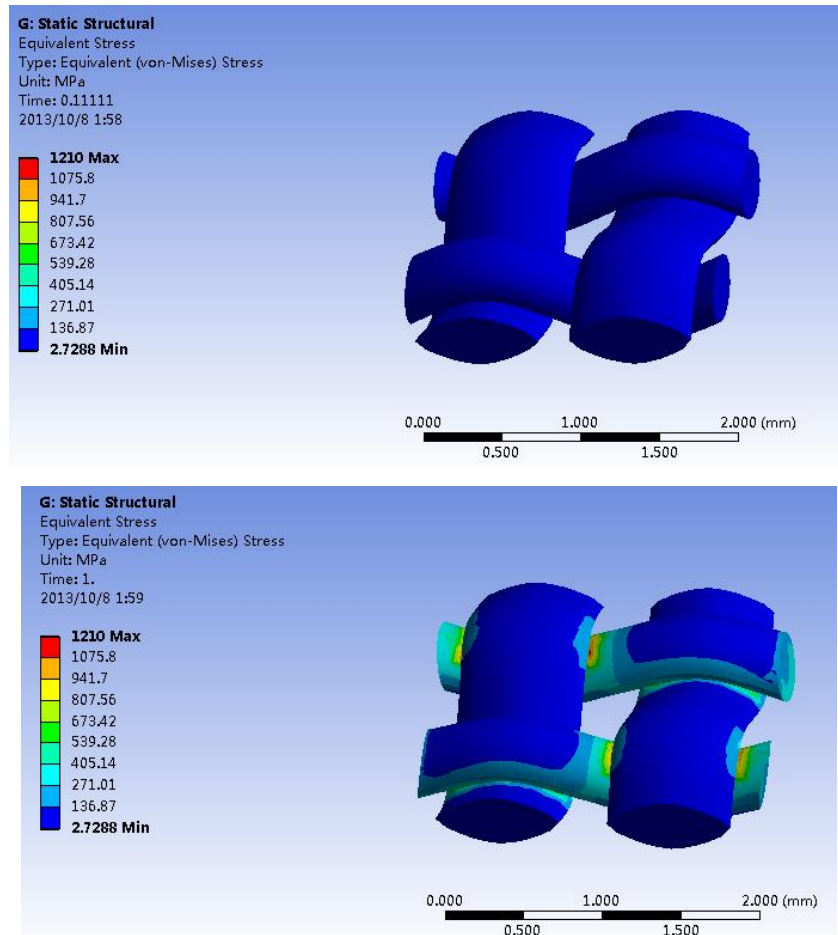


Figure 30 The contour of stress distribution throughout the unit cell of single-layer fabric 4 in undeformed state (top) and 10% deformed state (bottom) in the weft direction

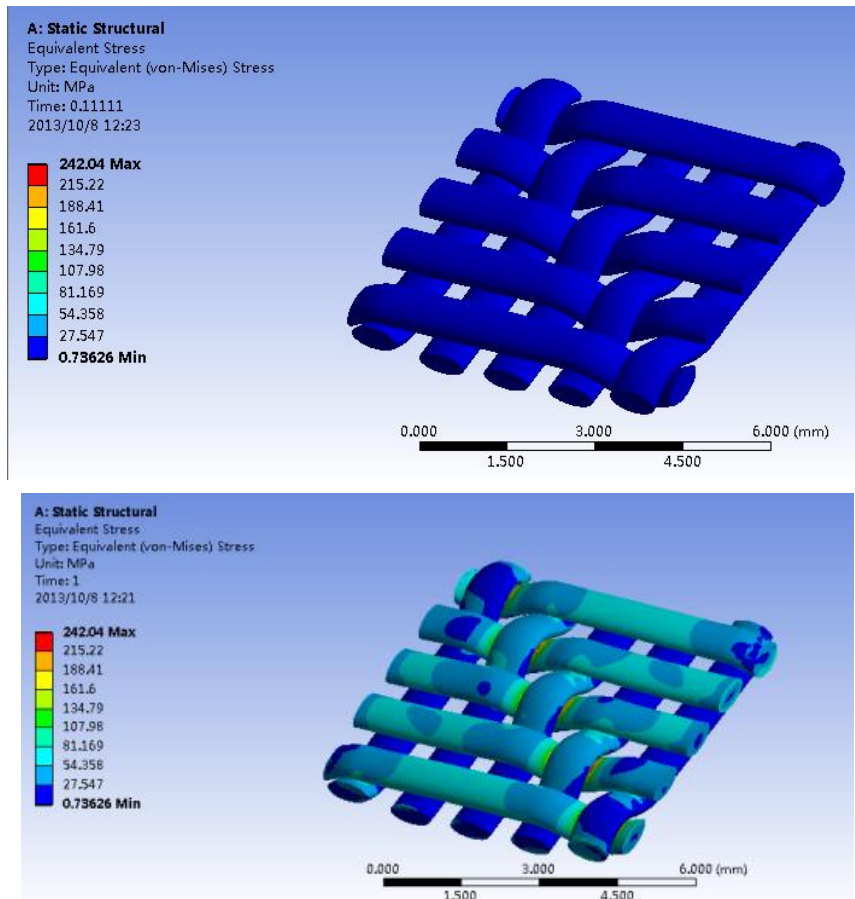


Figure 31 The contour of stress distribution throughout the unit cell of single-layer fabric 5 in undeformed state (top) and 10% deformed state (bottom) in the warp direction

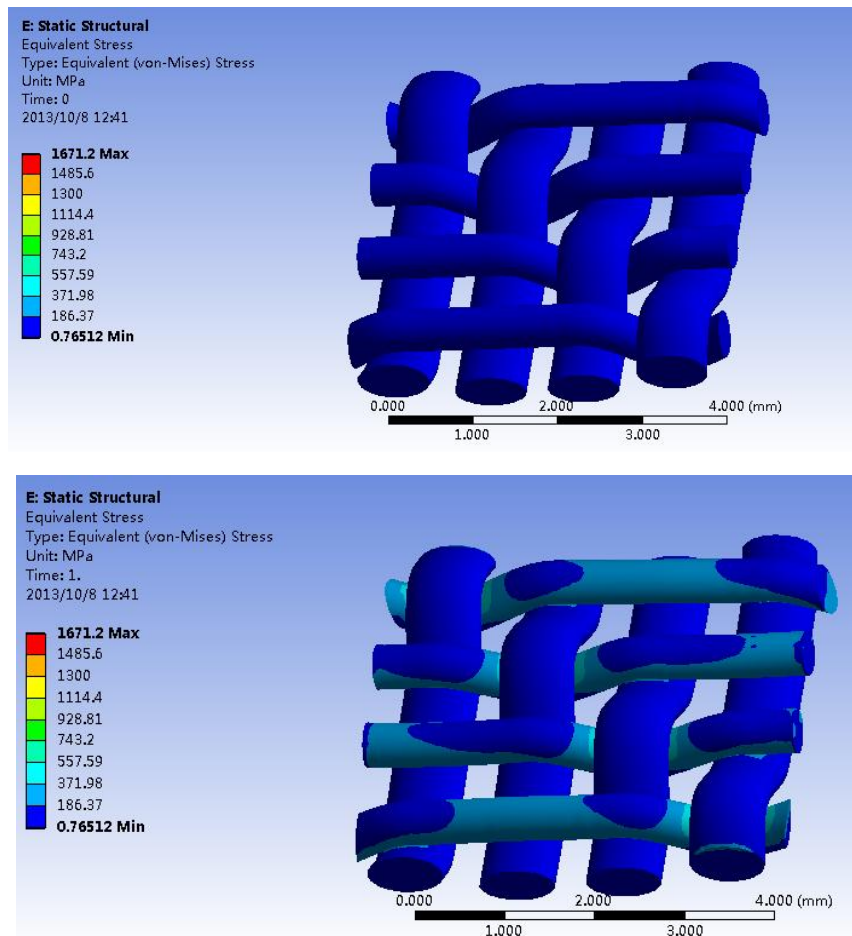


Figure 32 The contour of stress distribution throughout the unit cell of single-layer fabric 6 in undeformed state (top) and 10% deformed state (bottom) in the weft direction

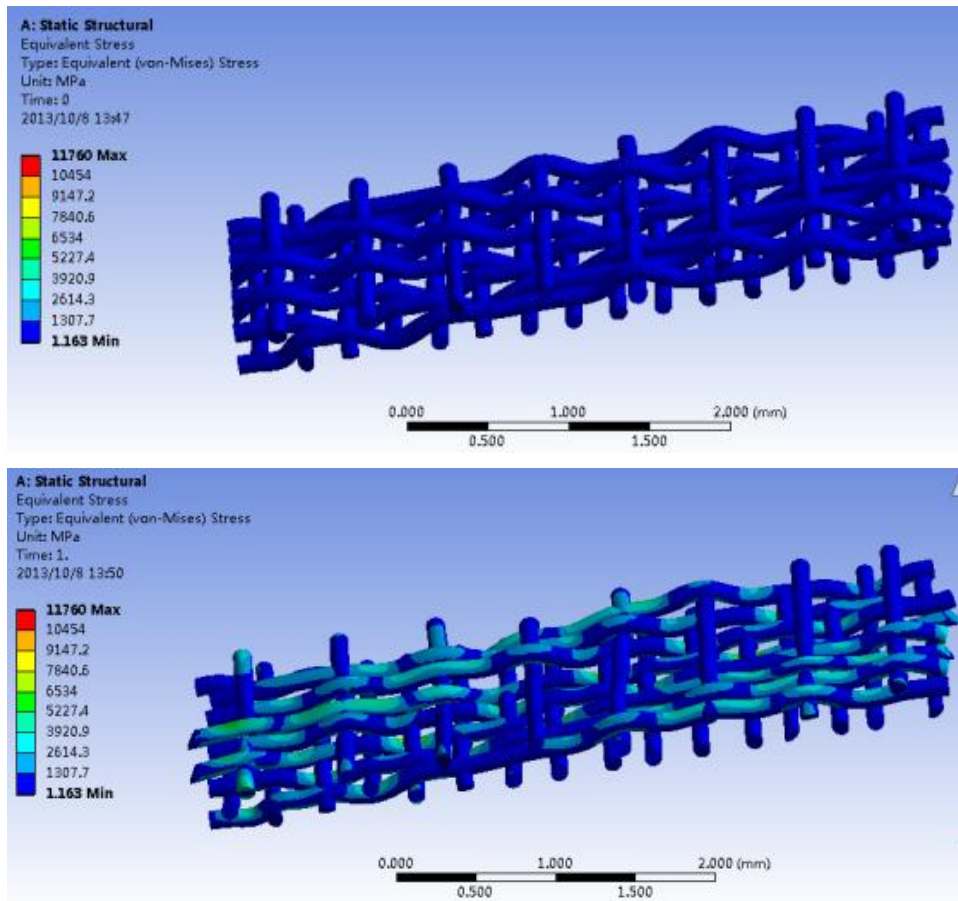


Figure 33 The contour of stress distribution throughout the unit cell of two-layer fabric 1 in undeformed state (top) and 10% deformed state (bottom) warp direction

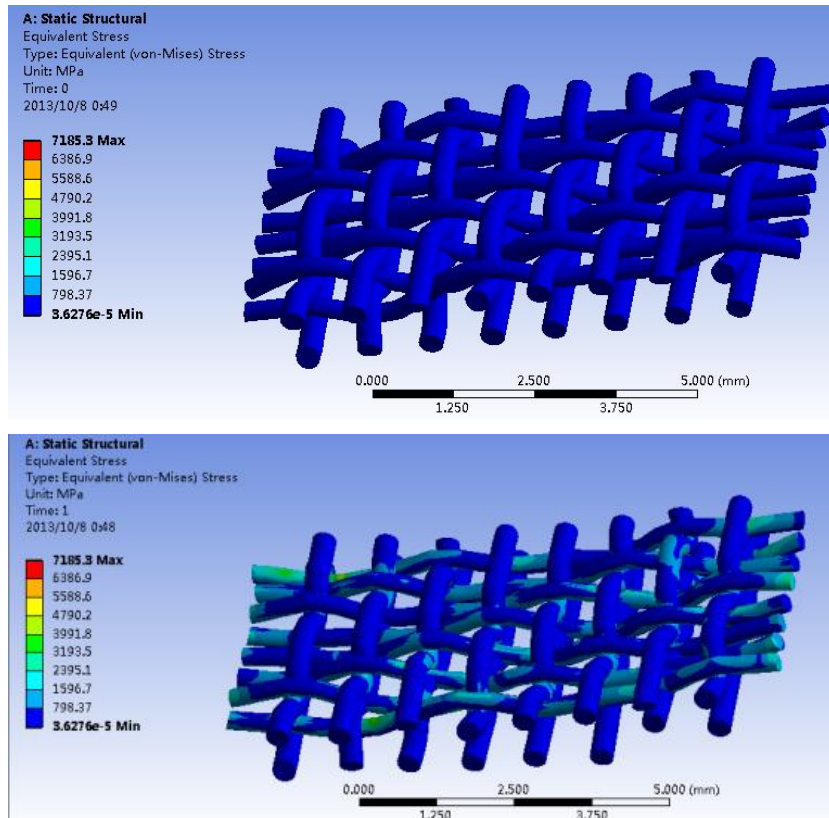


Figure 34 The contour of stress distribution throughout the unit cell of two-layer fabric 2 in undeformed state (top) and 10% deformed state (bottom) warp direction

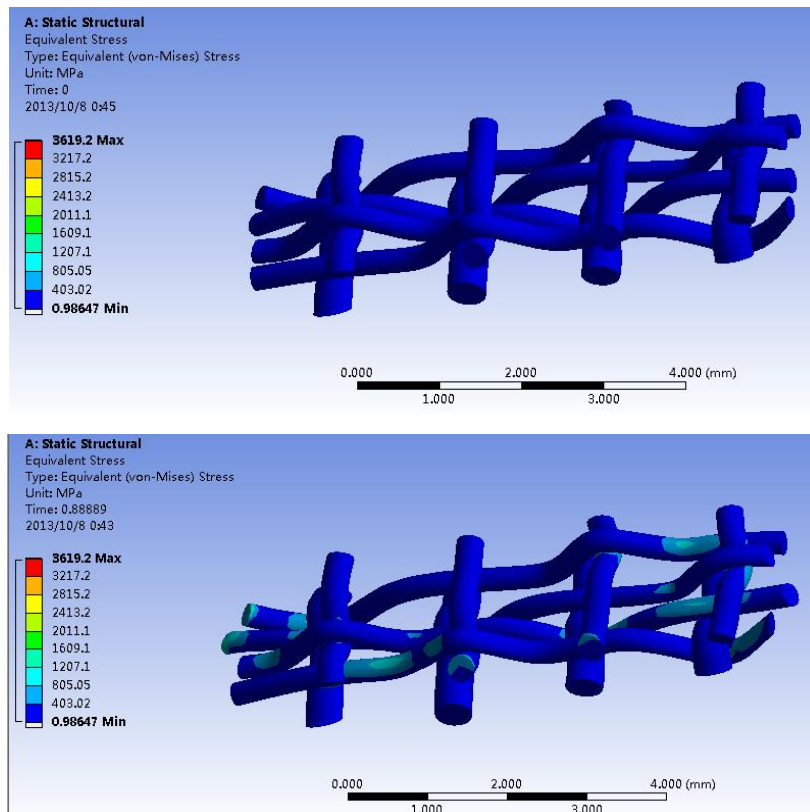


Figure 35 The contour of stress distribution throughout the unit cell of two-layer fabric 3 in undeformed state (top) and 10% deformed state (bottom) warp direction

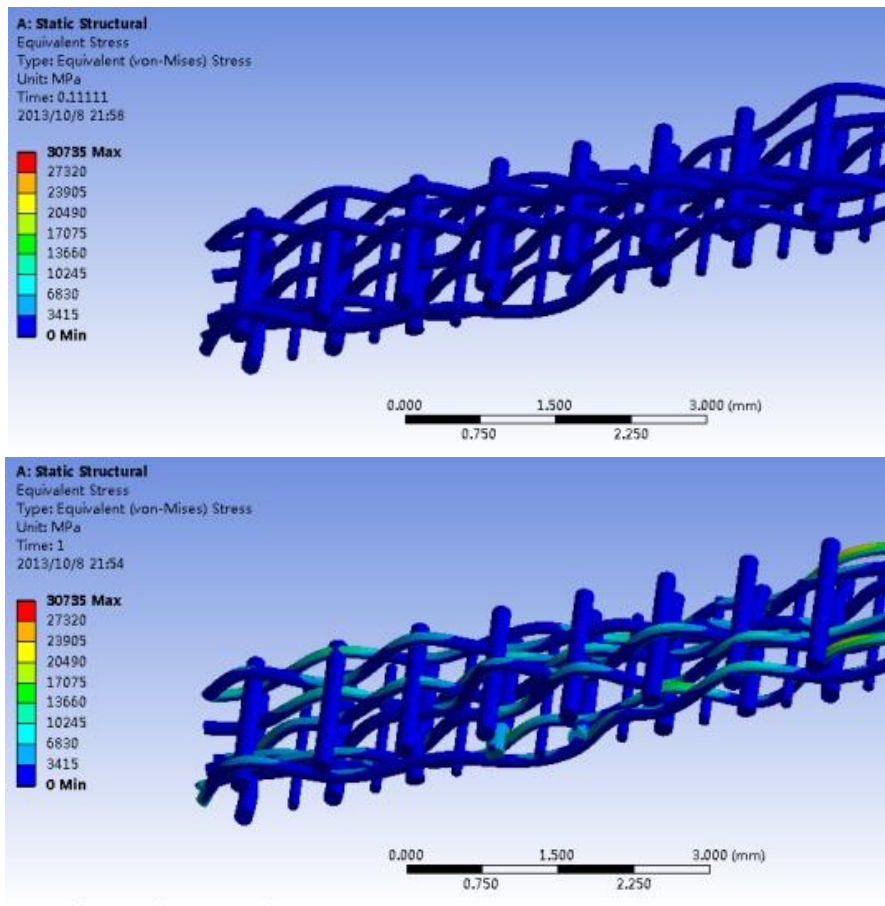


Figure 36 The contour of stress distribution throughout the unit cell of two-layer fabric 4 in undeformed state (top) and 10% deformed state (bottom) warp direction

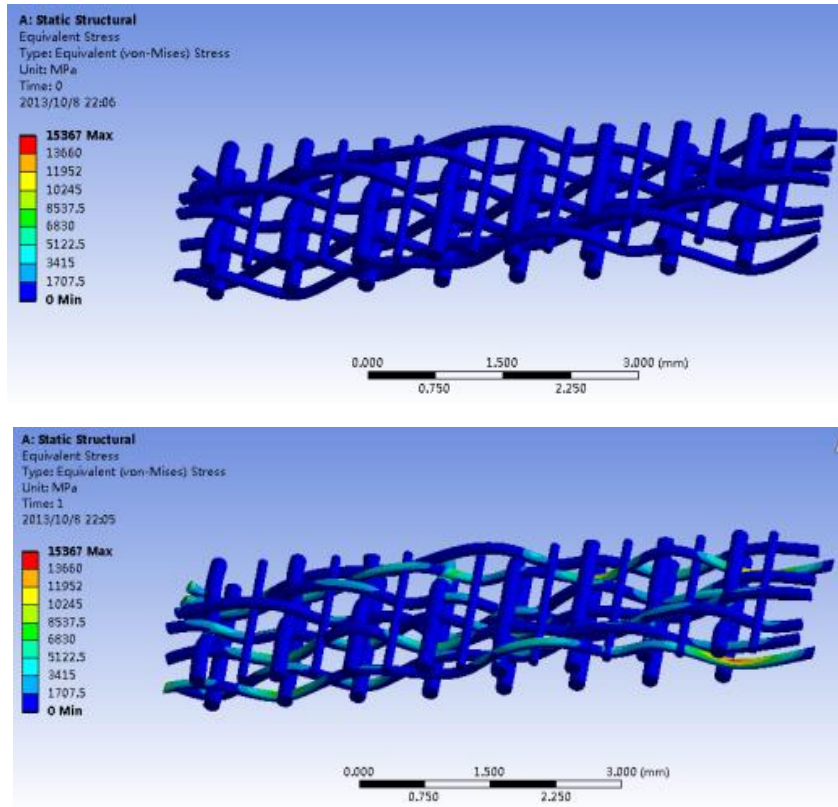


Figure 37 The contour of stress distribution throughout the unit cell of two-layer fabric 5 in undeformed state (top) and 10% deformed state (bottom) warp direction

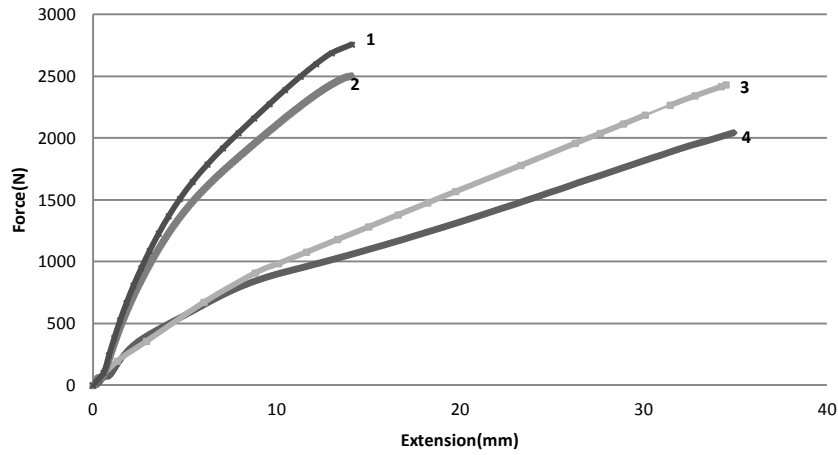


Figure 38 Comparison between experimental data and simulation data of single-layer fabric sample 1 (1: simulation data in warp direction, 2: experimental data for warp direction, 3: simulation data in weft direction, 4: experimental data in weft direction)

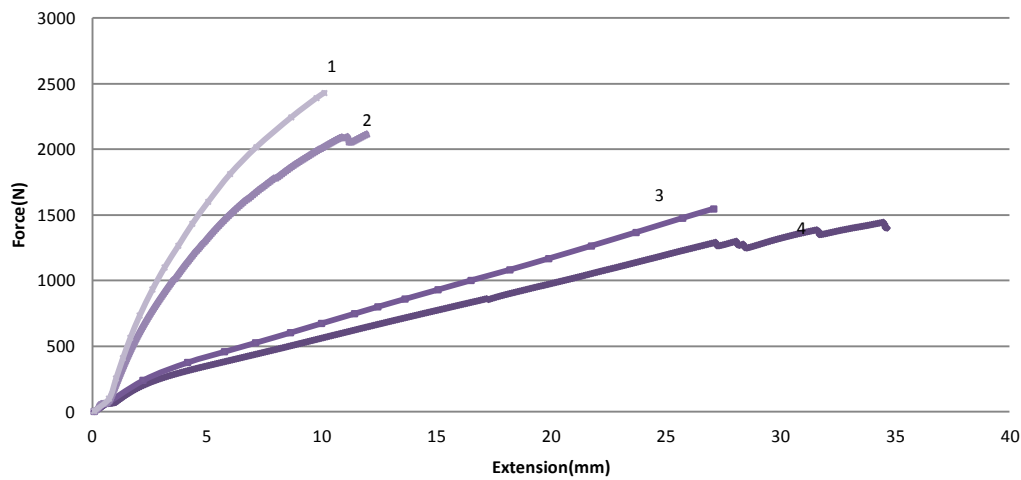


Figure 39 Comparison between experimental data and simulation data of single-layer fabric sample 2 (1: simulation data in warp direction, 2: experimental data for warp direction, 3: simulation data in weft direction, 4: experimental data in weft direction)

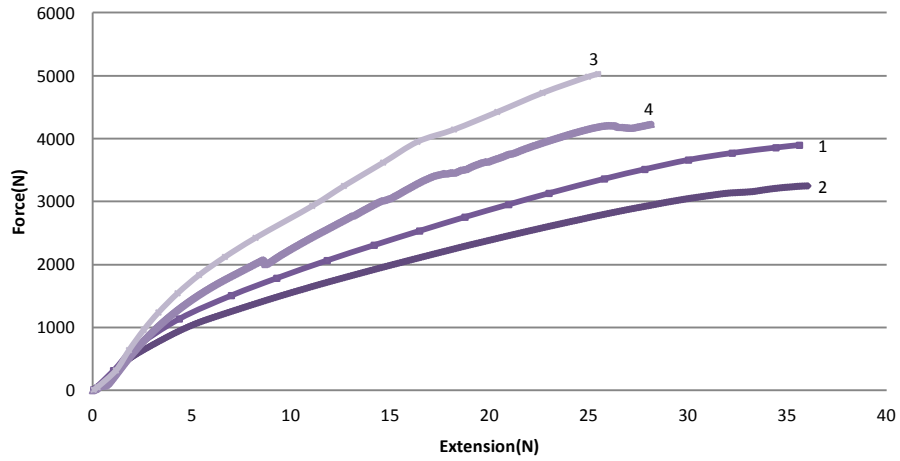


Figure 40 Comparison between experimental data and simulation data of single-layer fabric sample 3 (1: simulation data in warp direction, 2: experimental data for warp direction, 3: simulation data in weft direction, 4: experimental data in weft direction)

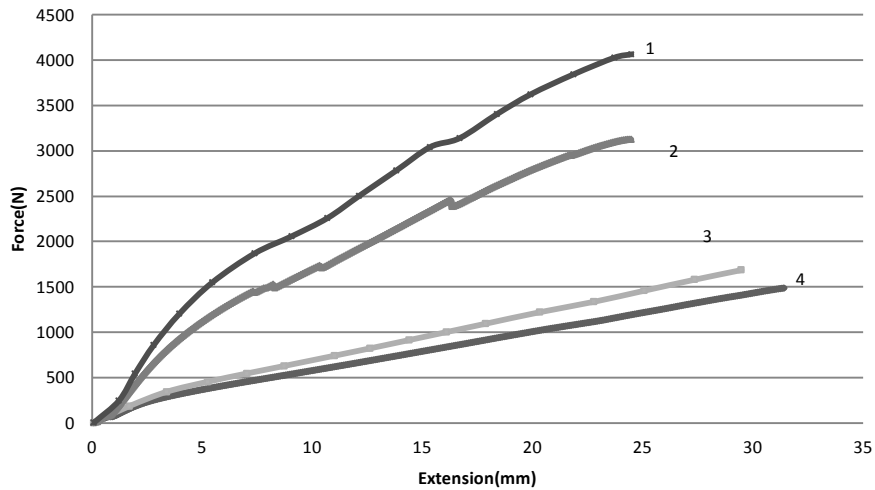


Figure 41 Comparison between experimental data and simulation data of single-layer fabric sample 4 (1: simulation data in warp direction, 2: experimental data for warp direction, 3: simulation data in weft direction, 4: experimental data in weft direction)

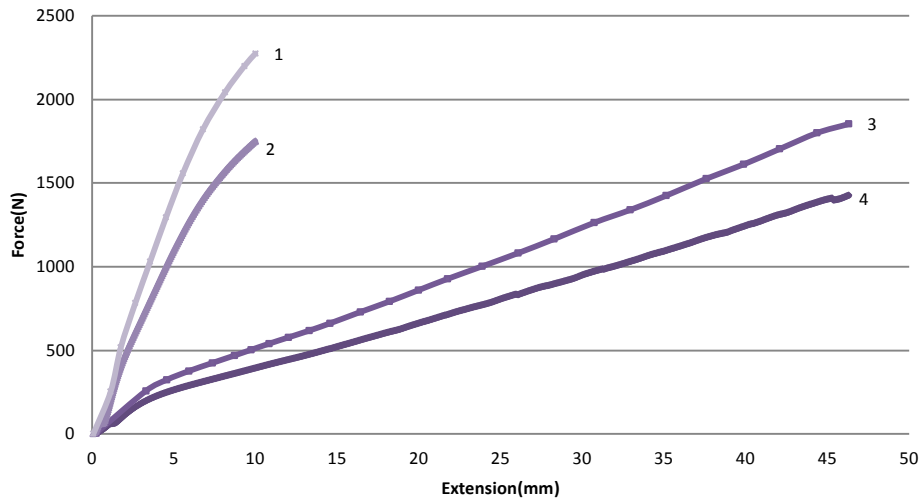


Figure 42 Comparison between experimental data and simulation data of single-layer fabric sample 5 (1: simulation data in warp direction, 2: experimental data for warp direction, 3: simulation data in weft direction, 4: experimental data in weft direction)

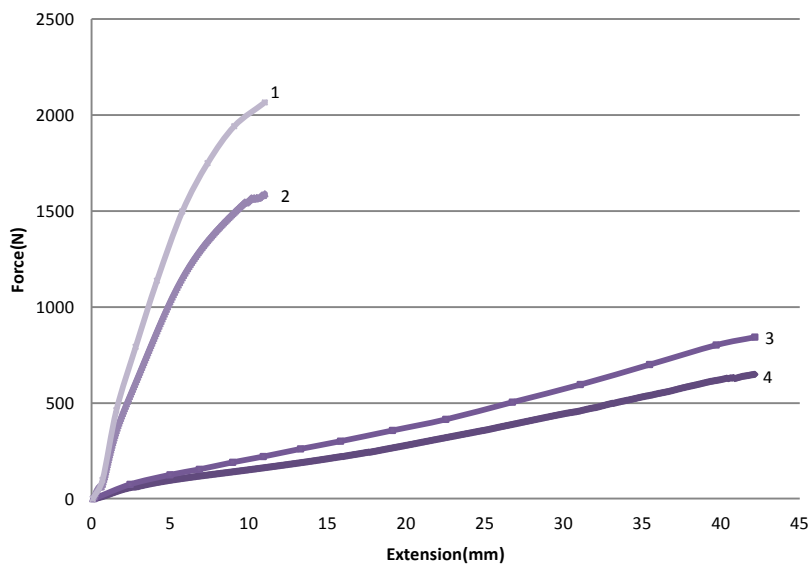


Figure 43 Comparison between experimental data and simulation data of single-layer fabric sample 6 (1: simulation data in warp direction, 2: experimental data for warp direction, 3: simulation data in weft direction, 4: experimental data in weft direction)

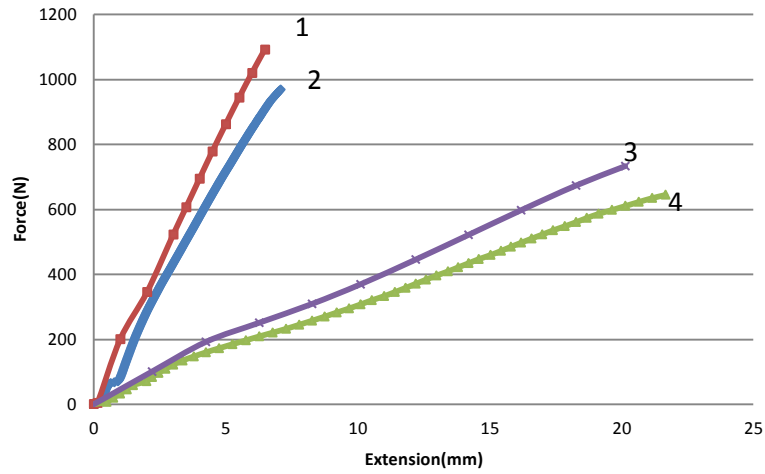


Figure 44 Comparison between experimental data and simulation data of two-layer fabric sample 1 (1: simulation data in warp direction, 2: experimental data for warp direction, 3: simulation data in weft direction, 4: experimental data in weft direction)

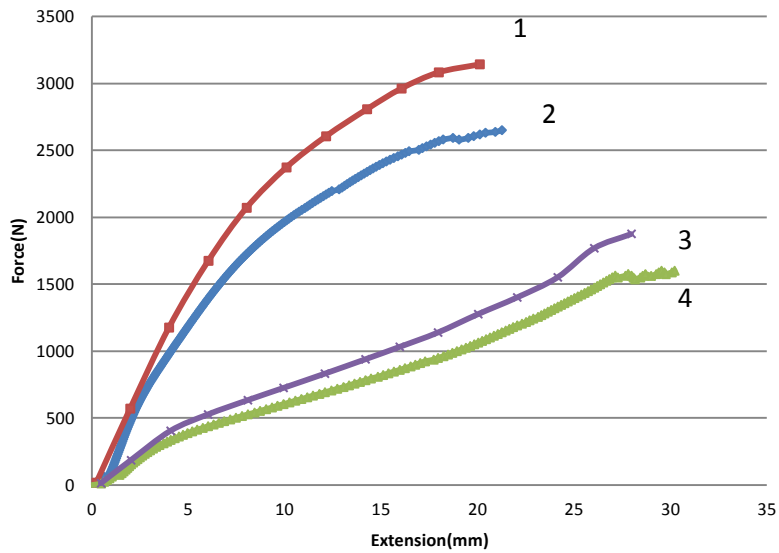


Figure 45 Comparison between experimental data and simulation data of two-layer fabric sample 2 (1: simulation data in warp direction, 2: experimental data for warp direction, 3: simulation data in weft direction, 4: experimental data in weft direction)

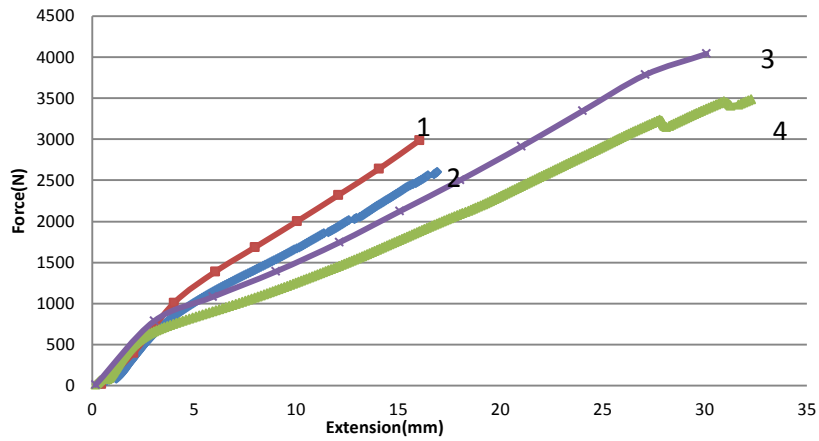


Figure 46 Comparison between experimental data and simulation data of two-layer fabric sample 3 (1: simulation data in warp direction, 2: experimental data for warp direction, 3: simulation data in weft direction, 4: experimental data in weft direction)

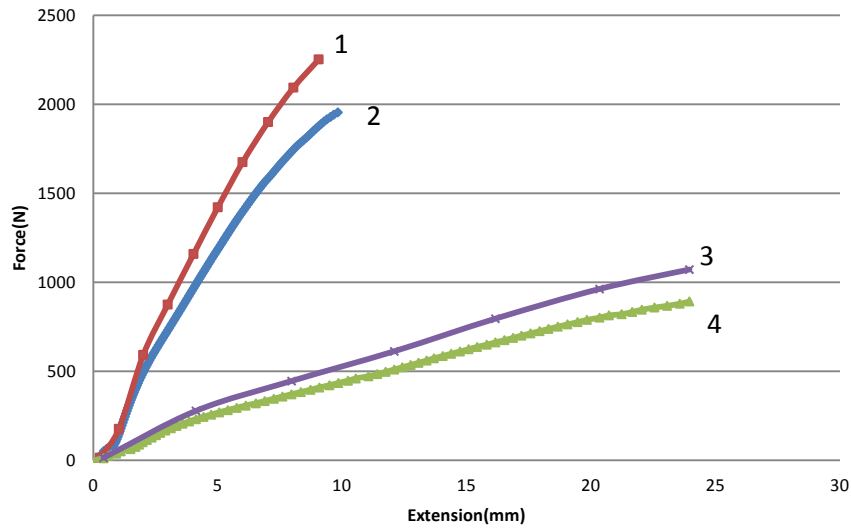


Figure 47 Comparison between experimental data and simulation data of two-layer fabric sample 4 (1: simulation data in warp direction, 2: experimental data for warp direction, 3: simulation data in weft direction, 4: experimental data in weft direction)

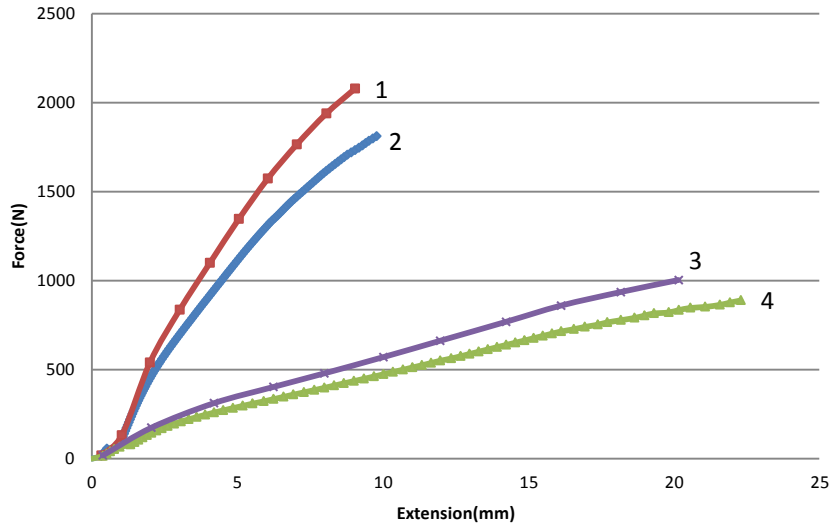


Figure 48 Comparison between experimental data and simulation data of two-layer fabric sample 5 (1: simulation data in warp direction, 2: experimental data for warp direction, 3: simulation data in weft direction, 4: experimental data in weft direction)

2.5 Conclusions

A mechanical model is built to simulate tensile behavior of monofilament woven fabrics. The model is based on the multi-level mechanical theory in which the properties of the yarn and geometry of the repeating unit are taken into account.

A generative model is used to efficiently generate the 3D solid model of woven fabrics. This technique can be further used to all sorts of complex fabric structures.

The simulation data is in reasonably good agreement with the experimental data for all. The variation between experimental data and simulation data probably result from the difference between isotropic material property and an-isotropic material property.

This model is based on FEA and shows the stress-strain field at local points. Stress concentration occurs at crossover points and stress translation takes place at crossover points, which can be further integrated into fatigue and damage analysis of fabrics and fabric reinforced composites.

Chapter 3 Mechanical Analysis of Auxetic Behavior of a Novel Braiding Tubular

Structure by FEM

3.1 Literature Review

Auxetic materials [63, 64] which are materials with negative Poisson's ratio, have received considerable attention over the last three decades because of their counter intuitive mechanical behavior: the auxetic material elongates in the force direction and expands perpendicularly to the force direction simultaneously. This interesting behavior has been studied and found that auxetic property could improve many fundamental bulk properties such as the indentation resistance, the shear modulus, fracture toughness and synclastic curvature [65]. The analysis of auxetic behaviour and exploration of auxetic materials demonstrated that auxetic materials exist in a wide range of fields from natural single crystals [66] and cubic metals [67] to biological materials such as skin [68] and bones [69] and synthetic materials such as foams [70], honeycomb structures [71] and composites [72]. Among all other auxetic materials discovered, synthetic auxetic materials are demonstrated to be very promising since they can be tailored for specific purpose by controlling the structure and properties.

Numerous efforts has been done to scope the fundamental mechanism behind auxetic behavior. The research of crystal arsenic [73] and zeolites [74] drew a conclusion that auxetic behavior attributes to molecular bond rotation. Meanwhile, auxetic fibers demonstrated that they can be woven into technical textiles endowing the auxetic property to the overall structure. Shanahan and Piccirelli [75] fabricated woven fabric which exhibited auxetic behavior as a result of geometric effect by woven structure. Ugbolue et al. [76] invented a

knitted textile structure by carefully knitting the structure resulting in a Poisson's ratio of -0.6 over the fabric width. Hall et al. [77] successfully produced carbon nanotube sheets with an in-plane Poisson's ratio as low as a -0.2 by combination of single and multi-walled carbon nanotubes. Auxetic yarn structure was fabricated by Hook et al. [1] by wrapping a monofilament yarn with higher modulus and smaller diameter onto another yarn with lower modulus and larger diameter. This helical structure of combination of two separate yarns indicated a net increase in the width of the structure when subjected to a tensile load. Miller et al. [78] used helical auxetic yarns in weaving to manufacture a woven fabric made of helical auxetic yarns and tested the respective mechanical properties.

In this research, a tubular fabric structure with auxetic behavior was made by braiding. Moreover, a finite element model of this tubular fabric structure was built for the analysis of auxetic behavior.

3.2 Material Preparation

Two polyester yarns were prepared for the manufacture of helical auxetic yarn. One polyester yarn has much higher modulus and smaller diameter than the other. The auxetic yarn was manufactured on the braiding machine and then helical auxetic yarns were used as yarn component to fabricate the tubular braided structure by braiding.

The modulus of warp yarn and core yarn are tested according to the ASTM D3822 – 07 Monofilament. The data are given in Table 9.

Table 9 Mechanical properties of wrap and core yarns as component of the helical auxetic yarn

| | Core | Wrap |
|-------------------------|------|------|
| Young's modulus (MPa) | 13 | 1360 |
| Ultimate strength (MPa) | 31 | 650 |
| Strain at break (%) | 88 | 6.2 |

3.3 Approach

The auxetic yarn is manufactured on braiding machine. The core yarn is inserted in the system taking place of the position of mandrel in the middle of the braiding machine. The core yarn is stationary. The wrap is wrapped onto the core yarn with spindle. An illustration of the manufacture process is given in Figure 49. Figure 50 presents one spindle rotating in the trajectory. Figure 51 shows the braiding machine used.

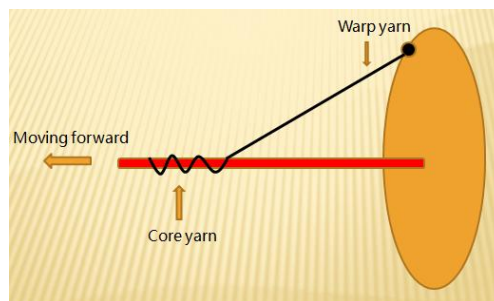


Figure 49 Schematic of manufacture of helical auxetic yarn

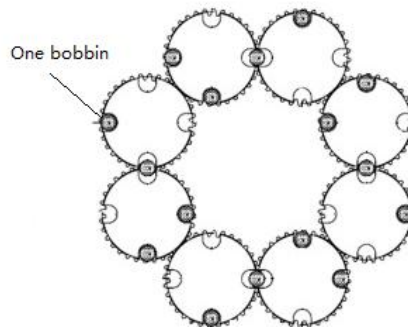


Figure 50 The cross sectional view of rotating surface

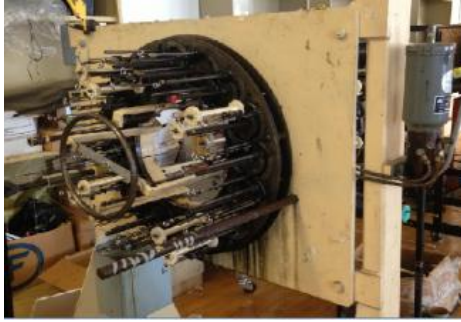


Figure 51 The braiding machine used

The geometry of helical auxetic yarn is analyzed by microscope. According to the manufacture process of helical auxetic yarn, the diameter of core and wrap yarns (D_c and D_w), the starting angle (α) and pitch (L) are three important parameters determining the geometry (Figure 52 and 53). The data are given in Table 10.

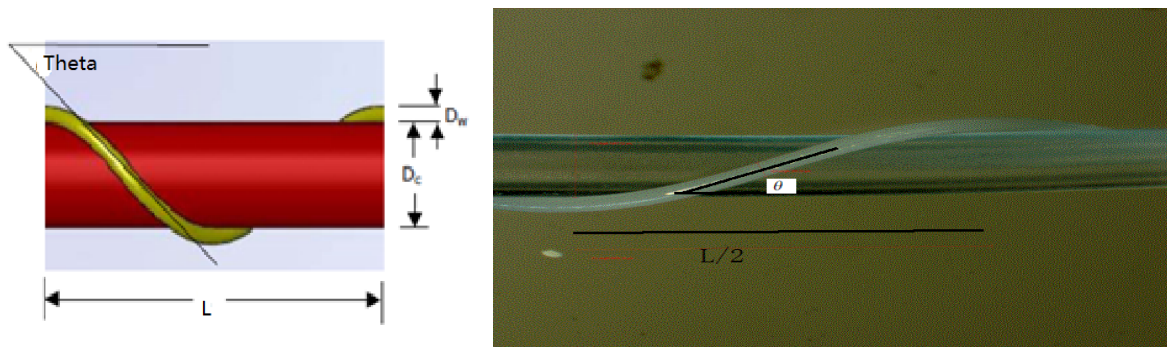


Figure 52 Geometry of a helical auxetic yarn

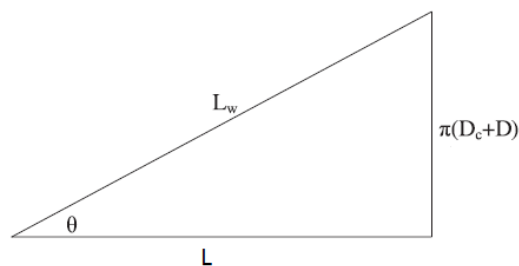


Figure 53 Geometrical parameters

Each geometric parameter is correlated by the following equations:

$$L = \frac{\pi(D_w + D_c)}{\tan\theta} \quad (55)$$

$$A_c = \frac{\pi D_c^2}{4} \quad (56)$$

$$A_w = \frac{\pi D_w^2}{4 \cos \theta} \quad (57)$$

$$A = A_c + A_w \quad (58)$$

A_c and A_w are the cross sectional area of core yarn and wrap yarn in helical auxetic structure.

Table 10 Geometric parameters for the auxetic yarn

| | |
|-----------------------------|---------|
| Core diameter (D_c) | 1.32 mm |
| Warp diameter (D_w) | 0.27 mm |
| Starting angle (θ) | 17.4° |
| Pitch (L) | 13.2mm |

Then, the biaxial tubular structure was fabricated on the braiding where 8 spindles of helical auxetic yarns were used. A mandrel was used in the core, around which 8 spindles of auxetic yarns are rotating. Figure 54 illustrates the geometric structure of the biaxial tubular structure. Figure 55 presents the picture of biaxial tubular structure.

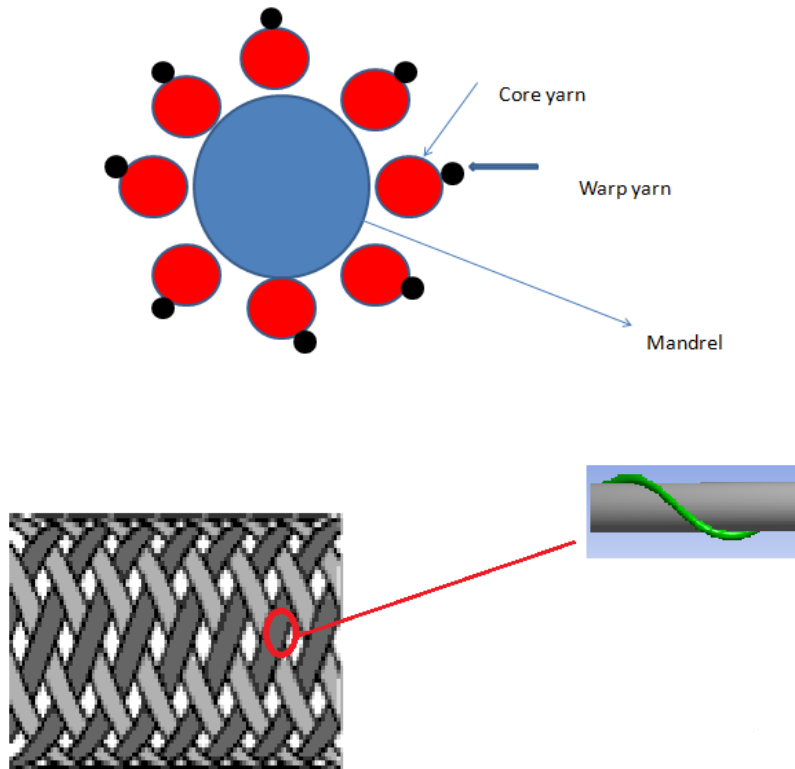


Figure 54 Schematic of the biaxial tubular structure

The geometry information of the biaxial tubular structure is given in Table 11.

Table 11 Geometry of the biaxial tubular structure

| | |
|-----------------------|-------|
| Starting angle | 47° |
| Pitch (mm) | 31.45 |
| Mandrel diameter (mm) | 10.75 |

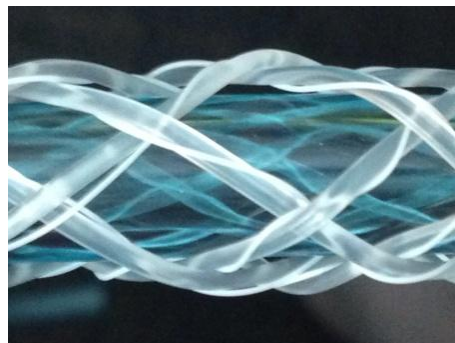


Figure 55 The biaxial tubular structure

3.4 Analysis of the Properties by FEM

The original purpose of the biaxial tubular fabric was to fabricate a novel 3D structure with variable permeability on the surface. This characteristic is achieved through the auxetic behavior of auxetic yarns in the biaxial tubular structure. Theoretically speaking, the increase of width of auxetic yarns in the structure would change the open area on the surface leading to variable permeability. The permeability can be quantified by measurement of open area on the surface under different longitudinal strain. The area of open surface can be measured by the universal mechanical test machine associated with a camera device while the biaxial structure is subjected to tensile loading. Then the curve of the open surface area versus longitudinal strain can be drawn according to the experimental data. The FEM model of the biaxial tubular structure is built to calculate the open surface area under different longitudinal strain. The results were validated by comparing the experimental data and simulation data.

The objective of FEM model of biaxial tubular structure is to obtain the open surface area as a function of longitudinal strain. The change of the open surface area is due to three parameters: the Poisson's ratio of helical auxetic yarn, the edge length of unit cell and the angle between the two cross yarns.

3.4.1 Micro-Mechanical Model

The micro-mechanical model of biaxial tubular structure is to simulate the mechanical properties of the helical auxetic yarn. An FEM model of the auxetic yarn is established. The 3D solid geometry model is made according to the geometric data experimentally measured. The same generative modeling technique in Chapter 2 is employed here for the 3D construction of the helical auxetic yarn. Figure 56 shows the 3D solid geometry of the helical

auxetic yarn.

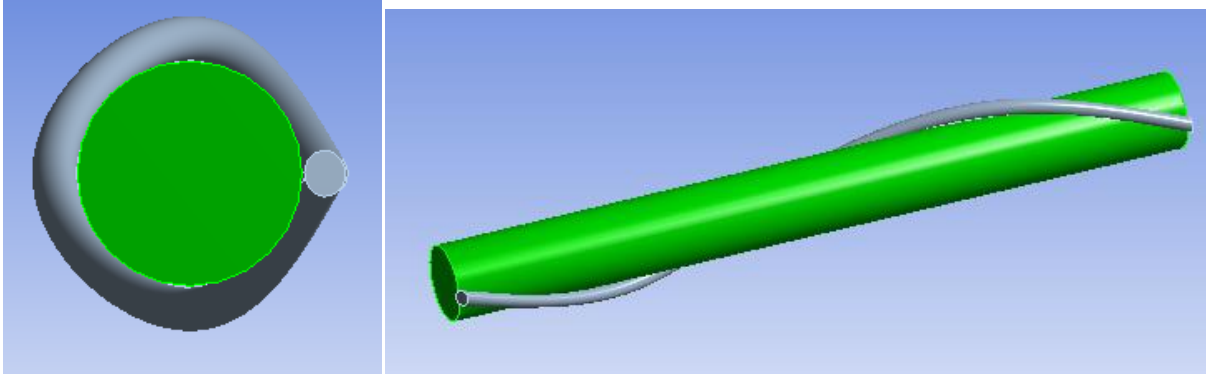


Figure 56 3D solid model of the helical auxetic yarn

The material is defined as isotropic material. The boundary conditions to simulate the tensile test are derived from the compatibility of equations on the two ends. The boundary conditions are given in the following equations.

$$U_{ac}=U_{aw}=U \quad (59)$$

$$U_{bc}=U_{bw}=-U \quad (60)$$

where U is the prescribed displacement which can be defined in an incremental form.

The FEM model is established such that the stress σ is determined with strain U prescribed. Then the stress-strain curve of auxetic yarn can be obtained and validated by comparison with experimental data.

The implementation of boundary conditions is illustrated in Figure 57. Figure 58 shows the contour of stress distribution of helical auxetic yarn before and after the deformation. The simulation and experimental data are exhibited in Figure 59. The simulation data is fit quite well with the experimental data below the strain point at around 0.05. The inaccuracy of simulation data increased probably due to the plastic deformation and the rough contact algorithm.

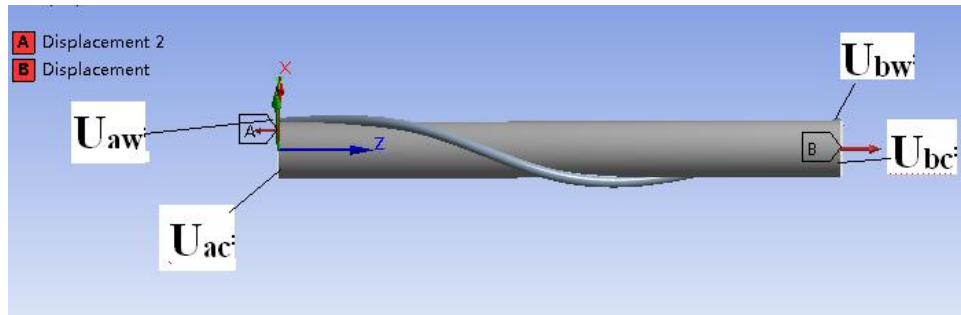


Figure 57 Application of boundary conditions

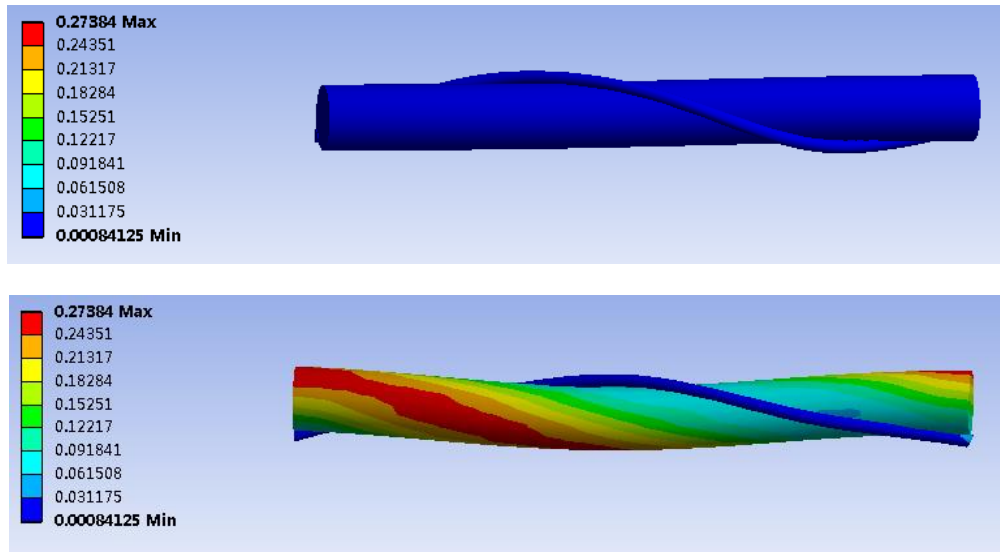


Figure 58 The contour of stress distribution before (up) and after (down) deformation

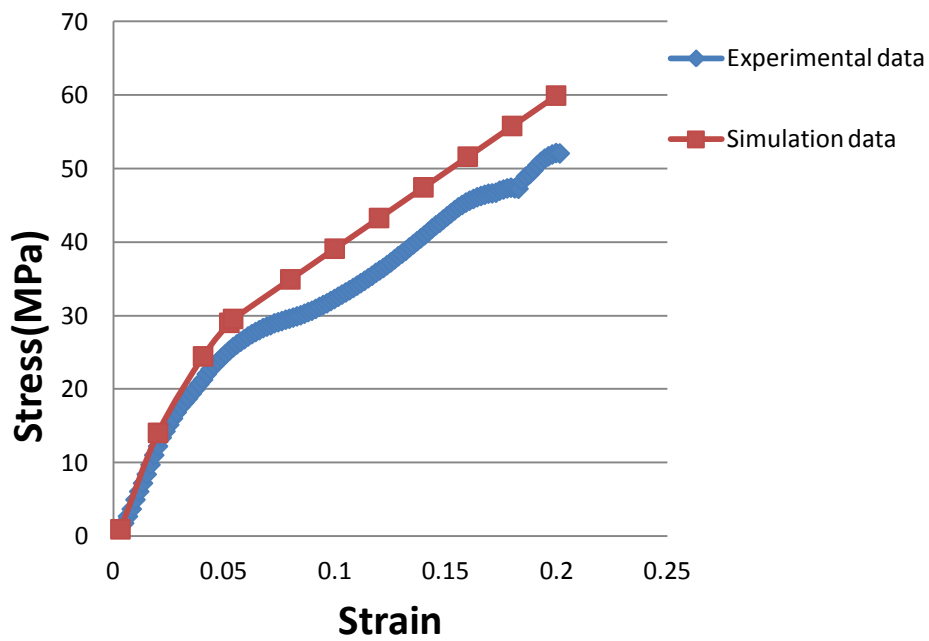


Figure 59 Comparison between simulation data and experimental data for tensile property

It is indicated in Figure 59 that the mechanical property of auxetic yarn is highly non-linear. Therefore, a bilinear isotropic property is defined for the material property of auxetic yarn. The stress-strain curve is divided into two parts by the onset point where the slope of the curve is changed abruptly. The turning of the curves can also be considered as the yield point. The first part is fitted with a linear function which represents the linear isotropic property; the second part is also fitted with another linear function which represents the plastic behaviour (Figure 60). These two linear functions are used to define the material property of the helical auxetic yarn in the meso-mechanical model.

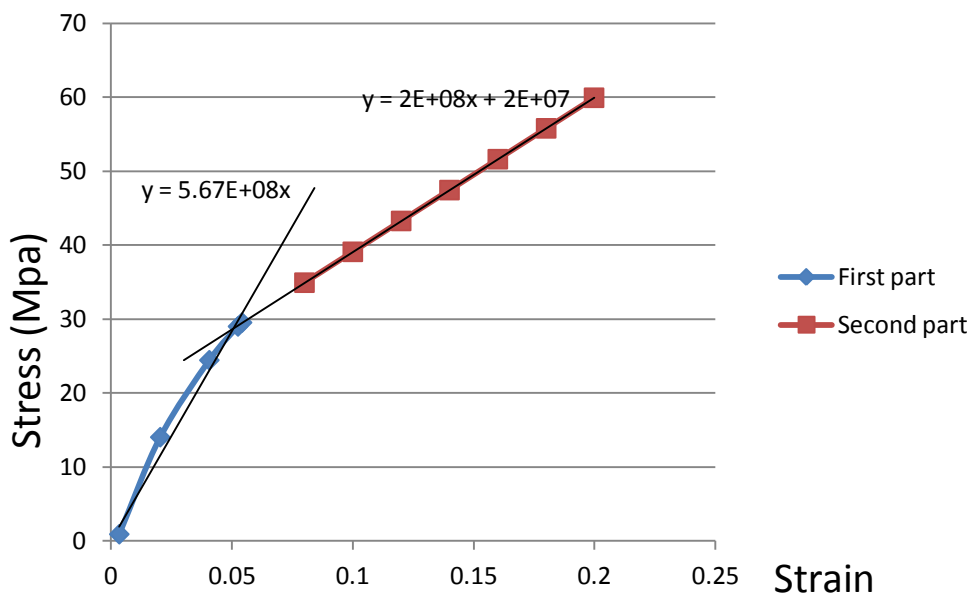


Figure 60 Curve fitting with bilinear function

After the stress-strain property of the helical auxetic yarn is obtained from the simulation, a 3D solid cylinder model with modified diameter is generated to represent the helical auxetic yarn (Figure 61). The modified diameter is given in the following equation:

$$D = D_c + 2D_w \tag{61}$$

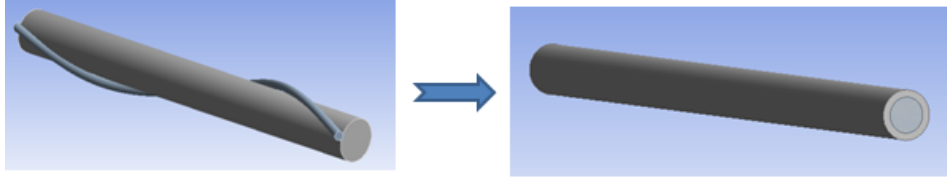


Figure 61 Representation of helical auxetic yarn

Then, the only mechanical property left for the helical auxetic yarn is the Poisson's ratio. A Poisson's ratio has to be no more than 0.5 for the linear isotropic part. According to the geometry of the modified yarn, the overall lateral strain is the sum of wrap yarn's lateral strain and core yarn's lateral strain. The Poisson's ratio for the linear isotropic property of the helical auxetic yarn can be calculated by considering the laminate theory of parallel structures in the following equation:

$$\frac{1}{\gamma} = \frac{1}{\gamma_w} + \frac{1}{\gamma_c} + \frac{1}{\gamma_w} \quad (62)$$

where γ_w and γ_c stand for the Poisson's ratio of wrap yarn and core yarn.

Furthermore, the probe can be defined in the FEM to measure the lowest position and highest position in transverse direction of the helical auxetic yarn, which gives the strain in transverse (ϵ_y) direction. Then the Poisson's ratio can be calculated by Equation (63). The curves of the Poisson's ratio versus longitudinal strain of the warp yarn, the core yarn, the experimental data of HAY and the simulation data of HAY are given in Figure 62.

$$-\frac{\epsilon_x}{\epsilon_y} = \nu \quad (63)$$

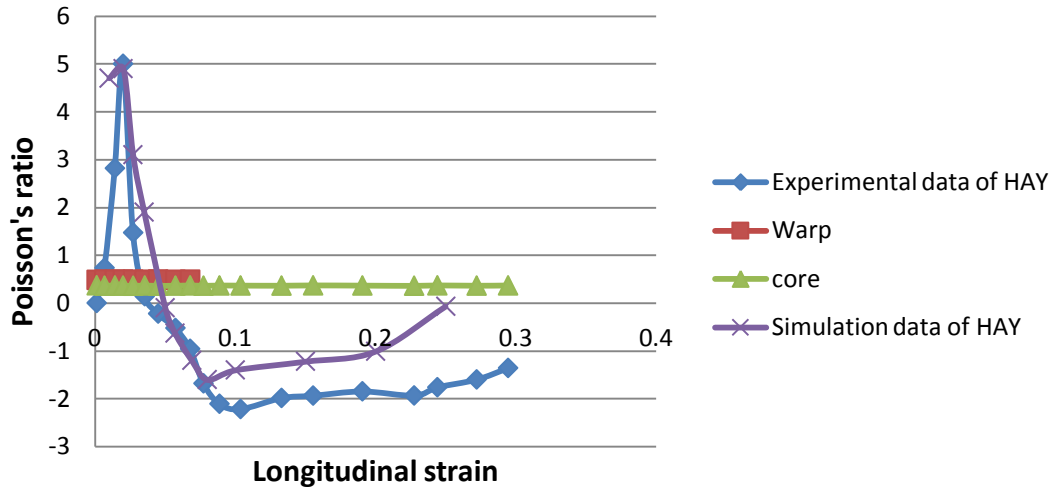


Figure 62 Poisson's ratio versus longitudinal strain

3.4.2 Meso-Mechanical Model

- Geometry of unit cell of the biaxial tubular structure

The biaxial tubular structure can be considered as a 2D interlaced fabric sheet by unwinding the structure. The periodic representative volume is a 2×2 plain woven structure with a certain angle between the warp and weft yarn at crossing point. The 3D solid geometric is generated by the same generative modelling technique used for woven fabrics. The geometry information of the unit cell of biaxial tubular structure is measured by microscope. It must be clarified that the crossing angle between the two interlaced yarns is 2θ , which is continuously changing while the shear force is increasing. Figure 63 shows the 3D solid model of the unit cell.

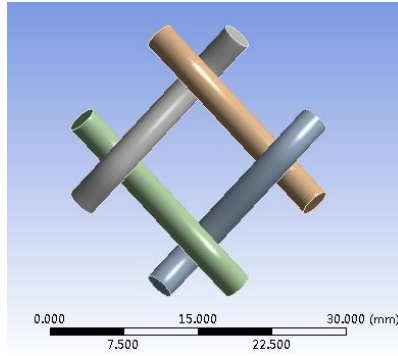


Figure 63 3D solid model of the unit cell

- Simulation

The tensile test of the biaxial tubular structure along the longitudinal direction is considered to be equivalent to pure shear test. The relationship between the longitudinal force and shear force is illustrated in Figure 64 and given in the following equations.

$$F = \cos\theta * F_{12} + \cos\theta * F_{32} \quad (64)$$

$$F_{12} = F_{32} = F_{21} = F_{23} \quad (65)$$

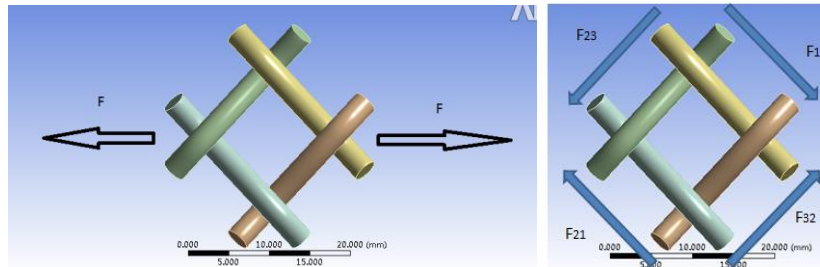


Figure 64 Illustration of tension and shear

The periodic boundary conditions are still valid for the unit cell of biaxial tubular structure due to the periodicity of the unit cell while the overall structure is subjected to deformation. In particular, periodic boundary conditions can be substituted by the boundary conditions of prescribed forces on the edges of unit cell. The nodes on both edges of one yarn have exactly the opposite forces to have periodicity. The displacement in x axis must be zero

to avoid rigid body displacement. Figure 65 shows the application of boundary conditions.

The boundary conditions in terms of displacements are given in the following equation:

$$\vec{U}(A + \vec{b}) - \vec{U}(A) = \langle \epsilon \rangle * \vec{b} \quad (66)$$

where $\langle \epsilon \rangle$ is the macro strain tensor which can be defined as an incremental form. This could be further transformed into the boundary condition in the form of forces:

$$F_A = F_B = F_C = F_D = -F_E = -F_F = -F_G = -F_H \quad (67)$$

where $F_A, F_B, F_C, F_D, F_E, F_F, F_G, F_H$ are four pairs of opposite forces which can be defined in Ansysworkbench.

In addition, the condition $U_{1x} = U_{2x} = 0$ is applied at the cross over point (Figure 65) to avoid the rigid displacement. A bonded tie contact is defined at each cross over point.

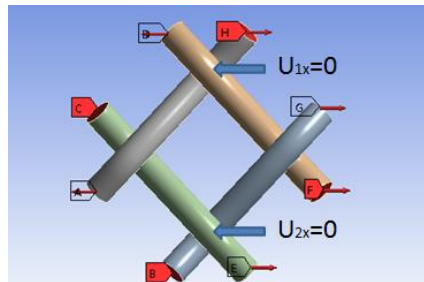


Figure 65 Application of boundary conditions

3.5 Results and Discussion

The shear deformation can be calculated by angle between the crossing yarns.

$$\Delta = \theta_d - \theta_0 \quad (68)$$

where Δ is the change of angle, θ_d is the angle after deformation and θ_0 is the angle before deformation

It is assumed that the shape of the unit cell is always a parallelogram regardless of different crossing angles. According to the geometry of the unit cell (Figure 66), the open

area (A) is:

$$A = l * l * \sin 2\theta \quad (69)$$

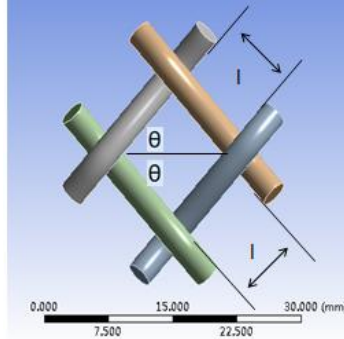


Figure 66 Geometry of the unit cell

Suppose the edge length at a given tensile force F is l' ; then the final edge length l is given by the following equation:

$$l = l' - \frac{\varepsilon_y(D_c + 2D_w)}{\sin 2\theta} \quad (70)$$

where ε_y is the lateral strain of the helical auxetic yarn,

$\varepsilon_y(D_c + 2D_w)$ is the displacement of the width of the helical auxetic yarn,

$\frac{\varepsilon_y(D_c + 2D_w)}{\sin 2\theta}$ is the displacement projected on the axis direction of the helical auxetic yarn, resulted from the increase of width of the helical auxetic yarn under tension.

The value l' and θ can be calculated from the FEM model of the unit cell as a function of incremental tensile force F . The lateral strain ε_y is a function of the longitudinal strain ε_x which equals to:

$$\varepsilon_x = \frac{l' - l_0}{l_0} \quad (71)$$

The initial length was $l_0 = 9.83$ mm

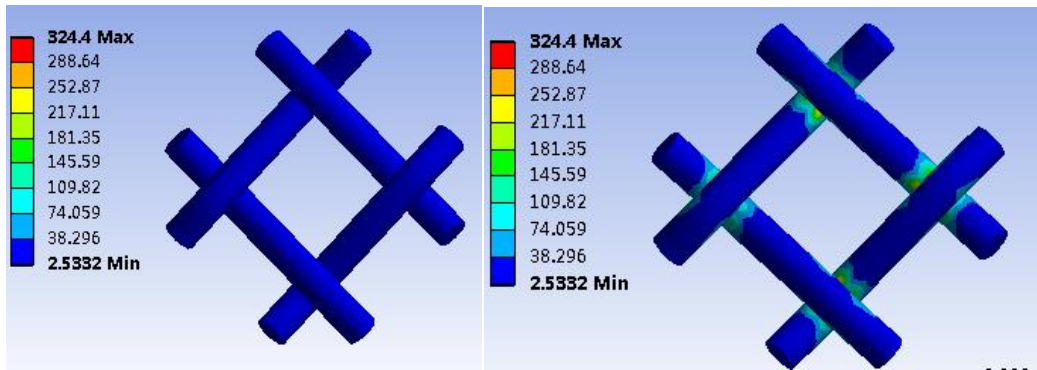


Figure 67 The contour of stress distribution before deformation (left) and after deformation (right)

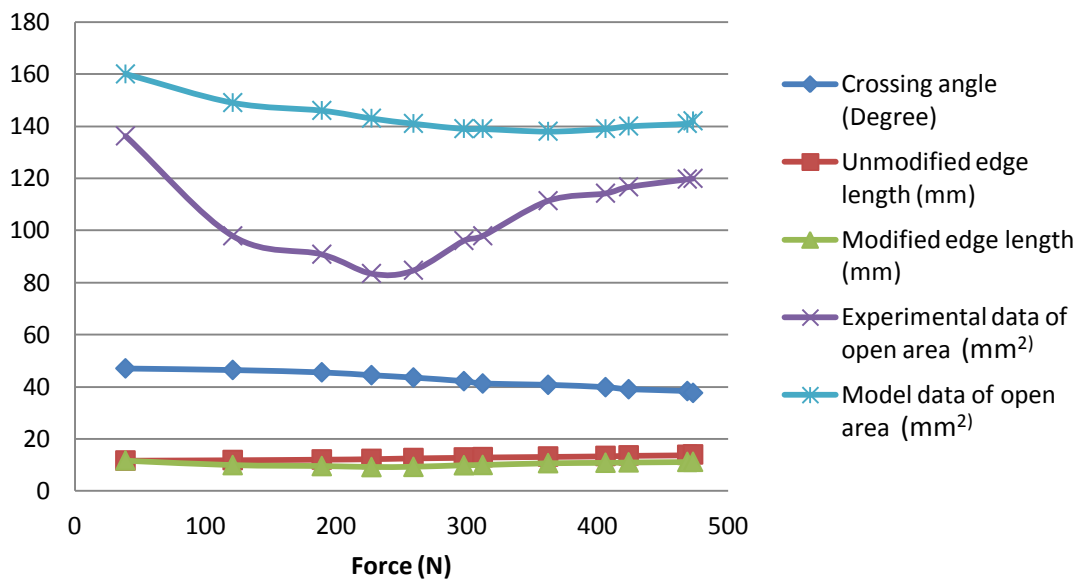


Figure 68 Experimental data and simulation results of each parameter

Figure 67 presents the contour of stress distribution before deformation and after deformation. Figure 68 shows the final results of the model. It is clearly observed that the open area is decreased while the structure is subjected to incremental tension. The experimental data of open area versus axial force indicates that the open area is going to decrease at the beginning stage and then gradually increase after the lowest point at around 250 N. This phenomenon can be explained by the combination effect of auxetic behaviour of the helical auxetic yarn and the decrease of the crossing angle under axial tension. The

increase in width of the auxetic yarn contributes to the decrease of the open area and the decrease of the crossing angle has the opposite effect. The FEM model based on auxetic behaviour and crossing angle is validated through the comparison between simulation data and experimental data. The major inaccuracy of the model is probably due to the relative sliding between helical auxetic yarns and measurement errors. The yarn's relative sliding, which occurs in reality, is not taken into account in the model. The relative sliding, if it is big enough, could severely damage the periodicity and stability of the unit cell. If the unit cells do not periodically constitute the overall structure, the model is no longer valid.

3.6 Conclusions

A novel biaxial tubular fabric made of helical auxetic yarn is fabricated by braiding method. The tubular braiding fabric has variable permeability property while it is subjected to incremental axial forces. An FEM based mechanical model including the micro-mechanical and meso-mechanical model is established to investigate the mechanical properties. The model is validated by comparison between simulation data and experimental data. The auxetic behaviour of the yarn and decreasing crossing angle under axial force are the two major parameters to influence the permeability.

References

- 1 Hook, P.B., Evans, K.E., Hannington, J.P., Hartmann-Thompson, C., Bunce, T.R., (2006). Patent number: KR20060009826.
- 2 Konopasek, M., Computational aspects of large deflection analysis of slender bodies. (1980) In: J.W.S. Hearle, J.J. Thwaites and J. Amirbaya, eds, *Mechanics of Flexible Fiber Assemblies*, Nato Advanced Study Institutes Series, Series E: Applied Science - No. 38. USA: Sijthoff & Noordhoff, pp. 275-292.
- 3 Postle, J.R. and Postle, R., (1996). Modelling Fabric Deformation as a Nonlinear Dynamical System Using Bäcklund Transformations. *International Journal of Clothing Science and Technology*, Vol.8, No.3, pp. 22-42.
- 4 Adanur, S., 1995. *Wellington Sears Handbook of Industrial Textiles*, CRC Press
- 5 Adanur, S. and Vakalapudi, J. S., (2013). Woven Fabric Design and Analysis in 3D Virtual Reality, Part 1: Computer Aided Design and Modeling of Interlaced Structures. *Journal of the Textile Institute*.
- 6 Adanur, S. and Vakalapudi, J. S., (2012). Woven Fabric Design and Analysis in 3D Virtual Reality, Part 2: Predicting Fabric Properties with the Model, *Journal of the Textile Institute*.
- 7 Adanur, S. and Liao, T., (1998). 3D Modeling of Textile Composite Preforms. *Composites. Part B: Engineering*, 29B, pp. 787-793.
- 8 Liao, T. and Adanur, S., (1998). A Novel Approach to Three Dimensional Modeling of Interlaced Fabric Structures. *Textile Research Journal*, Vol.68, No.11, pp. 841-847.
- 9 Liao, T. and Adanur, S., (2000). 3D Structural Simulation of Tubular Braided Fabrics for Net-Shape Composites. *Textile Research Journal*, Vol. 70 No.4, pp. 297-303.
- 10 Takano, N., Uetsuji, Y., Kashiwagi, Y. and Zako, M., (1999). Hierarchical Modelling of Textile Composite Materials and Structures by the Homogenization Method. *Modelling and Simulation in Materials Science and Engineering*, Vol.7, No.2, pp. 207-231.
- 11 Lomov, S.V., Ivanov, D.S., Verpoest, I., Zako, M., Kurashiki, T., Nakai, H. and Hirose, S., (2007). Meso-FE Modelling of Textile Composites: Road map, Data Flow and Algorithms. *Composites Science and Technology*, Vol.67, No.9, pp. 1870-1891.
- 12 Bogdanovich, A.E., (2006). Multi-Scale Modeling, Stress and Failure Analyses of 3-D Woven Composites. *Journal of Materials Science*, Vol.41, No.20, pp. 6547-6590.
- 13 Peirce, F.T., (1937). The Geometry of Cloth Structure. *Journal of the Textile Institute*, Vol.28, No.45, pp.43-77.
- 14 Hearle, J.W.S., El-Behery, H.M.A.E. and Thakur, V.M., (1959). The Mechanics of Twisted Yarns: Tensile Properties of Continuous-Filament Yarns. *Journal of the Textile Institute*, Vol.50, pp. T83-T111.
- 15 Önder, E. and Bacer, G., (1996). A Comprehensive Stress and Breakage Analysis of Staple Fiber Yarns Part I: Stress Analysis of A Staple Yarn Based on a Yarn Geometry of Conical Helix Fiber Paths. *Textile Research Journal*, Vol.66, No.9, pp. 562-575.
- 16 Backer, S., (1952). The Mechanics of Bent Yarns. *Textile Research Journal*, Vol.22, No.5, pp. 668-681.

- 17 Platt, M.M., Klein, W.G. and Hamburger, W.J., (1959). Mechanics of Elastic Performance of Textiles Materials, Part XIV: Some Aspects of Bending Rigidity of Single Yarns. *Textile Research Journal*, Vol.29, pp. 611.
- 18 Freeston, W.D. and Schoppee, M.M., (1975). Geometry of Bent Continuous-Filament Yarns. *Textile Research Journal*, Vol.45, No.12, pp. 835-852.
- 19 Choi, K.F. and Tandon, S.K., (2006). An Energy Model of Yarn Bending. *Journal of the Textile Institute*, Vol.97, No1, pp. 49-56.
- 20 Park, J. and Oh, A., (2006). Bending Rigidity of Yarns. *Textile Research Journal*, Vol.76, No.6, pp. 478-485.
- 21 Komori, T., (2001). A Generalized Micromechanics of Continuous-Filament Yarns Part I: Underlying Formalism. *Textile Research Journal*, Vol.71, No.10, pp. 898-904.
- 22 Dastoor, P.H., Ghosh, T.K., Batra, S.K. and Hersh, S.P., (1994). Computer-Assisted Structural Design of Industrial Woven Fabrics Part III: Modelling of Fabric Uniaxial/Biaxial Load-Deformation. *Journal of the Textile Institute*, Vol.85, No.2, pp. 135-137.
- 23 Kemp, A., (1958). An Extension of Peirce's Cloth Geometry to the Treatment of Non-Circular Threads. *Journal of the Textile Institute*, Vol.49, No.1, pp. 44-48.
- 24 Olofsson, B., (1964). A General Model of A Fabric as A Geometric-Mechanical Structure. *Journal of the Textile Institute*, Vol.55, No.11, pp. 541-557.
- 25 Freeston, W.D., Platt, M.M. and Schoppee, M.M., (1967). Mechanics of Elastic Performance of Textile Materials. XVIII. Stress-Strain Response of Fabrics Under Two-Demensional Loading. *Textile Research Journal*, Vol.37, No.11, pp. 948-975.
- 26 Grosberg, P. and Kedia, S., (1966) The Mechanical Properties of Woven Fabrics, Part I: The Initial Load Extension Modulus of Woven Fabrics. *Textile Research Journal*, Vol.36, No.1, pp. 71-79.
- 27 Dastoor, P.H., Ghosh, T.K., Batra, S.K. and Hersh, S.P., (1994). Computer-Assisted Structural Design of Industrial Woven Fabrics Part III: Modelling of Fabric Uniaxial/Biaxial Load-Deformation. *Journal of the Textile Institute*, Vol.85, No.2, pp. 135-137.
- 28 Huang, N.C., (1979). Finite Biaxial Extension of Completely Set Plain Woven Fabrics. *Journal of Applied Mechanics, Transactions ASME*, Vol.46, No.3, pp. 651-655.
- 29 Huang, N.C., (1979). Finite biaxial extension of partially set plain woven fabrics. *International Journal of Solids and Structures*, Vol.15, No.8, pp. 615-623.
- 30 Kawabata, S., Niwa, M. and Kawai, H., (1973). Finite-Deformation Theory of Plain-Weave Fabrics - 1. The Biaxial-Deformation Theory. *Journal of the Textile Institute*, Vol.64, No.1, pp. 21-46.
- 31 Dolatabadi, K. M.; Kovar, R. & Linka, A., (2009). Geometry of Plain Weave Fabric Under Shear Deformation. Part I: Measurement of Exterior Positions of Yarns. *J. Text. Inst.*, Vol.100, No.4, pp. 368-380
- 32 Dolatabadi, K. M. & Kovar, R., (2009). Geometry of Plain Weave Fabric Under Shear Deformation. Part II: 3D Model of Plain Weave Fabric Before Deformation And III: 3D Model of Plain Weave Fabric Under Shear Deformation. *J. Text. Inst.*, Vol.100, No.5, pp. 381-300

- 33 Konopasek, M., (1980). Classical Elastica Theory and Its Generalizations. In: J.W.S. Hearle, J.J. Thwaites and J. Amirbaya, eds, *Mechanics of flexible fiber assemblies*, Nato Advanced Study Institutes Series, Series E: Applied Science - No. 38. USA: Sijthoff & Noordhoff, pp. 255-274.
- 34 Konopasek, M., (1980). Textile Application of Slender Body Mechanics. In: J.W.S. Hearle, J.J. Thwaites and J. Amirbaya, eds, *Mechanics of flexible fiber assemblies*, Nato Advanced Study Institutes Series, Series E: Applied Science - No. 38. USA: Sijthoff & Noordhoff, pp. 293-310.
- 35 Lloyd, D.W., Mete, F. and Hussain, K., (1996). An Approach to The Theoretical Mechanics of Static Drape. *International Journal of Clothing Science and Technology*, Vol.8, No.3, pp. 43-58.
- 36 Stylios, G.K., Wan, T.R. and Powell, N.J., (1996) Modelling The Dynamic Drape of Garments on Synthetic Humans In A Virtual Fashion Show. *International Journal of Clothing Science and Technology*, Vol.8, No.3, pp. 95-112.
- 37 Hu, J., Chen, S. and Teng, J.G., (2000). Numerical Drape Behavior of Circular Fabric Sheets over Circular Pedestals. *Textile Research Journal*, Vol.70, No.7, pp. 593-603.
- 38 Hu, J.L. and Teng, J.G., (1996) Computational Fabric Mechanics: Present Status and Future Trends. *Finite Elements in Analysis and Design*, Vol.21, No.4, pp. 225-237.
- 39 Keefe, M., Edwards, D.C. and Yang, J., (1992) Solid Modeling of Yarn And Fiber Assemblies. *Journal of the Textile Institute*, Vol.83, No.2, pp. 185-196.
- 40 Provatidis, C. and Vassiliadis, S., (2002) On The Numerical Estimation of The Mechanical Behaviour of Fabrics, 2nd AUTEX World Textile Conference, pp. 88-97.
- 41 Provatidis, C.G., Vassiliadis, S.G. and Anastasiadou, E.A., (2005) Contact Mechanics in Twodimensional Finite Element Modelling of Fabrics. *International Journal of Clothing Science and Technology*, Vol.17, No.1, pp.29-40.
- 42 Munro, W.A., Carnaby, G.A., Carr, A.J. and Moss, P.J., (1997) Some Textile Applications of Finite-element Analysis. Part I: Finite Elements for Aligned Fiber Assemblies. *Journal of the Textile Institute*, Vol.88, No.4, pp. 325-338.
- 43 Vassiliadis, S., Kallivretaki, A. and Provatidis, C., (2010) Mechanical Modelling of Multifilament Twisted Yarns. *Fibers and Polymers*, Vol.11, No.1, pp. 89-96.
- 44 Toney, M.M., (2000) Computer Modeling of Fibrous Structures. *Journal of the Textile Institute*, Vol.91, No.3, pp. 133-139.
- 45 Durville, D., (2005). Numerical Simulation of Entangled Materials Mechanical Properties. *Journal of Materials Science* Vol.40, No.22, pp. 5941–5948
- 46 Tarfaoui, M. and Akesbi, S., (2001) Numerical Study of The Mechanical Behaviour of Textile Structures. *International Journal of Clothing Science and Technology*, Vol.13, No.3- 4, pp. 166-175.
- 47 Bartels, Beatty, and Barsky. (1987). *An Introduction to Splines for Use in Computer Graphics and Geometric Modeling*. Morgan Kaufmann.
- 48 Vassiliadis, S., Kallivretaki, A., Grancaric, A.M., Giannakis, S. and Provatidis, C., (2008) Computational Modelling of Twill and Satin Woven Structure, Proc. of the World Conference AUTEX 2008, June 2008, Biella, Italy.

- 49 Zhang, Y.C. and Harding, J., (1990) A Numerical Micromechanics Analysis of The Mechanical Properties of A Plain Weave Composite. *Computers & Structures*, Vol.36, No.5, pp. 839-844.
- 50 Naik, N.K. and Ganesh, V.K., (1992) Prediction of On-Axes Elastic Properties of Plain Weave Fabric Composites. *Composites Science and Technology*, Vol.45, No.2, pp. 135-152.
- 51 Whitcomb, J. and Srirengan, K., (1996) Effect of Various Approximations on Predicted Progressive Failure in Plain Weave Composites. *Composite Structures*, Vol.34, No.1, pp. 13-20.
- 52 Ng, S., Tse, P. and Lau, K., (1998). Numerical and Experimental Determination of In-Plane Elastic Properties of 2/2 Twill Weave Fabric Composites. *Composites Part B: Engineering*, Vol.29 No.6, pp. 735-744.
- 53 Choi, J. and Tamma, K.K., (2001) Woven Fabric Composites, Part I: Predictions of Homogenized Elastic Properties and Micromechanical Damage Analysis. *Int. J. Numer. Meth. Eng.*, Vol.50, pp. 2285-2298.
- 54 Verpoest, I. and Lomov, S.V., (2005) Virtual Textile Composites Software Wisetex: Integration with Micro-Mechanical, Permeability and Structural Analysis. *Composites Science and Technology*, Vol.65(15-16 SPEC. ISS.), pp. 2563-2574.
- 55 Lomov, S.V., Gusakov, A.V., Huysmans, G., Prodromou, A. and Verpoest, I., (2000) Textile Geometry Preprocessor for Meso-Mechanical Models of Woven Composites. *Composites Science and Technology*, Vol.60, No.11, pp. 2083-2095.
- 56 Lomov, S.V., Huysmans, G., Luo, Y., Parnas, R.S., Prodromou, A., Verpoest, I. and Phelan, F.R., (2001) Textile Composites: Modelling Strategies. *Composites - Part A: Applied Science and Manufacturing*, Vol.32, No.10, pp. 1379-1394.
- 57 Martin, S (2007). *Geometric and Mechanical Modelling of Textiles* (Doctoral dissertation), University of Nottingham, UK.
- 58 C. C. Wong, A. C. Long, M. Sherburn, F. Robitaille, P. Harrison, and C. D. Rudd. (2006). Comparisons of Novel and Efficient Approaches for Permeability Prediction Based On The Fabric Architecture. *Composites Part A*, Vol.37, No.6, pp.847-57.
- 59 J. W. S. Hearle and W. J. Shanahan., (1978). An Energy Method for Calculations in Fabric Mechanics. *Journal Textile Institute*, Vol.69, No.4, pp. 81-110.
- 60 ANSYS® Academic Research, Release 14.0. (2011). Help System, ANSYS, Inc.
- 61 Carvelli, V., Corazza, C. and Poggi, C. (2008). Mechanical Modelling of Monofilament Technical Textiles. *Computational Materials Science*, Vol.42, pp.679-691.
- 62 Carvelli, V. and Poggi, C. (2001). A Homogenization Procedure for A Numerical Analysis of Woven Fabric Composite. *Composites - Part A: Applied Science and Manufacturing*, Vol.32, pp.1425-1432.
- 63 Lakes, R.S., (1987). Foam Structure with a Negative Poisson's Ratio. *Science*, Vol.235, pp.1038.
- 64 Evans, K.E., Nkansah, M.A., Hutchinson, I.J., Rogers, S.C., (1991). Molecular Network Design. *Nature*, Vol.353, pp.124.
- 65 Evans, K.E., Alderson, A., (2000). Auxetic Materials: Functional Materials and Structures from Lateral Thinking. *Advanced Materials*, Vol.12, No. 9, pp.617-628.

- 66 Williams, J.J., Smith, C.W., Evans, K.E., Lethbridge, Z.A.D., Walton, R.I., (2007). An Analytical Model for Producing Negative Poisson's Ratios and Its Application in Explaining Off-Axis Elastic Properties of The Nattype Zeolites. *Acta Materialia*, Vol.55, No.17, pp.5697–5707.
- 67 Baughman, R.H., Shacklette, J.M., Zakhidov, A.A., Stafstrom, S., (1998). Negative Poisson's Ratios as A Common Feature of Cubic Materials. *Nature*, Vol.392, pp.362.
- 68 Lees, C., Vincent, J.E.V., Hillerton, J.E., (1991). Poisson's Ratio in Skin. *Biomedical Materials and Engineering* 1, pp.19–23.
- 69 Williams, J.L., Lewis, J.L., (1982). Properties and an Anisotropic Model of Cancellous Bone from The Proximal Tibial Epiphysis. *Trans. ASME, Journal of Biomechanical Engineering* 104.
- 70 Chan, N., Evans, K.E., (1997). Fabrication Methods for Auxetic Foams. *Journal of Materials Science*, Vol.32, pp.5945–5953.
- 71 Gaspar, N., Ren, X.J., Smith, C.W., Grima, J.N., Evans, K.E., (2005). Novel Honeycombs with Auxetic Behaviour. *Acta Materialia*, Vol.53, pp.2439–2445.
- 72 Kocer, C., McKenzie, D.R., Bilek, M.M., (2009). Elastic Properties of A Material Composed of Alternating Layers of Negative and Positive Poisson's Ratio. *Materials Science and Engineering A505*, pp.111–115.
- 73 Gunton, D.J., Saunders, G.A., (1972). The Young's Modulus and Poisson's Ratio of Arsenic, Antimony And Bismuth. *Journal of Materials Science*, Vol.7, pp.1061–1068.
- 74 Grima, J. N., Alderson, A., Evans, K. E., (2005). An Alternative Explanation for The Negative Poisson's Ratios in Auxetic Foams, *J. Phys.Soc. of Japan*, Vol.74, pp.1341-1342.
- 75 Shanahan, M.E.R., Piccirelli, N., (2008). Elastic Behaviour of A Stretched Woven Cloth. *Composites Part A Applied Science and Manufacturing*, Vol.39, pp.1059–1064.
- 76 Ugbolue, S.C, Warner, S.B., Kim, Y.K., Fan, Q., Yang, C.L., Kyzymchuk, O., Feng, Y., (2007). The Formation and Performance of Auxetic Textiles, Report, National textile centre, USA, NTC project: F06-MD09, pp. 1–10.
- 77 Hall, L.J., Coluci, V.R., Galvao, D.S., Kozlov, M.E., Zhang, M., Dantes, S.O., Baughman, R.H., (2008). Sign Change of Poisson's Ratio for Carbon Nanotube Sheets. *Science*, Vol. 320, pp.504.
- 78 Miller, W., Hook, P.B., Smith, C.W., Wang, X., Evans, K.E., (2009). The Manufacture and Characterisation of A Novel, Low Modulus, Negative Poisson's Ratio Composite. *Composites Science and Technology*, Vol.69, No.5, pp.651–655.